ROLE OF OCEAN-ATMOSPHERE COUPLING IN REGIONAL CLIMATIC IMPACTS OF ANTHROPOGENIC SULFATE AEROSOLS

A Dissertation

by

TARUN VERMA

Submitted to the Office of Graduate and Professional Studies of
Texas A&M University
in partial fulfillment of the requirements for the degree of

DOCTOR OF PHILOSOPHY

Chair of Committee,	Ramalingam Saravanan
Committee Members,	Ping Chang
	Gerald R. North
	Mikyoung Jun
Head of Department,	Ping Yang

December 2017

Major Subject: Atmospheric Sciences

ABSTRACT

Using a suite of coupled and uncoupled climate model experiments, we explore the impacts of anthropogenic sulfate aerosols on tropical Pacific climate and its variability. The role of sea surface temperature (SST), ocean dynamics, and ocean-atmosphere interaction in climate response to aerosols is examined by appropriately choosing the ocean component namely, full ocean general circulation model (OGCM), slab ocean model (SOM) or prescribed climatological SST. The ensemble of shorter responses versus a long-term response highlights processes and coupled feedbacks that are active on seasonal-interannual timescales versus on multi-decadal timescales. We find that an abrupt increase in tropospheric sulfate aerosols gives rise to El Niño like warming of the eastern tropical Pacific on seasonal-interannual timescales. Dynamical interaction between the ocean and the atmosphere causes this equatorial warming, whereas the thermodynamic interaction is responsible for the off-equatorial warming. These two interactions are related to the presence of Bjerknes feedback over the equator versus the off-equatorial WES (Wind-Evaporation-SST) feedback in the tropical climate system. In long-term, ocean dynamics will remove the initial tropical warming leaving a weaker and negative SST in response to increased aerosols in the fully-coupled case. Absence of ocean dynamics in the partially-coupled case, on the other hand, will lead to amplification of the off-equatorial warming via positive WES feedback. These coupled feedbacks, therefore, control the intertropical convergence zone (ITCZ) shift in response to aerosols over the eastern tropical Pacific. In this study, we also identify a cloud

microphysics based mechanism for the high cloud increase over the tropical Indian Ocean. This regional increase in high clouds results in local net positive radiative forcing in comparison to negative forcing elsewhere on the globe.

CONTRIBUTORS AND FUNDING SOURCES

Contributors

This work was supervised by a dissertation committee consisting of Professors Ramalingam Saravanan [chair], Ping Chang, and Gerald R. North of the Department of Atmospheric Sciences and Professor Mikyoung Jun of the Department of Statistics.

The initial experiments were designed and performed in collaboration with Dr. Salil Mahajan of the Oak Ridge National Laboratory.

All work for the dissertation was completed by the student, under the advisement of Professor Ramalingam Saravanan of the Department of Atmospheric Sciences.

Funding Sources

The research was funded by Department of Energy Grant Number SC0008569, "Impacts of Aerosols and Air-Sea Interaction on Community Earth System Model Biases in the Western Pacific Warm Pool Region".

TABLE OF CONTENTS

Page

ABSTRACT ii

CONTRIBUTORS AND FUNDING SOURCES iv

TABLE OF CONTENTS v

LIST OF FIGURES vii

LIST OF TABLES xi

CHAPTER I INTRODUCTION & LITERATURE REVIEW 1

1.1 Introduction 1
1.2 Background 2
1.3 Scientific Hypotheses & Questions 8
1.4 Summary 9

CHAPTER II MODEL & EXPERIMENT DETAILS 10

2.1 Introduction 10
2.2 Model Details & Advancements 11
2.3 Model Integrations and Experiments 15
2.4 Model Validation 23
2.5 Conclusions 29

CHAPTER III TRANSIENT OCEAN DYNAMICAL RESPONSE 31

3.1 Introduction 31
3.2 Method & Model Details 32
3.3 Results 35
3.4 Conclusions 48

CHAPTER IV THERMODYNAMIC & DYNAMICAL COUPLED RESPONSE 53

4.1 Introduction 53
4.2 Methodology 58
4.3 Results 66
4.4 Conclusions 75

Page

CHAPTER V TROPICAL HIGH CLOUD RESPONSE 78

5.1 Introduction 78
5.2 Model Details 79
5.3 Results 83
5.4 Conclusions 90

CHAPTER VI CONCLUSIONS 93

REFERENCES 97

LIST OF FIGURES

FIGURE		Page
1.1	Schematic representing a simplified aerosol-climate interaction	5
2.1	Mean increase in sulfate aerosol concentration and its seasonality	16
2.2	Schematic differences between short- and long-term experiments.....	18
2.3	Global mean annual mean trajectories of long-term control and perturbed runs for (a,b,c) fully- and (d,e,f) partially-coupled cases	21
2.4	ENSO temporal characteristics (Niño3.4) in 20th century observed SST data (grey; HadISST) and preindustrial fully-coupled integration (blue; 1850S)	22
2.5	Pacific Meridional Mode (PMM; spatial pattern and associated seasonal variance) in observations, preindustrial fully-coupled (1850S), and present-day perturbed (2000S_long) integrations	25
2.6	Mean local Walker and Hadley Circulation in observations (NCEP/ NCAR Reanalysis), and preindustrial fully-coupled integration (1850S).....	26
2.7	Total sulfate aerosol radiative forcing	28
3.1	Ensemble mean first 2-year mean differences between ‘2000S’ and ‘1850S’ runs.....	34
3.2	Ensemble mean first 2-year mean differences between ‘2000S_som’ and ‘1850S_som’ runs	37
3.3	Ensemble mean monthly mean differences between (a,c,e) ‘2000S’ and ‘1850S’ runs, and (b,d,f) ‘2000S_som’ and ‘1850S_som’ runs over equatorial Pacific (5S-5N)	38
3.4	Ensemble mean second year October-December mean differences between ‘2000S’ and ‘1850S’ runs	39
3.5	Ensemble mean second year April-June mean differences between ‘2000S’ and ‘1850S’ runs	41

FIGURE Page

3.6 Ensemble mean second year October-December mean differences between ‘2000S’ and ‘1850S’ runs 42

3.7 Ensemble mean monthly mean differences between ‘2000S’ and ‘1850S’ runs 44

3.8 Ensemble based lead-lag cross-correlation between Niño3.4 SST response (‘2000S’ – ‘1850S’) and zonal wind stress response (‘2000S’ – ‘1850S’) in a fully-coupled experiment 45

3.9 Ensemble mean monthly mean differences between ‘2000S’ and ‘1850S’ runs over equatorial Pacific (5S-5N) 47

3.10 Ensemble based lead-lag cross-correlation between area averaged time series of SST and zonal wind stress responses (‘2000S’ – ‘1850S’). 48

3.11 Ensemble mean fourth-year mean differences between ‘2000S’ and ‘1850S’ runs 51

4.1 Simultaneous linear regression coefficient between monthly mean SST (ERSST v4) and net downward heat flux (NCEP/ NCAR Reanalysis) at the surface for 1950-2015 period..... 54

4.2 Area-averaged differences in mean and variance (of annual mean time series shown in Figure 2.2) of surface temperature, net downward radiative flux at top of the model and precipitation in (a,c,e) long-term fully- (‘2000S_long’ – ‘1850S’) and (b,d,f) partially-coupled (‘2000S_som_long’ – ‘1850S_som’) experiments 56

4.3 Schematic of surface-layer heat budget in slab ocean versus full (or dynamical) ocean model 59

4.4 Near-surface layer heat budget in a fully-coupled control run (‘1850S’) over (a) Niño3 region, (b) southeast tropical Pacific, and (c) northeast tropical Pacific Ocean 63

4.5 Annual cycle of near-surface layer heat budget in a fully-coupled control run (‘1850S’) over (a) Niño3 region, (b) southeast tropical Pacific, and (c) northeast tropical Pacific Ocean 64

4.6 Long-term mean differences between (a) ‘2000S_som_long’ and ‘1850S_som’, and (b) ‘2000S_long’ and ‘1850S’ runs 65

FIGURE Page

4.7 Ensemble mean short-term mean differences between (a) '2000S_som' and '1850S_som', and (b) '2000S' and '1850S' runs 66

4.8 Long-term mean differences in downward surface shortwave radiative flux (in W/m^2) between (a) '2000S_som_long' and '1850S_som', and (b) '2000S_long' and '1850S' runs. Ensemble mean short-term mean differences in downward surface shortwave radiative flux between (c) '2000S_som' and '1850S_som', and (d) '2000S' and '1850S' runs 68

4.9 Same as in Figure 4.8 except for changes in surface latent heat flux (positive into the ocean). 69

4.10 Area averaged ensemble mean monthly mean SST changes between (a) '2000S_som' and '1850S_som' for two-years in the partially-coupled experiment, and (b) '2000S' and '1850S' for four years in the fully-coupled experiment 70

4.11 Surface-layer heat budget analysis for short-term partially-coupled experiment. Each curve represents an area average ensemble mean monthly mean difference between '2000S_som' and '1850S_som' runs . 73

4.12 Surface-layer heat budget analysis for short-term fully-coupled experiment. Each curve represents an area average ensemble mean monthly mean difference between '2000S' and '1850S' runs..... 74

4.13 KDE based probability density function of Niño3 region monthly mean SST in (a) partially-coupled, and (b) fully-coupled long-term integrations 77

4.14 Linear regression of monthly mean sea level pressure and windstress fields with principal component time series of Pacific Meridional Mode shown in Figure 2.5 77

5.1 Simplified schematic representation of process-ordering in CAM5 81

5.2 Ensemble mean first-year mean difference between uncoupled control ('1850S_pres') and perturbed ('2000S_pres_short') integrations 85

5.3 Ensemble mean first-year mean difference between fully-coupled control ('1850S_pres') and perturbed ('2000S_pres_short') integrations 86

FIGURE Page

5.4 Ensemble mean first-year mean differences between fully-coupled control (‘1850S’) and perturbed (‘2000S_short’) integrations ... 88

5.5 Area-averaged ensemble mean first-year mean difference between fully-coupled control (‘1850S’) and perturbed (‘2000S_short’) integrations 89

5.6 Total sulfate aerosol radiative forcing..... 92

LIST OF TABLES

TABLE Page

2.1 Summary of model integrations using CESM 1.1.2..... 20

4.1 Variance explained by terms in near-surface layer heat budget analysis... 65

CHAPTER I

INTRODUCTION & LITERATURE REVIEW

1.1 INTRODUCTION

This study is relevant to two important fields in climate research, namely, atmospheric aerosols and El Niño Southern Oscillation (ENSO). While increased tropospheric aerosol concentration since the pre-industrial era is a major driver of anthropogenic climate change, ENSO is the dominant natural variability of the climate system. Both these components cannot only influence weather and climate patterns globally, but they have significant effect on earth's ecosystem and world's economy (McPhaden et al. 2006; Mahowald et al. 2011; Carslaw et al. 2010). This study considers potential interactions between the radiative effects of atmospheric aerosols and the dynamical processes that drive ENSO.

Atmospheric aerosols, based on their interaction with radiation, are classified into two types: 1) absorbing and 2) scattering aerosols. Black carbon and sulfate aerosols are examples of these two, respectively. Not only they affect radiation differently but they yield contrasting climate responses (Ocko et al. 2014). Sulfate aerosols (also referred to as sulfates) because of their chemical composition and hygroscopic nature can also interact with clouds and affect precipitation further modifying earth's energy budget and hydrological cycle (Haywood and Boucher 2000; Jones et al. 2007; IPCC 2013 and references therein). The proximity of tropical Pacific to East Asia, a major source region of industrial sulfates (Figure 8.23 in IPCC 2013), makes it susceptible to variations in emissions. Hence, we restrict our focus to understanding the effect of sulfate aerosols on

the tropical Pacific climate. Given the nonlinearity and complexity of the climate system, limiting to single external forcing will make the problem more tractable with simpler interpretation of the response.

ENSO is a quasi-periodic and a zonally asymmetric fluctuation of the tropical Pacific with El Niño (La Niña) phase being associated with warmer (cooler) than average SST over eastern Pacific. This 2-7 year period fluctuation is a collective result of the upper ocean dynamics and Bjerknes positive feedback- a change in the strength of trade winds excites an upper ocean thermocline response which reinforces the initial change (Philander 1990). Previous studies suggest modification of ENSO characteristics in recent past. Both its amplitude and spatial location in the tropical Pacific are affected. Whether this dynamical ocean-atmosphere mode of variability is affected by an increase in sulfates around the world or not, presents us with an opportunity to better understand the coupled climate response to aerosols and perhaps identify a potential source of seasonal to interannual predictability.

1.2 BACKGROUND

An important consequence of anthropogenic climate change is the modification of tropical atmospheric circulation. Under greenhouse gas warming, the tropical circulations weaken (Held and Soden 2000; He and Soden 2015). Climate model studies show the southward displacement of Intertropical Convergence Zone (ITCZ) in response to anthropogenic sulfate aerosol forcing (Rotstayn and Lohmann 2002; Shindell et al. 2012; Allen et al. 2015). These changes can cause droughts and floods over the tropical landmasses (Nobre and Shukla 1996; Giannini et al. 2003; Biasutti and Giannini 2006)

and can spur long-term climatological impacts across the tropics. This zonal mean displacement can be predicted based on simple energetics (Donohoe et al. 2012; Frierson et al. 2013; Schneider et al. 2014); the ITCZ shifts in order to compensate for the hemispheric excess or scarcity in energy caused by greater anthropogenic emissions over the Northern Hemisphere. On a regional scale, however, one needs to consider local factors like sea surface temperature (SST), lower level circulation, and their interaction, which determines extent of the shift (Nobre and Shukla 1996; Chang et al. 1997; Xie 2004; Chiang and Vimont 2004). The real world, however, is inherently complex and cannot be simplified. Both the strength and the position of the ITCZ during the past century are jointly controlled by more than one forcing type and are strongly modulated by intrinsic climate variability (Chang et al. 2011; Hwang et al. 2013; Friedman et al. 2013; Green et al. 2017). The observed displacement during the 20th century is, therefore, not fully understood.

The effect on zonally asymmetric circulation, namely, the Walker cell, is even less understood. The interannual variations associated with El Niño-Southern Oscillation (ENSO) greatly reduces the signal to noise ratio. Additionally, the Walker circulation is inherently tied to the meridional cell, through the returning equatorward flow, which makes it conceptually difficult to separate the two. As a result, the 20th century changes in Walker cell and their causes is still an unresolved problem and actively studied (Tokinaga et al. 2012; L'Heureux et al. 2013; McGregor et al. 2014; England et al. 2014). Like the meridional cell, the Walker cell weakens in the warming world partly through the thermodynamical constraint proposed by Held and Soden 2000. The other

contribution comes from the reduction in the tropical Pacific zonal SST gradients and changes in the ocean thermocline (Vecchi and Soden 2007; He and Soden 2015; Cai et al. 2015). The impact of aerosols on the Walker cell is unclear, but recent studies link weakening of the south Asian monsoon (and the Walker cell) since 1950s to increase in aerosols, particularly over Asia (Bollasina et al. 2011).

Others have also linked the Walker circulation strength to variations in the global mean surface temperature (Kosaka and Xie 2013; England et al. 2014). The 20th century global mean climate is characterized by a long-term warming trend that slows down and speeds up, intermittently. The increasing trend is typically attributed to the steady increase in well-mixed greenhouse gases. The short-term changes are either attributed to intrinsic climate variability or changes in short-lived radiative gases and aerosols. Their relative contribution to modulating the warming is uncertain as separating a robust response (to an external forcing) from the intrinsic noise is extremely challenging and is still actively debated. Some studies based on the observational record and climate model simulations (Swanson et al. 2009; DelSole et al. 2011; Wu et al. 2011) suggest that 20th century climate is primarily modulated on multidecadal timescales by processes internal to the climate system. Others (Smith et al. 2016; Takahashi and Watanabe 2016) highlight the importance of aerosols in driving recent decadal to multidecadal variations. Fundamental to this ambiguity is the poor understanding of how aerosol radiative forcing interacts with natural modes of climate variability as well their imperfect representation in climate models.

Figure 1.1 is a simplified representation of how aerosols can affect climate. Aerosols affect atmospheric state by modifying radiative fluxes, and clouds. The changes in clouds include many small-scale cloud microphysical, macrophysical and dynamical adjustments. Changes in atmospheric state can feedback into aerosols, radiation and clouds. This initial response constitutes the rapid atmospheric adjustments, or fast response of the climate system. The slow response of the system is associated with changes in SST and upper ocean. The SST change in response to aerosols affect atmosphere state and modifies the initial fast response. The total response of the climate system is, therefore, a combination of rapid atmospheric adjustments and slower ocean mediated feedback processes.

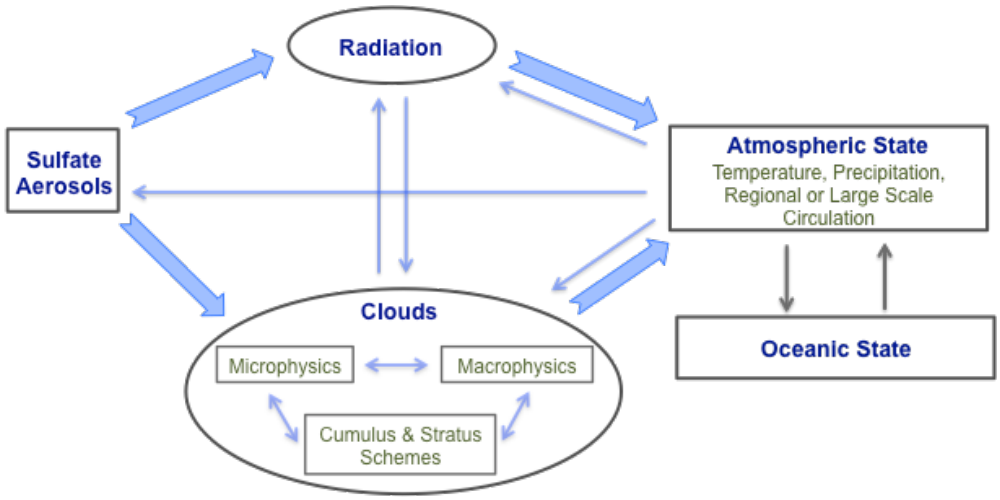

Figure 1.1 Schematic representing a simplified aerosol-climate interaction. Aerosols impact atmospheric state through radiation and clouds (rapid adjustment) that in turn interacts with oceanic state (slower feedbacks). Thick arrows represent direct impacts and thin arrows represent feedbacks.

After decades of research on the aerosol effect on climate, many aspects of its impacts are still unresolved (Stevens and Feingold 2009). According to the last IPCC report, large error bars in the global anthropogenic radiative forcing result from uncertainty in quantifying aerosol related processes. The error bars in the radiative forcing (RF) in turn translate into an uncertain climate response to the aerosol forcing, especially on regional scales. An additional uncertainty in climate response can stem from the inability to fully account for various feedbacks. The effects of missing or inaccurate short-term feedbacks have already been accounted for in the RF uncertainty. On the other hand, the long-term feedbacks that are mediated through SST and/or upper ocean changes are typically stronger (on longer timescale) and can have greater impact on the climate (IPCC 2013; Boucher 2015).

One of the difficulties in identifying well defined statistical relationships between aerosol, clouds and precipitation, needed to parameterize their effect in climate models, is the inability to constrain meteorology which can independently affect such relationships. The literature suggests the use of regime-dependent (with uniform large-scale environment) studies to resolve this issue (Stevens and Brenguier 2009). Previous studies have shown observational evidence of both 'cloud albedo' and 'cloud lifetime' effects for one such regime- shallow marine clouds over the subtropical ocean (Christensen and Stephens 2011; Russell et al. 2013). Both these effects can be distinguished from each other depending upon whether cloud macrostructure (spatial extent and water content) is affected by changes in precipitation formation ability (cloud lifetime effect), or if cloud albedo is modified by changes in cloud drop size distribution

keeping the macrostructure constant (cloud albedo effect). Understanding of aerosol-warm cloud interactions, although not fully resolved, have significantly improved over past decades, with aerosol effect on ice clouds emerging as an important area of research (Stevens and Feingold 2009; Rosenfeld et al. 2008; Tao et al. 2012).

In spite of improvements in basic processes, the role of SST (and ocean) feedback is poorly understood resulting sometimes in ambiguous climate response attribution to aerosols. For example, Booth et al. 2012 attribute twentieth century north Atlantic decadal climate variability to aerosol effects whereas Zhang et al. 2012 argue against it. The major challenge in attributing twentieth century regional climate change to an external forcing is the difficulty in removing the effects of internal climate variability, which are in turn tied to the ocean response. The importance of ocean mediation of climate response to aerosol changes are also regularly stressed in geoengineering (Amman et al. 2010) and in studies of climate response to volcanic eruptions.

Effect of volcanic eruption on tropical climate variability is an example of naturally occurring interaction between sulfate aerosols (stratospheric) and the tropical Pacific. The large-scale surface cooling post-eruption is a robust climate response (Collins 2003), however, the regional effects are less well understood. Recent studies on decadal scale predictability suggests volcanic forcing can significantly affect forecast skill over the eastern tropical Pacific (Timmreck et al. 2016; Pohlmann et al. 2013). Others (Maher et al. 2015; Ohba et al. 2013) show increased likelihood of El Niño 6-12 months after peak volcanic forcing. An inverse study by Lehner et al. 2016 also indicates that large-scale volcanic cooling is modulated by the phase of ENSO.

1.3 SCIENTIFIC HYPOTHESES & QUESTIONS

Aerosol effect on climate is unresolved in part due to imperfect process-level understanding of its effect on clouds and precipitation but also because of gaps in understanding various large-scale feedback processes which emerge on modifying aerosol concentrations. Many of these feedbacks (at least in part) are connected to ocean response. In order to address these gaps, we will be testing following hypotheses with focus on ocean-mediated response to aerosol forcing,

H1 *- Subtropical radiative forcing associated with sulfate aerosol can excite remote tropical ocean response through atmosphere-ocean interaction.*

H2 *- Ocean dynamics can moderate the impact of anthropogenic sulfate aerosol on tropical atmospheric circulation.*

The first hypothesis (H1) is motivated by the proximity of a major source of aerosol emissions, East Asia, to the tropical Pacific region. This hypothesis could also have implications for geoengineering studies, ENSO variability in future climate simulations, and seasonal forecasting of the response to volcanic eruptions. Second hypothesis (H2), on the other hand, is related to comprehending meridional shift of Hadley cell in response to sulfates' hemispherically asymmetric forcing. The displacement of tropical rain band has previously been tied to long-term droughts over semi-arid regions of Sahel and Nordeste. In addition to above hypotheses, we would be addressing following scientific questions,

Q1 *- What role does thermodynamic and dynamical ocean-atmosphere coupling play in tropical response to aerosols (of H1)?*

Q2 *- How does the tropical response scale with increasing aerosol forcing?*

Q3 *- Does sulfate-induced extratropical cooling affects the tropical response?*

Q4 *- What role do convective and microphysical processes play in model simulated tropical cloud response to sulfate forcing?*

1.4 SUMMARY

The dissertation is organized as follows: Chapter 2 describes climate model experiments carried out along with model details, advancements and validation. Chapter 3 addresses ocean dynamical response to short-term sulfate aerosol forcing over the equatorial Pacific. It is followed by comparison of short- and long-term tropical Pacific responses to aerosols in chapter 4 which brings out the role of thermodynamic versus dynamical ocean-atmosphere coupling. Chapter 5 examines tropical cloud response to increased atmospheric aerosols and studies the competing role of convection and cloud microphysics.

CHAPTER II

MODEL & EXPERIMENT DETAILS

2.1 INTRODUCTION

The spatial pattern of sulfate aerosol radiative forcing (RF) is highly inhomogeneous when compared to that of well-mixed greenhouse gases (Figure 8.23 in IPCC 2013). It is asymmetric between northern and southern hemispheres, which can lead to southward shift of ITCZ. It is also asymmetric across the tropical/subtropical Pacific ocean in the zonal direction due to maxima in aerosol loading over the Asian continent. However, climatic impacts of this zonally asymmetric RF are poorly understood. Whether it affects the zonal circulation over the tropics (Walker cell) or the zonally asymmetric mode of natural variability (ENSO) are important problems in understanding of past and future regional climatic changes and needs to be addressed.

In this study, we rely on numerical modeling approach to understand aforementioned issues. The carefully designed experiments with climate models, having the most accurate and complete representation of the processes involved, can provide us with robust answers. The observation-based approach to study the climate effects of aerosols would be ideal, but is often hampered by the insufficient data. Observations are, however, important as they play a role in evaluating the climate model's ability to accurately represent fundamental interactions e.g., between aerosols and the fast atmospheric processes like clouds and radiation.

We use version 1.1.2 of National Center for Atmospheric Research's (NCAR's) Community Earth System Model (CESM; Hurrell et al. 2013) as a tool to identify and

study regional climatic impacts of sulfate aerosols. The CESM 1.1.2 was publicly released in July 2013 and is scientifically validated on multi-decadal time scales for number of resolutions including the one used in this study. It is highly updated over its predecessor with respect to the atmospheric physics package - a suite of parameterization schemes (Neale et al. 2010). The relevant advancements and their impacts are discussed in section 2.2. These advances in atmospheric physics make CESM 1.1.2 one of the leading candidates to study aerosol-climate interaction.

Rest of the chapter is organized as follows: section 2.2 describes different components of CESM, coupling between ocean and atmospheric General Circulation Models (GCMs), and advances in representation of aerosol related processes. It is followed by the description of model integrations and experiments in section 2.3. Section 2.4 compares the simulated tropical climate to the observations along with brief validation of simulated aerosol effects on shorter timescales. Conclusions and some important caveats of the methodology are discussed in section 2.5.

2.2 MODEL DETAILS AND ADVANCEMENTS

CESM being an earth system model is a collection of atmosphere (atm), ocean (ocn), sea ice (cice), land (lnd), land ice, and river runoff models that interact through a program called coupler. The CESM framework with seven components each representing a different subsystem provides tremendous flexibility in studying the earth system as a whole or in parts. The interactions between any two or more subsystems can be studied with relative ease. Its applications span across variety of topics including climate change, climate dynamics, biogeochemistry, aerosol-cloud interaction, sea ice

and ocean dynamics, air-sea interaction, land-atmospheric interaction and so on. The CESM or climate models in general, have quite rapidly advanced and expanded in the last fifty years (Donner et al. 2011). The earliest version of the model was called Community Climate Model (CCM) and was released in early 1980s (Williamson et al. 1987). It only included the most fundamental dynamics and physics of the atmosphere, in contrast, the current version of the model is able to track various chemical species through different components of the climate system e.g. the carbon cycle is predicted across ocean, atmosphere and land models in CESM 1.1.2.

From the perspective of simulating aerosols' effect on the climate, CESM 1.1.2 with CAM5 physics has advanced in the way aerosols, their characteristics and interactions with other physical parameterizations are modeled (Neale et al. 2010). The previously used bulk approach of predicting only the mass-mixing ratio of externally mixed aerosol species is replaced by a more generic "modal" approach. In the new approach, aerosols are classified into either seven or three different lognormal modes, which are referred to as MAM7 and MAM3 (MAM being an acronym for Modal Aerosol Module) (Liu et al. 2012; Ghan et al. 2012). In this study, we use the three-mode version in order to keep the computational cost low. The new model predicts both the mass-mixing ratio for each species within different modes and an individual modes' number concentration. These two predicted values then determine the parameters for each mode's lognormal size distribution. In contrast, the bulk approach prescribed a fixed lognormal size distribution everywhere and at all times and only predicted the mass-mixing ratio. The principal advantage comes from being able to simulate the

spatiotemporal variability of the size distribution and to an extent the internal mixing between various aerosol species within the mode. The improvements in size and mixing state have implications for how aerosols interact with the radiation, microphysics and other schemes in atmospheric GCM (Boucher 2015).

Representing aerosol-cloud interaction in climate models is imperative to simulating aerosols' effect on the climate. This interaction includes many fine scale processes that account for aerosols' affect on cloud micro and macrostructure, cloud dynamics and resulting changes to the earth's radiative budget. The term interaction here suggests highly interconnected nature of different components with strong feedbacks among them. The presence of aerosols reduces the effective size of cloud particles, resulting in higher cloud reflectivity and lesser downward radiative flux. Simultaneously, it affects clouds' precipitation forming ability resulting in longer lasting clouds and an overall increase of cloud fraction further reducing the downward radiative flux. The changes in radiative balance by itself can affect back the cloud micro and macrostructure through changes in cloud dynamics. The interaction highlighted above is relatively simplistic in comparison to the surplus of processes and feedbacks present in the real atmosphere. These fine scale processes cannot be explicitly resolved on climate model's spatial and temporal scales, and therefore need to be parameterized. The model not only needs to get the distribution of various aerosol species right, but need physically realistic interaction among various physical parameterization schemes. Both the instantaneous adjustment of clouds due to increase in cloud condensation nuclei as well as rapid adjustments comprising radiative and dynamical effects on clouds which take

finite amount of time need to be modeled correctly. In this regard, CAM5 improves over its predecessor by introducing sub grid scale parameterizations (Shallow Convection, Microphysics and Macrophysics; Neale et al. 2010) as well as their interactions that are more physically realistic (Park et al. 2014; Ghan et al. 2012).

On climate timescales, the radiative perturbation caused by an increased aerosol loading results in significant changes in upper ocean thermal structure and sea surface temperature. The overall climate response to aerosols is a combination of slower feedbacks due to changes in SST and the previously mentioned rapid atmospheric adjustments of clouds and radiation (Figure 7.01 in IPCC 2013; Voigt et al. 2017). The tropical Pacific climate is characterized by a strong coupling between atmospheric and oceanic circulations. As a result, the tropical Pacific climate response could be further influenced by the upper ocean dynamics. These three contributions from rapid atmospheric adjustment, SST and ocean dynamics can easily be separated in the CESM framework by appropriately choosing an ocean component. Most advanced option includes the use a full ocean GCM (POP2 stands for Parallel Ocean Program) where the three-dimensional ocean state is predicted using dynamical and thermodynamic equations. In contrast, the Slab Ocean Model (SOM) is greatly simplified over POP2 and neglects all the ocean dynamics and only predicts an average mixed layer temperature using a simple thermal balance at the ocean surface. The third and the simplest option include the prescription of SST, either observed or from previous coupled model integration. Comparing the climate system response obtained using different hierarchy of

ocean components can help separate out the contributions from rapid atmospheric adjustment, SST or ocean dynamics (look at section 2.3 for more details).

Over the tropical Pacific, the representation of ENSO in current generation climate models has been much improved; they do fairly well in simulating its period, variability, asymmetry between El Niño and La Niña, and to an extent its spatial diversity (Guilyardi et al. 2012; Capotondi et al. 2015a, 2015b; Chen et al. 2017). A brief evaluation of the model with respect to the tropical Pacific climate and aerosols is presented in section 2.4.

2.3 MODEL INTEGRATIONS AND EXPERIMENTS

The role of ocean-atmosphere coupling in regional climate response to anthropogenic sulfate aerosols is examined by first carrying out three long control simulations using CESM 1.1.2. Each of these climate model integrations are subjected to preindustrial forcings due to greenhouse gases, aerosols etc. and use ~2 degree horizontal resolution for 'atm' and 'lnd' and ~1 degree for 'ocn' and 'cice' components. They differ from each other only in the choice of the ocean component being used. Whether the atmospheric GCM is coupled to the full ocean GCM, slab ocean model or if SSTs are prescribed determine the strength and the kind of climate responses that would be simulated. The suffixes 'som' and 'pres' will be used in the naming of model integrations to indicate the choice of the ocean component being used. The fully coupled model integrations, which use the full ocean GCM, have no suffix in their names. In future, we often will be referring the climate model integrations with SOM as partially coupled integrations (or experiments) analogous to fully coupled integrations.

The global emissions of tropospheric sulfate aerosols and their precursor gases (SO_2, DMS) are based on Lamarque et al. 2010 emission inventory. These emission fluxes are prescribed in the atmospheric GCM; the aerosol particles introduced into the atmosphere are allowed to advect with the circulation and interact with various cloud processes, and are eventually removed by various chemical and physical sinks. In order to examine the climate response to sulfate aerosols, the emissions are raised from their preindustrial values to the present day level. The present day minus the preindustrial sulfate emissions is used as the perturbation for generating different kinds (due to differences in ocean component) and timescales of climate responses. The simulated annual mean increase in sulfate aerosol burden (vertically-integrated column amount) in the fully coupled case is shown in Figure 2.1a. We find that the mean pattern of the increase is not sensitive to the choice of ocean-atmosphere coupling (not shown).

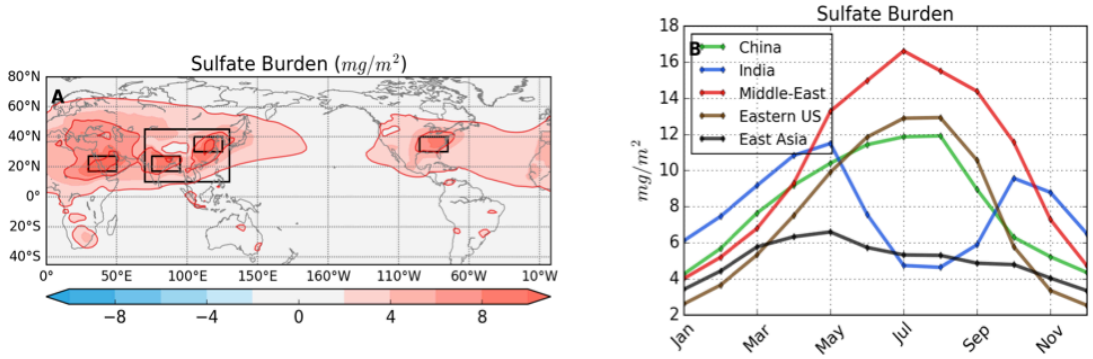

Figure 2.1 Mean increase in sulfate aerosol concentration and its seasonality. (a) Ensemble mean 4-year mean increase in column-integrated sulfate aerosol amount between '2000S' and '1850S' fully-coupled runs. (b) Ensemble mean monthly mean increase in column-integrated sulfate aerosol amount for regions highlighted in (a).

As mentioned earlier, the total climate response is a combination of the fast atmospheric adjustments and the slow ocean mediated feedbacks. Prescribing SSTs (or fixing the SST) brings out the fast response when compared to the use of slab or full ocean model. Later options, on the other hand, contain SST mediated effects. The temporal dependence of the response can be further studied by conducting perturbed simulations that are longer versus generating an ensemble of shorter (up to two to four years) perturbed simulations. The long-term climate response would be a result of long-term SST mediated feedbacks and is desirable for understanding multi-decadal to century timescales climate change. On the other hand, the short-term response would bring out seasonal-interannual timescales SST feedbacks that are relevant for short-term predictability. These two approaches are illustrated schematically in Figure 2.2 and their response is formally referred to as "long-term" (or equilibrium) and "short-term" (or transient) climate response. The suffixes "long" and "short" will be used to differentiate between these two approaches. The following paragraphs describe experiments conducted along with their goals and details like integration length, ensemble size, initial conditions, spin up time and naming convention etc.

Long-term fully coupled experiment consists of two 75-year long simulations: (a) a preindustrial control simulation denoted by '1850S', (b) a perturbed simulation with present day concentration of sulfate aerosols denoted by '2000S_long'. Both of these are initialized from the preindustrial spin up from NCAR's repository. The first twenty years of the simulations are neglected to allow '2000S_long' to reach a new equilibrium state. The mean difference between the two 55-year long simulations is the long-term climate

response to sulfate aerosol forcing. *Short-term fully coupled* experiment consists of a set of ensembles of four-year long simulations: (a) a control ensemble of size 108 with each member being four-year long is generated from a single 111-year long preindustrial control simulation and is again denoted by '1850S', (b) an ensemble (size=108) of four-year long perturbed simulations with each member initialized from 108 Januaries in '1850S' and denoted by '2000S_short'. This approach is extremely useful in constraining the variability coming from the deeper ocean esp. over the tropical Pacific Ocean thus enhancing signal to noise ratio. As the name suggests, the experiment determines the seasonal-interannual timescale transient response of the climate system.

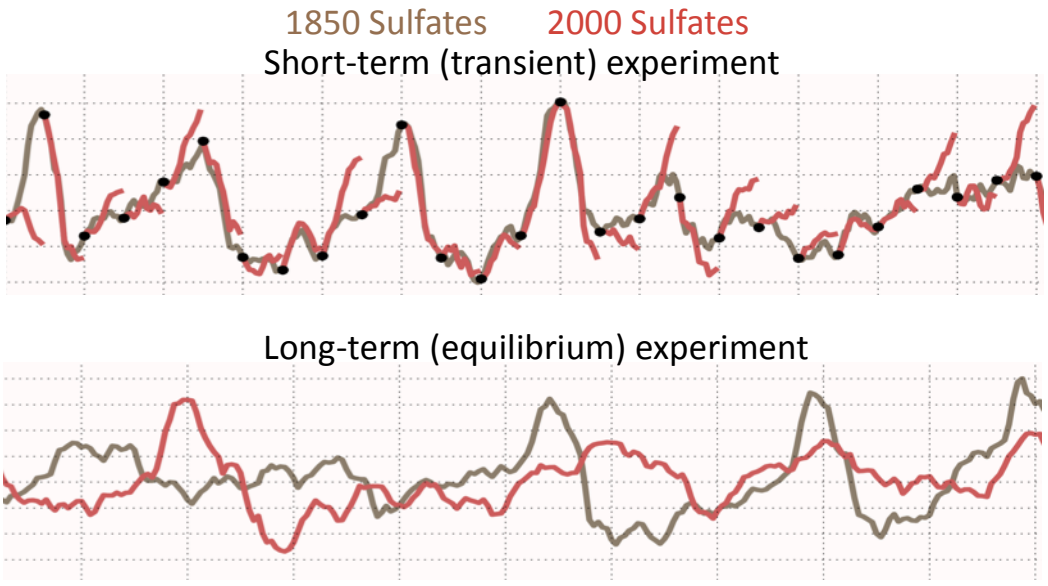

Figure 2.2 Schematic differences between short- and long-term experiments. Brown curve represents trajectory of preindustrial control simulation. Red curve represents perturbed trajectory on increasing sulfate aerosols from preindustrial to present-day level.

Long-term partially coupled experiment, like the fully coupled case, has two long simulations but with POP2 being replaced by SOM. The control simulation is 80-year long and is initialized from the same spin up initial condition used in the fully coupled cases. It is denoted by '1850S_som'. The first 20 years were discarded to allow it to reach the new partially coupled equilibrium. The perturbed simulation denoted by '2000S_som_long' is started from the 21st year of '1850S_som' and integrated forward for 60 years. The last 50 years of the two simulations are used to determine the equilibrium response. Replacing the full ocean GCM with the slab ocean results in the coupled response without the contribution from ocean dynamics. *Short-term partially coupled* experiment is analogous to the fully coupled case except for SOM being the ocean component and each member is only two-year long instead of four. The two ensembles (size=50) are denoted by '1850S_som' and '2000S_som_short'. Comparing its response with that of short-term fully coupled experiment can bring out the short-term effects of ocean dynamics.

Table 2.1 Summary of model integrations using CESM 1.1.2
(**1850S** refers to pre-industrial sulfate level; **2000S** refers to present day sulfate level)

Index	Model Runs	Duration (years)	Ensemble Size	Spin-up (years)	Initial Conditions
Fully Coupled (CAM5-POP)					
1	1850S (CONTROL1)	111	1	0	Pre-industrial spin-up (from NCAR repository)
2	2000S_long (long-term)	75	1	20	do.
3	2000S_short (transient)	4	108	0	Each January from CONTROL1
Partially Coupled (CAM5-SOM)					
4	1850S_som (CONTROL2)	80	1	20	Same as in CONTROL1
5	2000S_som_long (long-term)	50	1	10	Spin-up from CONTROL2
6	2000S_som_short (transient)	2	50	0	Each January from CONTROL2
Fully Coupled (CAM5-POP)					
7	2X_2000S_short	4	20	0	Januaries from CONTROL1
Uncoupled (CAM5)					
8	1850S_sst CONTROL3	30	1	0	Pre-industrial spin-up from NCAR repository
9	2000S_sst_short	1	30	0	Januaries from CONTROL3

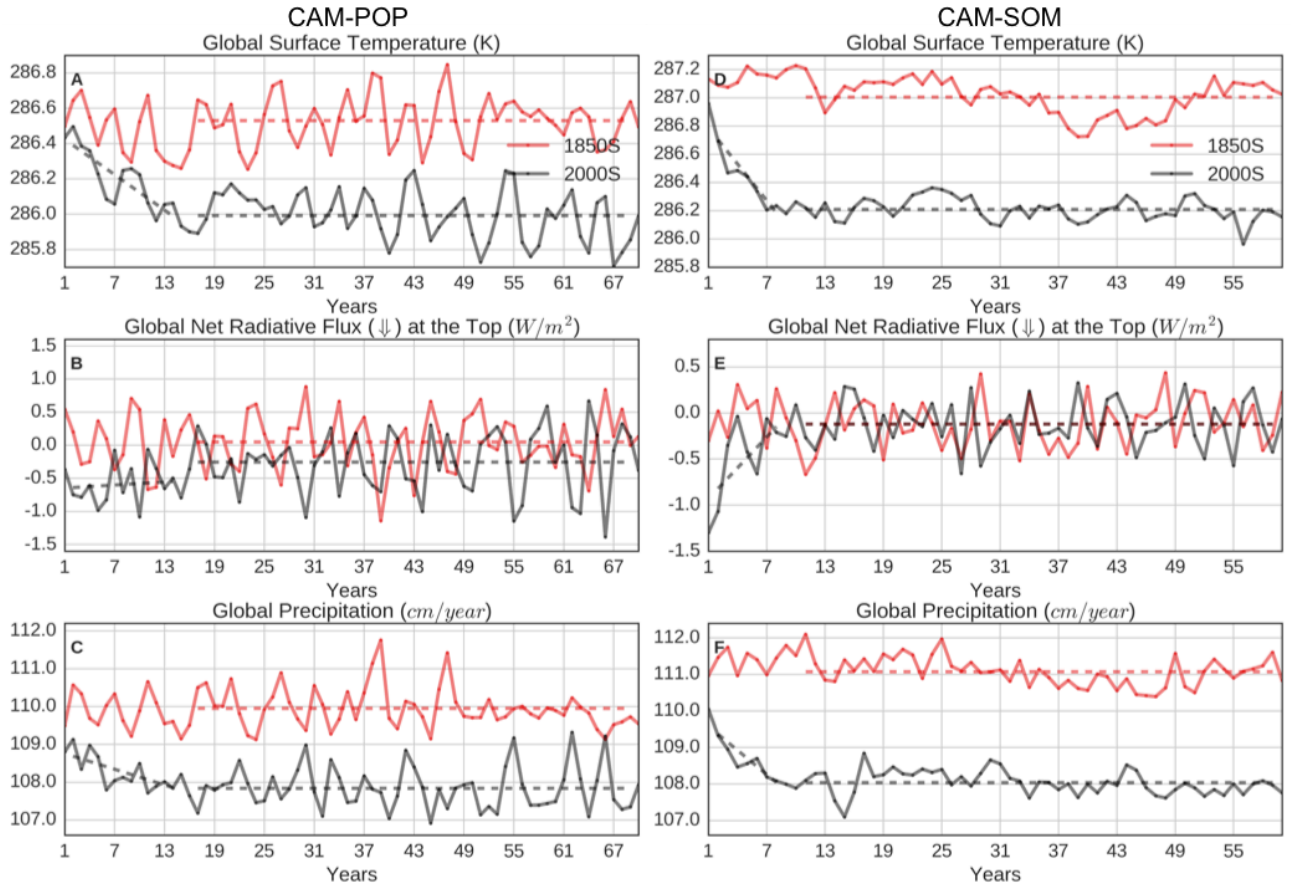

Figure 2.3 Global mean annual mean trajectories of long-term control and perturbed runs for (a,b,c) fully- and (d,e,f) partially-coupled cases. Brown curve represents trajectory of preindustrial control simulation. Red curve represents perturbed trajectory on increasing sulfate aerosols from preindustrial to present-day level.

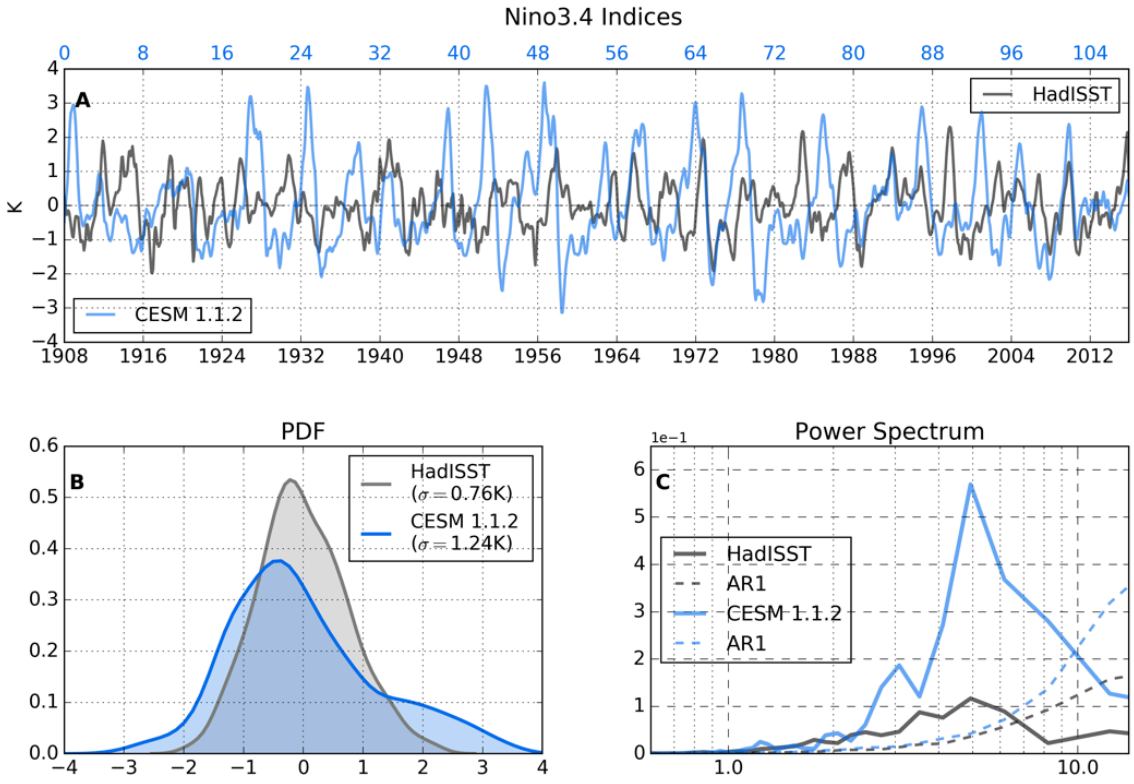

Figure 2.4 ENSO temporal characteristics (Niño 3.4) in 20th century observed SST data (grey; HadISST) and preindustrial fully-coupled integration (blue; 1850S). (a) 110-year long time series of Niño3.4 indices. (b) Corresponding kernel density estimation of probability density function, and (c) corresponding power spectra (in solid lines). The dashed lines in (c) are spectra of AR1 time series generated using autocorrelation estimate of original time series.

Long-term and short-term uncoupled experiments are fixed SST experiments. The 30-year climatology of sea surface temperature from '1850S' is used to generate all the control and the perturbed integrations. The uncoupled experiments are ideal for determining the fast atmospheric response to sulfate aerosols. An additional experiment known as *double perturbation short-term fully coupled* experiment is conducted to test the nonlinearity of the tropical Pacific climate response. In this experiment the perturbation is doubled and the ensemble size is considerably reduced from 108 to 20. Details of the various integrations are summarized in table 2.1. The time series of annual mean global mean radiative imbalance and corresponding surface temperature and precipitation for long-term fully and partially coupled experiment is shown in Figure 2.3.

2.4 MODEL VALIDATION

In this section, we briefly review the model performance with respect to two different modes of tropical Pacific climate variability, namely ENSO (or zonal mode) and the Pacific meridional mode. The characteristics of these modes are compared to those obtained from standard reanalysis datasets including Hadley Center Sea Ice and Sea Surface Temperature (HadISST), Extended Reconstructed Sea Surface Temperature (ERSST v4), and NCEP/NCAR Reanalysis data. In addition to the variability, the characteristics of the simulated mean tropical atmospheric cells over tropical Indian and Pacific Oceans are compared against the observations. Finally, the magnitude and spatial pattern of the simulated sulfate radiative forcing is compared against previous literature.

2.4.1 Temporal characteristics of ENSO

Figure 2.4a compares ~100-years long time series of Niño3.4 indices calculated from preindustrial control run, '1850S', and the HadISST data. Since, they do not span

the same time period, an individual event is not comparable and it is more pertinent to compare the overall characteristics of the two time series. The model seems to produce stronger El Niño with higher regularity than observed during the 20th century. The corresponding probability density functions (PDF) are plotted in Figure 2.4b and further highlight a larger El Niño-La Niña asymmetry (with respect to magnitude) in the model. The significantly longer tails in the model than the observation implies more extremes (El Niño and La Niña) and relatively lesser normal years in the model world. Figure 2.4c compares the power spectra of the two time series. Both shows periodicity of roughly 4 years but the power in the interannual band is much stronger in the model than the observation (look at Capotondi et al. 2015a for ENSO representation in CMIP5 models).

2.4.2 Pacific Meridional Mode

The meridional mode is prevalent in both Atlantic and Pacific basin and is characterized by cross-equatorial winds across the meridional SST gradient that primarily fluctuates on the decadal timescale. This decadal scale variability is known to contribute variability (Chiang et al. 2004; Chang et al. 2007) to ENSO in the Pacific basin. Recent studies also suggests meridional modes role in creating the diversity in the spatial pattern of ENSO, e.g. the central versus east Pacific Niño (Lorenzo et al. 2010; Yu et al. 2010; Capotondi et al. 2015B; Johnson et al. 2013). Figure 2.5a,b,c compares the spatial pattern of the meridional mode between observations (ERSST v4 & NCEP/NCAR Reanalysis) and the model. Associated seasonal variance of co-varying SST and surface winds time series are also plotted (Figure 2.5d,e,f). The model tends to overestimate equatorial zonal winds and the associated zonal SST gradient. The overestimation is considerably reduced in present day perturbed simulation,

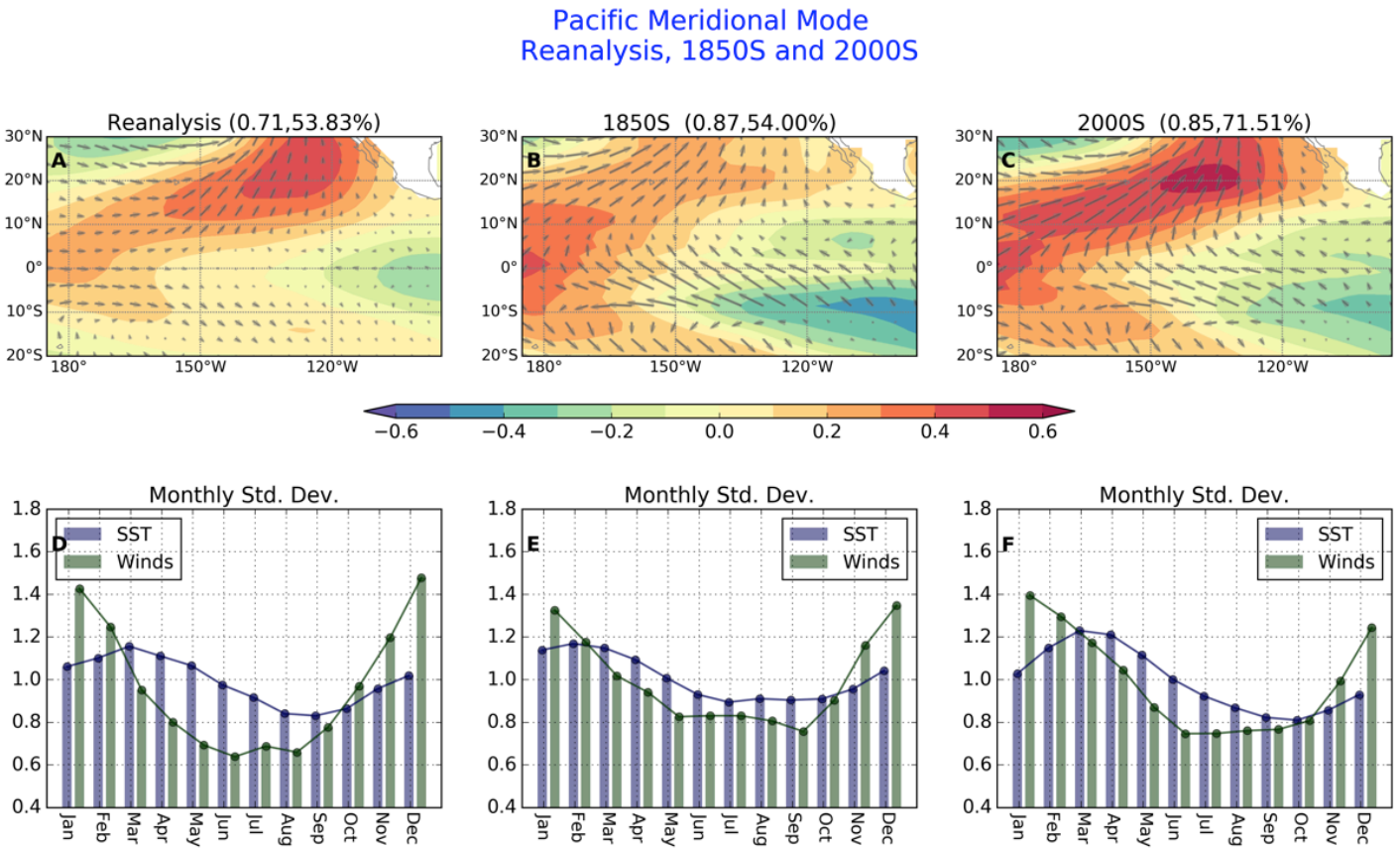

Figure 2.5 Pacific Meridional Mode (PMM; spatial pattern and associated seasonal variance) in observations, preindustrial fully-coupled (1850S), and present-day perturbed (2000S_long) integrations. Spatial pattern of PMM in (a) observed SST (from ERSST v4) and windstress (from NCEP/NCAR Reanalysis) during 1950-2015, (b) 60-years of preindustrial control simulation, and (c) 60-years of present-day perturbed simulation. The annual cycle of interannual variance in covarying SST and windstress principal components (PCs) are plotted in (d, e and f). The decomposition of monthly mean fields into PMM along with their PCs is based on maximum covariance analysis described in Chiang et al. 2004.

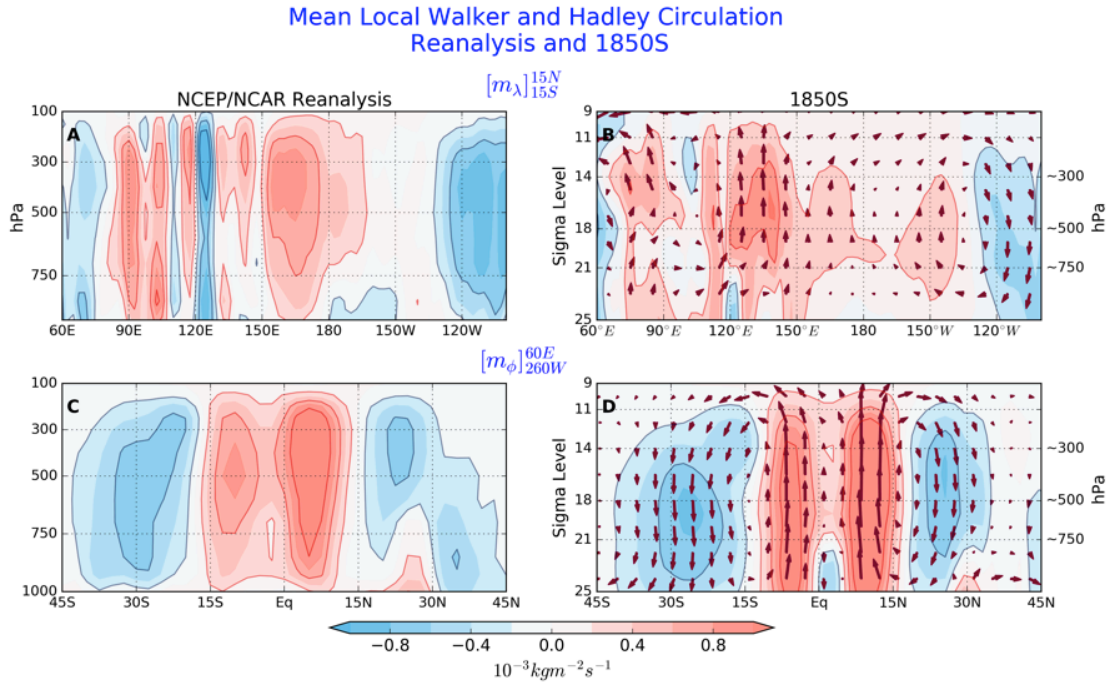

Figure 2.6 Mean local Walker and Hadley Circulation in observations (NCEP/NCAR Reanalysis), and preindustrial fully-coupled integration (1850S). Local Walker cell averaged between 15S-15N over tropical Indian and Pacific Ocean sector (a) in observations for 1950-2015 period, (b) 60 years of preindustrial control simulation. Local Hadley cell zonally averaged over Indian and Pacific Ocean sector (c) in observations for 1950-2015 period, (d) 60 years of preindustrial control simulation. The vectors in (b, d) represent corresponding winds (drawn not to scale). Also, note the different vertical coordinates between observations and simulation. The local partitioning into orthogonal cells is based on Schwendike et al. 2014.

'2000S_long' along with improvements in the spatial pattern and seasonal variance of the meridional mode. These preliminary results along with their implications will be further discussed in Chapter 4.

2.4.3 Hadley and Walker Cell

As mentioned previously, the tropical atmospheric cells and associated rainfall are affected by anthropogenic aerosols. Here, we briefly compare the spatial structure and the magnitudes of theses circulations between the model and the observation (Figure 2.6). Vertical mass flux is locally partitioned into two orthogonal directions based on Schwendike et al. 2014 and then averaged over latitudinal or longitudinal bands to calculate the local Walker and local Hadley circulation. The overall structure of the simulated cells is comparable to the one obtained from reanalysis data. But there are significant regional differences. For example, ascending branch of the simulated Walker circulation is displaced eastward with respect to the reanalysis. The associated subsidence to the east is also weaker in the model. The simulated Hadley cells have stronger ascent and descent and are displaced north with respect to the observations. Note the difference in the vertical coordinates between model and observations.

2.4.4 Sulfate Radiative Forcing

Total sulfate aerosol radiative forcing is calculated from the fixed SST experiment. It is the first-year mean radiative imbalance at the top (of the model) created after sulfate aerosols are raised from their preindustrial level to the present day level and is shown in Figure 2.7. It results from fast atmospheric adjustments that include direct and indirect effects as well as fast (without SST feedback) changes in clouds and atmospheric

circulation. The negative value over a region implies reduction in the energy available to heat both the atmospheric column and the underlying earth's surface, e.g. North Pacific Ocean. The tropical Indian Ocean, on the other hand, experiences positive radiative forcing, perhaps a result of indirect changes in the monsoonal circulation. The global mean estimate of the radiative forcing is 1.08 (±0.17) W/m^2 and is consistent with many previous studies' estimate e.g. (IPCC 2013; Ghan 2013; Deandreis et al. 2012; Boucher 2015).

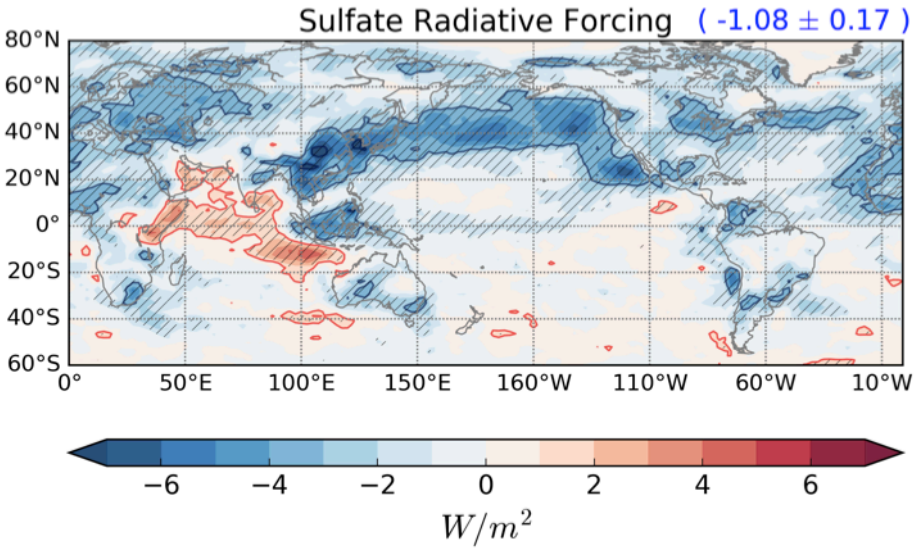

Figure 2.7 Total sulfate aerosol radiative forcing. Calculated as ensemble mean first-year mean difference in net radiative imbalance (at top of the model) between uncoupled preindustrial control ('1850S_sst') and uncoupled present day perturbed ('2000S_sst_short') integrations.

2.5 CONCLUSIONS

• *CAM5 has significantly advanced in parameterizing aerosol-cloud interaction.*

• *Poor understanding of aerosols' effect on mixed and ice phase clouds.*

• *Role of ocean-atmosphere interactions in climatic impacts of aerosols not well studied.*

The fundamental aerosol-radiative and aerosol-cloud interactions that eventually determine the climate response takes place at extremely small and fast-time scales relative to typical climate model spatiotemporal resolution. These processes, therefore, cannot be explicitly resolved in current generation climate models and need to be parameterized. There are numerous known and unknown processes and feedbacks associated with aerosol-radiative and aerosol-cloud interactions that need to be accounted for in order to get accurate results. It has proven to be a challenge to represent all these effects in climate models. Large error bars in aerosol radiative forcing is for example a reminder of uncertainty in emissions- natural or anthropogenic, aerosol-radiation, and aerosol-cloud interactions. This uncertainty eventually translates into erroneous climate response and causing inter-model spread in predicting the response.

In last two decades, there are significant advances in both theoretical understanding as well as in modeling of aerosols' effect on climate. One such advancement has come in aerosols' interaction with (shallow) warm clouds. The CAM5 physics is much more physically realistic than its predecessor in representing warm cloud-aerosol interactions. Whereas, the treatment of aerosols' interaction with mixed

phase and ice clouds is still minimal in the model along with poor theoretical understanding and will need to be improved in future generation climate models.

On climatic timescales, the role of ocean-atmosphere feedbacks in determining climate response to aerosols becomes important. While large-scale ocean-atmosphere interaction and coupled climate modes are extensively studied, their role in climate response to aerosols perturbation is hardly explored and needs to be studied.

CHAPTER III

TRANSIENT OCEAN DYNAMICAL RESPONSE

3.1 INTRODUCTION

Anthropogenic increase in sulfates since pre-industrial period has resulted in widespread cooling of Northern Hemisphere (NH) where most emission sources are located. This hemispheric asymmetry leads to changes in meridional energy transports that shift Inter-Tropical Convergence Zone (ITCZ) southward and affect zonal mean tropical atmospheric circulation (Williams et al. 2001; Hwang et al. 2013; Chiang et al. 2012; Schneider et al. 2014). These long-term or equilibrium climate responses are observed in nature and are to an extent simulated by climate models. However, on shorter time and regional scales, the response remains poorly understood. Specifically, the effect of aerosols on Walker cell, and ENSO over the tropical Pacific, is not well understood. We address this limitation by carefully examining the potential interactions between the radiative effects of sulfate aerosols (or sulfates; IPCC 2013 and references therein; Ocko et al. 2014; Boucher 2015) and the dynamical processes that drive ENSO (Neelin et al. 1998; Wang and Picaut 2004; Dijkstra 2006).

The proximity of tropical Pacific to East Asia, a major source region of industrial sulfates, makes it susceptible to variations in aerosol emissions and, therefore, an important problem to study. This study differs from earlier studies, of long-term climate response to aerosols, in being focused entirely on the tropical Pacific region. We ask the fundamental question: How does the tropical Pacific climate system respond on seasonal-to-interannual timescales to an abrupt increase in tropospheric sulfate aerosols?

Improving our understanding of aerosols affect ENSO will not only assist in the attribution of past climates, but could potentially enhance externally-forced predictability on these timescales. The possible interference between the radiative effects of tropospheric sulfate aerosols and those from volcanic sulfates makes this study relevant to decadal scale climate response after a volcanic eruption (Pohlmann et al. 2013; Maher et al. 2015; Timmreck et al. 2016).

Considering a notable zonal asymmetry in the tropical Pacific mean state (warm pool and cold tongue) and variability (seasonal cycle, El Niño and La Niña), it would be appropriate to ask, if a zonally asymmetric aerosol perturbation (high sulfates concentrations over east Asia) project on zonally asymmetric mode of climate variability or the zonally asymmetric tropical Pacific mean state? Rest of the chapter is organized as follows, section 3.2 explains model and experimental details followed by analysis and results in section 3.3. Finally, section 3.4 summarizes the results and discusses their implications.

3.2 METHOD AND MODEL DETAILS

We used the NCAR Community Earth System Model (CESM) with either full ocean or a slab ocean model in this study. To test the sensitivity of the tropical Pacific climate, sulfates and its precursor gases emissions are increased abruptly from preindustrial to present day level (based on Lamarque et. al. 2010 emission inventory) and a difference in ensemble mean climate simulated by CESM for the two cases is examined.

To characterize the control climate, a 110-year long fully-coupled control simulation with preindustrial settings, denoted '1850S', was carried out. An ensemble of four year long perturbed simulations, denoted '2000S', was created by starting integrations every January from the control simulation with modified sulfate emissions (both natural and anthropogenic sources). This approach is an effective way to study the transient tropical Pacific adjustment to the sulfate aerosol forcing. Limiting the simulations to a four year period restricts adjustment to the upper ocean, and thus limits the influence of any deep oceanic drifts in the climate model. In other words, it improves signal (response) to noise (internal variability) ratio.

Another set of control and shorter perturbed integrations, worth 50 years, were carried out which differs from previous set only in the use of Slab Ocean Model (SOM) in place of full ocean general circulation model (POP2). These are respectively called '1850S_som' and '2000S_som' and corrects for Q-Flux calculated from 40 years of '1850S' control run. Use of SOM removes dynamical ocean feedbacks, and thus ENSO, from the coupled climate model and thus provides an opportunity to further explore sulfates and ENSO interaction. We refer to these two experiments as fully- versus partially-coupled experiments in later sections.

Specifically, we used CESM version 1.1.2 (all components active) with ~2 degree finite volume grid for atmospheric component (CAM5) and ~1 degree displaced pole grid for oceanic component (POP2). These components had 30 and 60 levels in the vertical, respectively. Standard parameterizations for CAM5 which include moist turbulence scheme (Bretherton and Park 2009), Deep Convection (Neale et al. 2008),

Shallow Convection (Park and Bretherton 2009), a double moment stratiform microphysics (Morrison and Gettelman 2008) etc. were used. These choices are described using the run labels 'B_1850_CAM5_CN' and '1.9x2.5_gx1v6', corresponding to a standard configuration of the CESM.

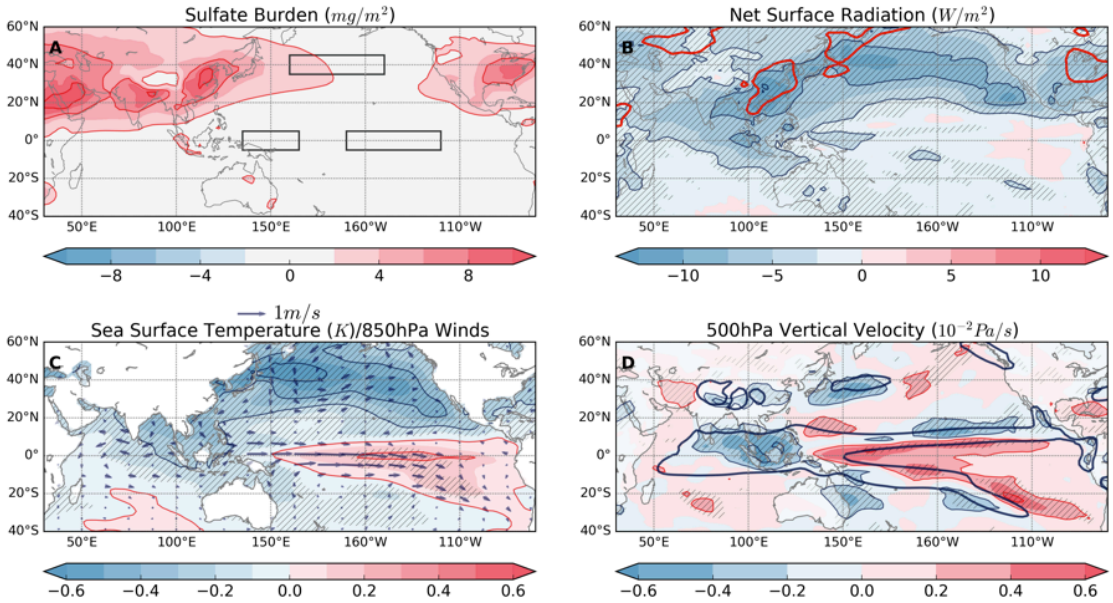

Figure 3.1 Ensemble mean first 2-year mean differences between '2000S' and '1850S' runs. (a) Increase in column-integrated sulfate aerosol amount, (b) change in net surface radiation (positive into the surface; colors), (c) change in sea surface temperature (colors) and 850hPa winds (vectors), and (d) change in 500hPa vertical velocity (colors). Red contours (-1.5 W/m^2) in (b) highlight regions with maximum decrease in net surface radiation under clear sky conditions. Blue contours (0.02 Pa/s) in (d) highlight regions with maximum 500hPa vertical velocity in '1850S'. Stippling indicate regions exceeding 90% statistical significance according to standard t-test.

In the following section, most of the results presented are from the fully-coupled experiment (2000S-1850S). The partially coupled experiments with SOM (2000S_som-

1850S_som) will be used used to highlight the improtance of dynamical ocean-atmosphere coupling.

3.3 RESULTS

An increase in atmospheric aerosols reduces the amount of energy available to heat Earth's surface through scattering of solar radiation and modification of clouds. Figure 3.1 shows the initial two-year mean response to sulfate aerosols in the fully-coupled experiment. The mean increase in the column-integrated sulfate aerosols during the first two years is shown in Figure 3.1a with high concentrations in the vicinity of emission sources like east and southeast Asia. The notable increase in aerosols over the northern hemisphere is due to larger anthropogenic emissions in the northern hemisphere and atmospheric circulation that is primarily zonal on timescales relevant to the aerosols. As a result, the corresponding net radiative imbalance at the surface (Figure 3.1b) also exhibits hemispheric asymmetry. A greater reduction over the north Pacific Ocean, further away from the aerosol maxima, is indicative of increase in cloud amount (in parts from aerosol-cloud interaction). The direct effect, however, is largely confined to regions closer to the emission sources as evident from the red contours (Figure 3.1b) that demarcate regions of negative radiation anomaly under clear sky conditions.

There is a widespread cooling over the northern hemisphere oceans (Figure 3.1c) similar to the pattern of reduced radiation (Figure 3.1b). Over the northern Pacific, the decrease in SST is accompanied with cyclonic lower level wind response (vectors in Figure 3.1c) suggesting weakening of the subtropical high. Surprisingly, tropical eastern Pacific Ocean exhibits warming along the equatorial channel, which then extends

southeast to 20°S. This warming is accompanied with (south) westerly wind response over the tropics and could be related to changes in equatorial ocean dynamics or turbulent heat fluxes i.e., dynamic versus thermodynamic coupled response. The focus of this study is to bring out the role of equatorial ocean dynamics in aforementioned response and its relation to zonally asymmetric atmospheric circulation.

The response of mid-tropospheric vertical velocity (proportional to the precipitation) in the fully-coupled experiment (Figure 3.1d) shows significant decrease over the maritime continent and increase over relatively dry areas above eastern Pacific cold tongue. This zonally asymmetric response over the tropical Pacific is consistent with underlying zonal asymmetry in the SST response (Figure 3.1c). Additionally, the band of negative (along 10°N) and positive (along the equator) anomalies over eastern tropical Pacific Ocean could be interpreted as a regional outcome of a southward shift of the ITCZ. In addition to the well studied southward shift of the ITCZ, sulfate aerosols also alter the zonally asymmetric circulation over the tropics (commonly referred to as the Walker Cell).

Despite similarities in the large-scale response simulated in the partially- and the fully-coupled cases, there are significant regional differences (compare Fig. 3.1 & Fig. 3.2). The most relevant of them are changes in tropical vertical motion and tropical eastern Pacific warming. There is a stronger ITCZ shift, but a weaker Walker cell response in the partially-coupled experiment where ocean dynamical feedbacks are omitted. The representation of ocean dynamics in the fully-coupled experiment allows warming of the equatorial channel over the eastern Pacific compared to exclusive off-

equatorial warming in the partially-coupled case. Henceforth, we focus on understanding this equatorial response to sulfate aerosol forcing and defer off-equatorial response to another study.

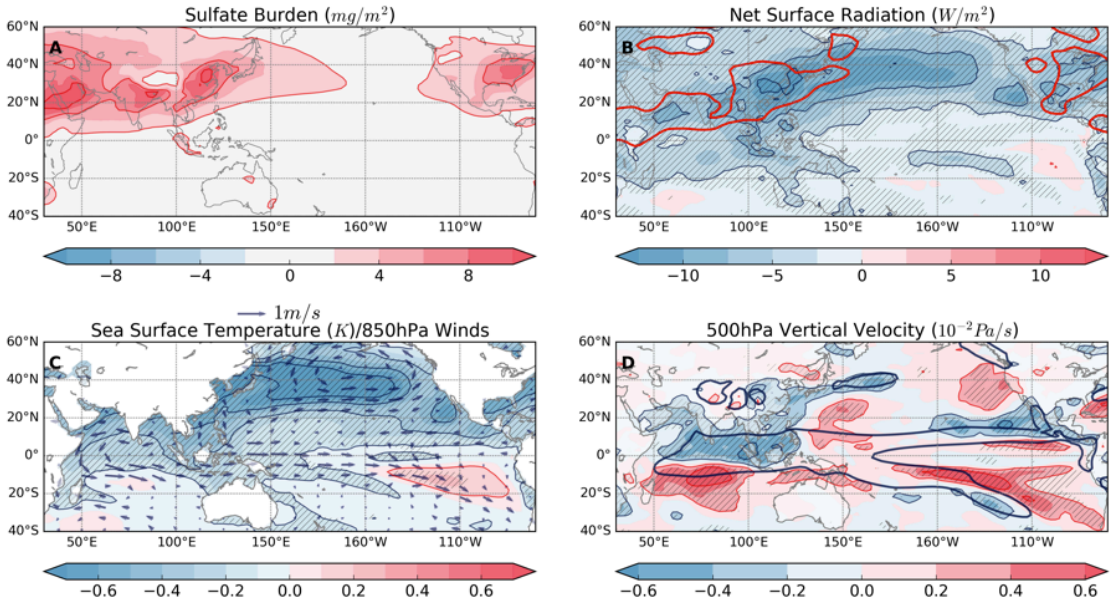

Figure 3.2 Ensemble mean 2-year mean differences between '2000S_som' and '1850S_som' runs. Same as in Figure 3.1 but for partially-coupled experiment.

Figure 3.3 compares two-year long spatiotemporal evolution (averaged between 5°S to 5°N) of zonal wind stress, SST and upper ocean heat content responses between the two experiments. In the fully-coupled case, the eastern Pacific warming undergoes seasonal modulation with maximum warming during the winter months (Figure 3.3c). The warming is not limited to the sea surface alone but extends to the subsurface (shown in Figure 3.4a) resulting in a similar pattern of upper ocean heat content response (Figure 3.3e).

These warm anomalies over the equator are preceded by westerly wind stress response (Figure 3.3a). There is a co-located wind stress and SST maxima during winter

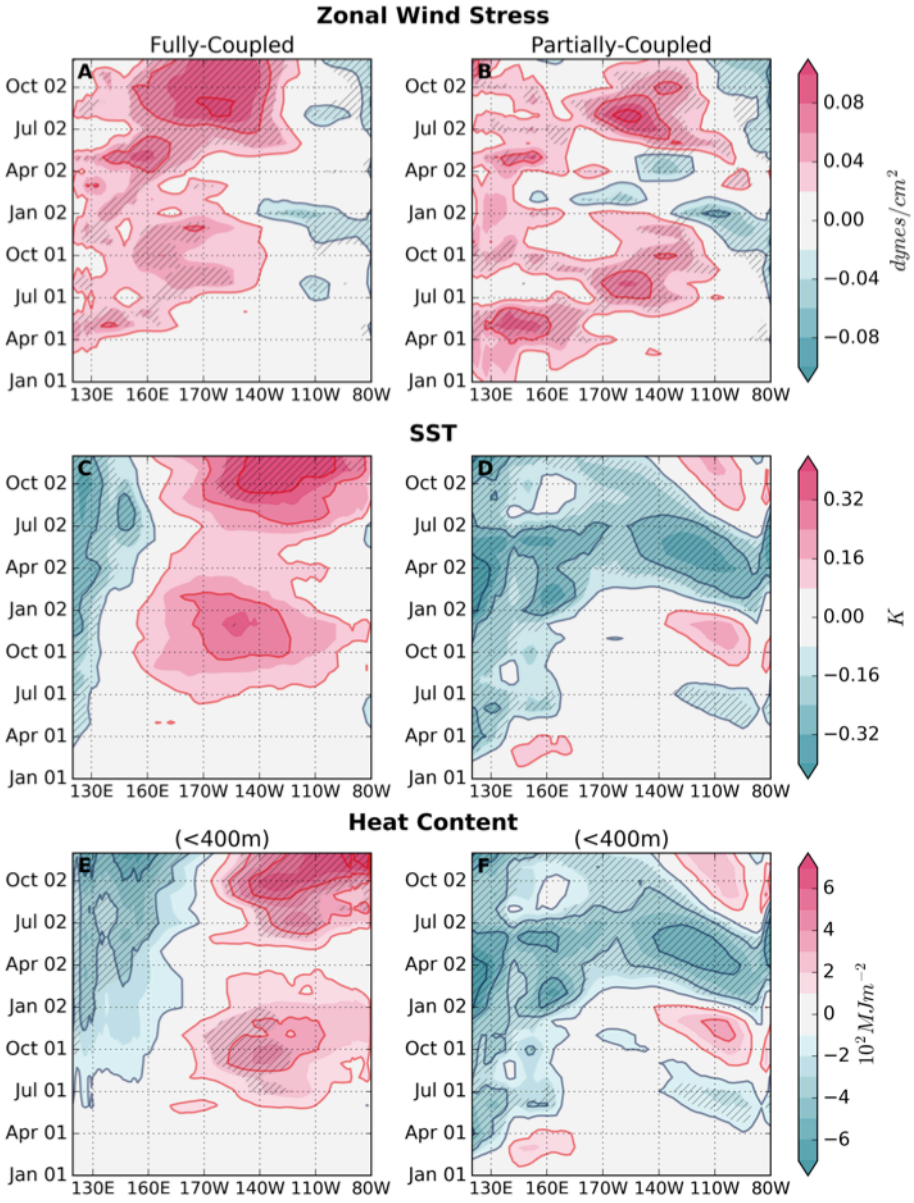

Figure 3.3 Ensemble mean monthly mean differences between (a,c,e) '2000S' and '1850S' runs, and (b,d,f) '2000S_som' and '1850S_som' runs over equatorial Pacific (5S-5N). Initial two-year evolution of (a) zonal wind stress, (b) sea surface temperature, and (c) Upper ocean heat content (up to 400m depths) responses in the fully-coupled experiment. Two-year evolution of (d) zonal wind stress, and (e) sea surface temperature responses in the partially-coupled experiment. Stippling indicate regions exceeding 90% statistical significance according to standard t-test.

months in the central Pacific. Another maxima in westerly wind stress is seen over the west Pacific during early summer months. These wind stress maxima are also observed in partially-coupled response, however, the slab ocean doesn't warm along the equator in response to increased sulfates. Similar pattern of wind stress response is observed in the two experiments (Figure 3.3a and 3.3b) but a greater amplitude during the second year in the fully-coupled case suggests a positive ocean-atmosphere feedback. The dependence of equatorial Pacific warming on the presence of ocean-atmosphere coupling along with the presence of westerly wind stress response points towards dynamical changes in upper ocean due to sulfate aerosols.

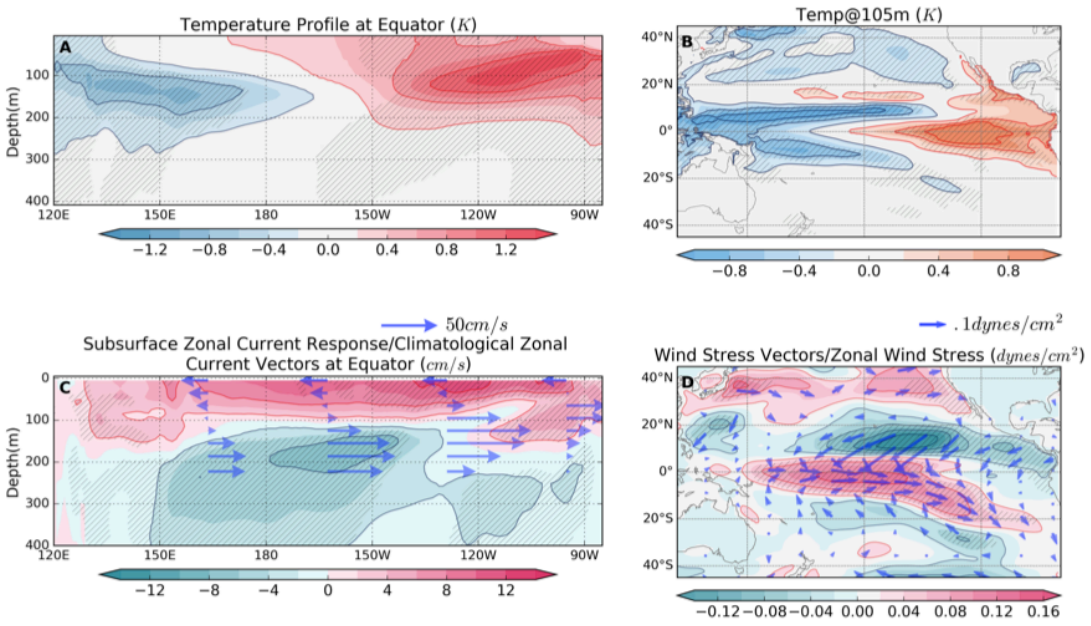

Figure 3.4 Ensemble mean second year October-December mean differences between '2000S' and '1850S' runs. (a) Equatorial cross-section (5S-5N) of temperature response, and (c) zonal current response (colors) along with vectors of climatological zonal currents based on '1850S' run. (b) Temperature response at 105m depth below the surface. (d) Zonal wind stress (colors) and wind stress vector responses. Stippling indicate regions exceeding 90% statistical significance according to standard t-test.

A cross section of temperature response across the Pacific Ocean (averaged between 5°S and 5°N) during October-December of the second year is shown in Figure 3.4a. This period corresponds to the maximum warming along the equatorial channel. A dipolar pattern with warm anomalies in the eastern side and cold anomalies in the western side of the basin is present with local maxima located around 100 m below the ocean surface. The pattern is characteristic of an El Niño event where a 'seesaw' like motion of thermocline results in opposite anomalies on either side of the basin. Deepening of thermocline in the east brings warm mixed layer water downwards, and its shoaling in the west transports colder water from beneath the thermocline upwards (Neelin 2010). The spatial subsurface temperature (105m) response is shown in Figure 3.4b. The off-equatorial cold anomalies to the north and the south of the equator represent thermocline shoaling, a dynamical response.

The tropical Pacific mean ocean temperature is zonally asymmetric (warm pool and cold tongue) and is maintained by upper ocean zonal circulation with westward directed surface currents and an eastward undercurrent (as shown by vectors in Figure 3.4c). The response in the equatorial Pacific zonal circulation to sulfate aerosols (shown as shading in Figure 3.4c) has a positive anomaly in the surface ocean and negative anomaly in the subsurface ocean which amounts to slow down of an existing zonal circulation, thereby causing an accumulation of heat on the eastern side of the basin. Figure 3.4d shows westerly windstress response which results in anomalous eastward surface currents shown earlier.

The westerly wind stress response over the western Pacific is a part of changes in the large-scale Walker circulation. The ascending branch of this zonal atmospheric cell which is typically located around the maritime continent (alongside western Pacific) is perturbed in response to increased sulfate aerosols. The atmospheric response to increased sulfate aerosols averaged over April-June of the second year is shown in Figure 3.5. This period corresponds to the windstress maxima over the western Pacific prior to the peak warming (Figure 3.4). Figure 3.5a shows a vertical cross section of change in zonal vertical mass flux averaged meridionally over 10°S to 10°N. The quantity represents the strength of the local Walker cell, and is calculated based on Schwendike et al. 2014.

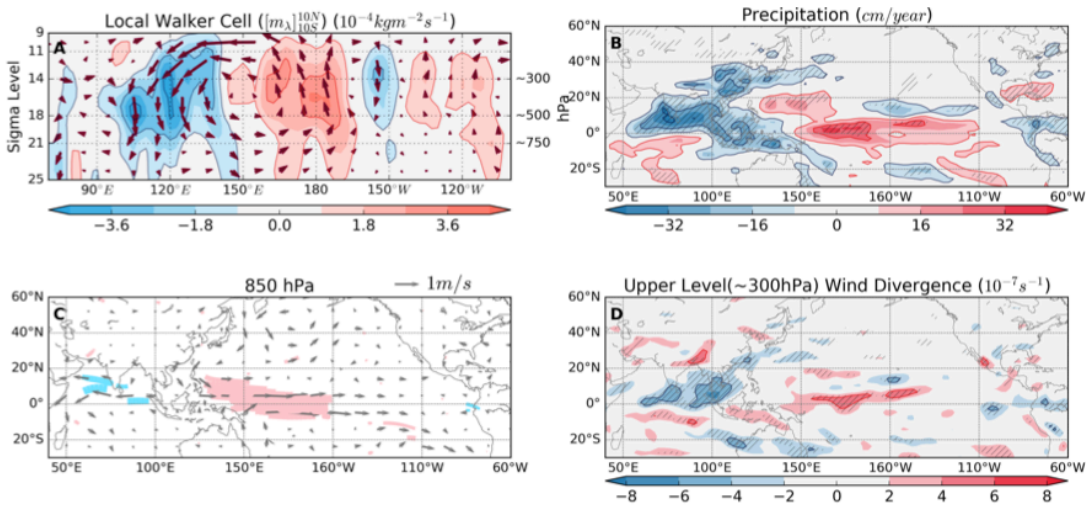

Figure 3.5 Ensemble mean second year April-June mean differences between '2000S' and '1850S' runs. (a) Local walker cell response (vertical mass flux partitioned into zonal direction) averaged over 10S to 10N (colors) along with corresponding winds response (vectors). (b) Precipitation response. (c) 850hPa wind response (vectors) with colors indicating regions of statistically significant zonal wind response (blue for easterly; red for westerly). (d) Changes in divergence at sigma level = 14 (~300hPa) between '2000S' and '1850S'. Stippling indicate regions exceeding 90% statistical significance according to standard t-test.

The anomalous circulation response shows descent over the Indian Ocean and ascent over the western Pacific. The low level westerlies over the equatorial western Pacific, which impart westerly momentum to underlying ocean, form the lower limb of this anomalous circulation.

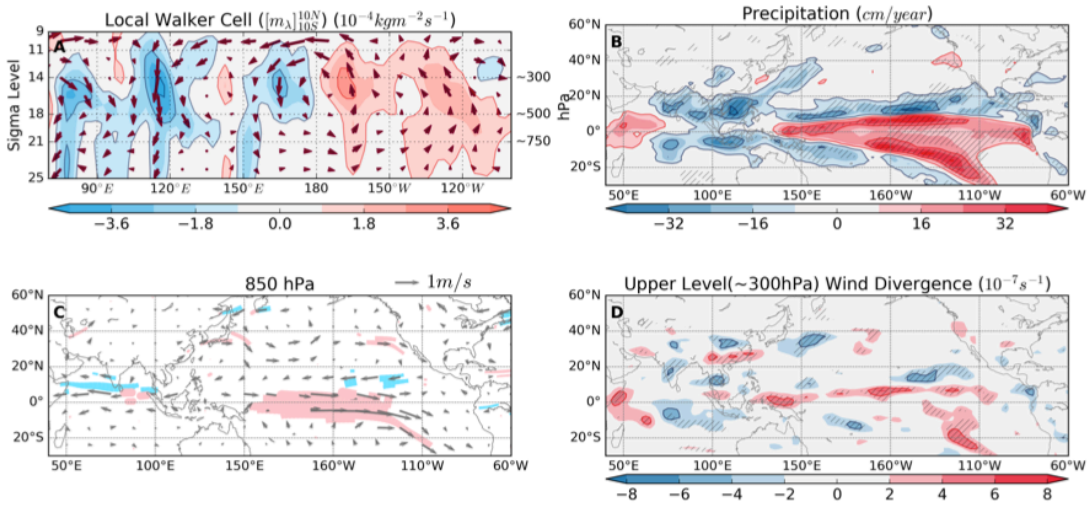

Figure 3.6 Ensemble mean second year October-December mean differences between '2000S' and '1850S' runs. Same as in Figure 3.5 except for following winter season.

Figure 3.5b, 3.5c and 3.5d are the corresponding responses in precipitation, low level (850 hPa) winds and upper level (~300 hPa) divergence. As expected, all of them point towards the existence of a large scale subsidence over east Asia as was seen in Figure 3.5a. The significant reduction in precipitation (Figure 3.5b) over east Asia is related to anomalous downward motion that diverges in lower levels with westerlies to the west and easterlies to the east of the maritime continent (Figure 3.5c). The non-zero convergence (Figure 3.5d) in the upper levels close to the equator thus explains the cyclic nature of the vertical zonal circulation response.

The Walker circulation response when the warming is greatest, i.e., October-December of the second year, is weaker and shifted eastward relative to April-June response (compare Figure 3.5a and 3.6a) which gives rise to westerly wind anomalies over the central/eastern Pacific instead of western Pacific (compare Figure 3.5c and 3.6c). The zonal asymmetry in precipitation is also reduced during winter months (Figure 3.6b) and no significant upper level equatorial convergence over the maritime continent is observed (Figure 3.6d).

Spatial maps showing vertically integrated temperature response (down to 400m depth) illustrate the growth of the equatorial warming during the first year (Figure 3.7a to 3.7d). The warm (positive) anomaly in vertically integrated temperature implies deepening of the thermocline. The anomaly first appears during May when westerly wind stress response is confined to the west, closer to the Asian continental emissions. Later, the anomaly grows and moves eastward and peaks during October. The eastward propagation of the warm anomaly and its spread along the coast brings to mind downwelling equatorial and coastal Kelvin waves. The reflection of the equatorial Kelvin wave from the eastern boundary into the downwelling off-equatorial Rossby wave can also be noticed in westward propagating warm anomaly over the northern tropics (near central American Coast) (Figure 3.7c and 3.7d). The equatorial warming, therefore, could be understood in terms of aforementioned equatorial wave dynamics.

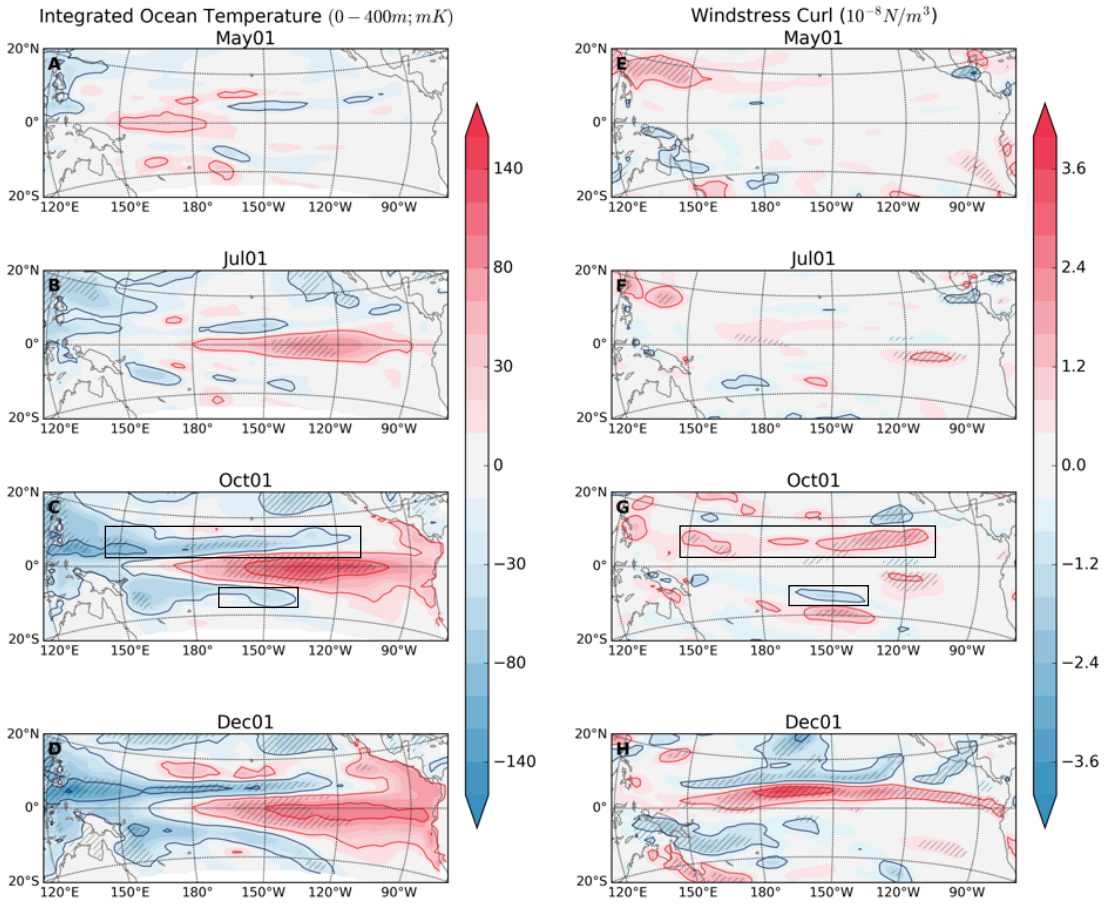

Figure 3.7 Ensemble mean monthly mean differences between '2000S' and '1850S' runs. (a-d) Vertically-integrated temperature (up to 400m depth) response for May, July, October and December of the first year, and (e-h) corresponding vertical component of curl of wind stress response. Stippling indicate regions exceeding 90% statistical significance according to standard t-test.

The off-equatorial thermocline response can be largely explained through changes in wind-driven Ekman pumping/suction. The curl of wind stress response for the corresponding months is shown on the right hand side in Figure 3.7e to 3.7h. Negative off-equatorial anomalies (refer to the black boxes in figure 3.7c) on either side of the equator are associated with shoaling of thermocline driven by positive (negative) wind

stress curl in the northern (southern) tropics. During December of the first year (Figure 3.7h), a band of positive wind stress curl, which stretches across the basin, brings colder water upwards and partially cancels the eastern Pacific warming. This wintertime increase in curl of wind stress is observed during all four years (not shown) of the simulation and could be contributing to seasonal decay of the warm anomaly.

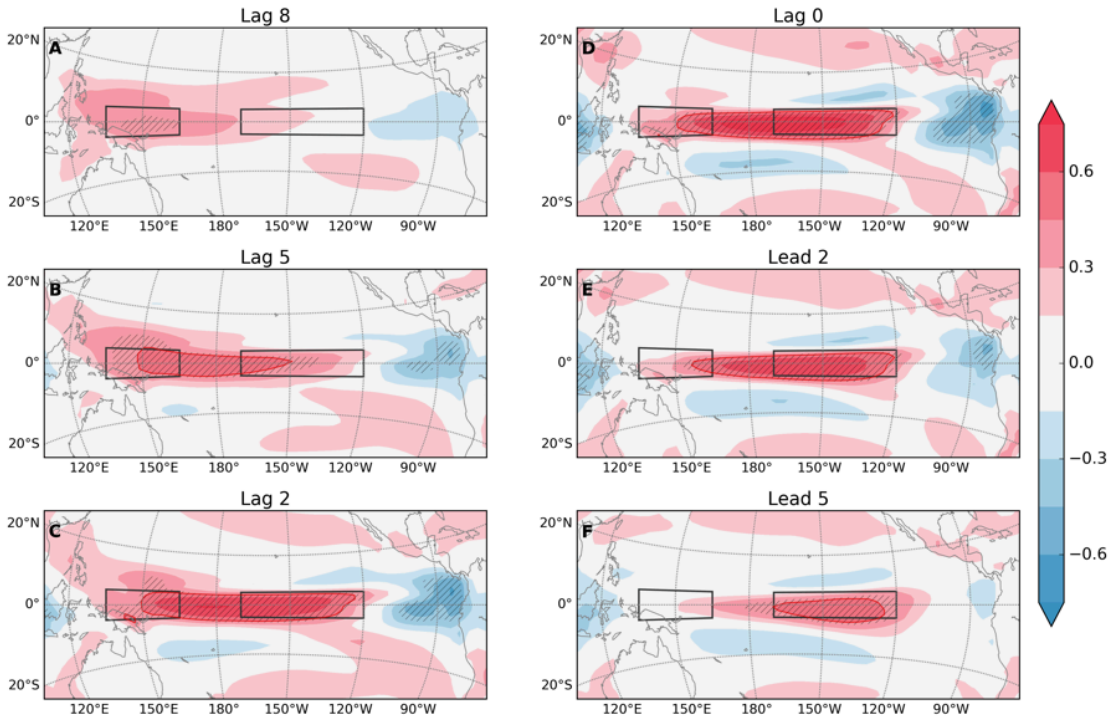

Figure 3.8 Ensemble based lead-lag cross-correlation between Niño 3.4 SST response ('2000S' – '1850S') and zonal wind stress response ('2000S' – '1850S') in a fully-coupled experiment. Change in zonal wind stress between '2000S' and '1850S' at each grid point is correlated to corresponding area averaged (170W – 120W, 5S-5N; Niño 3.4 region) SST change for SST lagging wind stress by (a) 8, (b) 5, (c) 2, and (d) 0 months, and SST leading wind stress by (e) 2, and (f) 5 months. Stippling indicates regions exceeding 90% statistical significance based on standard test using t-statistics.

Figure 3.8 shows maps of cross-correlation between Niño 3.4 SST response and zonal wind stress response for different lags and leads. The highest positive correlations

(up to 0.75) are found over the equatorial regions confirming the direct dependence of the equatorial warming on westerly wind stress response. The significant positive correlation first appears over the western Pacific about 8 months prior to the peak warming. Subsequently, the correlation grows and moves eastward along the equatorial channel. It peaks over the central Pacific when lag equals zero and then starts to decay with increasing lead times. The two maxima in wind stress response shown earlier in Figure 3.3a, one over the western Pacific, which leads and another over the central Pacific, which is in-phase with the warming. Figure 3.10a compares cross-correlation functions between Niño3.4 SST response and Niño3.4 (local) wind stress response versus Niño3.4 SST response and west Pacific (remote) wind stress response. The asymmetry around the zero lag reiterates that warming is remotely forced (at least partially) by the western Pacific westerly wind stress response. On the other hand, the symmetric curve implies local coupling between wind stress and SST responses, which might enhance their coupled response. The equatorial pacific warming is remotely forced by the springtime westerly wind stress response over the far west through changes in the equatorial thermocline.

Figure 3.9 extends the evolution of the equatorial response (from Figure 3.3a,c and e) in the fully-coupled case to another two-years. The seasonal warming is observed for another year and then replaced by the basin wide cooling in the fourth year. The associated westerly wind stress response reduces and shrinks in its extent during an anomalously cold equatorial Pacific in the fourth year. The overall time series of four-year evolution along with the twelve-month running mean over the Niño3.4 region is

shown in blue curve in Figure 3.10b. The phase reversal during the fourth-year implies the transient nature of the observed warming response.

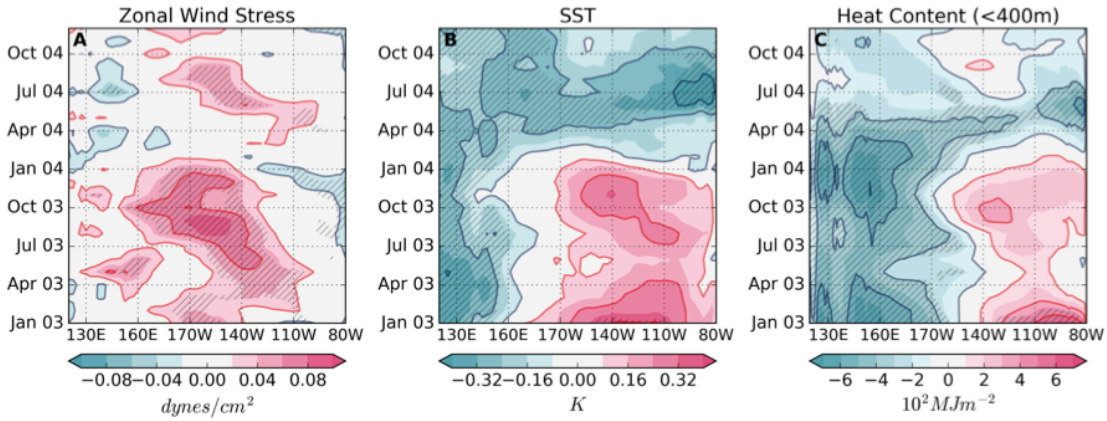

Figure 3.9 Ensemble mean monthly mean differences between '2000S' and '1850S' runs over equatorial Pacific (5S-5N). Last two-year evolution of (a) zonal wind stress, (b) sea surface temperature, and (c) Upper ocean heat content (up to 400m depths) responses in the fully-coupled experiment. Stippling indicate regions exceeding 90% statistical significance according to standard t-test.

We have demonstrated dynamical forcing of the ocean by the atmosphere circulation response, but, how do sulfate aerosols affect tropical zonal atmospheric circulation? Tropical atmospheric circulation (both zonal and meridional), referred to as 'thermally driven' circulations, has been studied for a long period of time, and significant advances in its understanding have been made in last few decades (Schneider 2006). There is a sizable evidence that SST and SST gradient play an important role in setting up of tropical circulation and its undulations (Gill 1980; Lindzen and Nigam 1987; Sobel 2007). Continuing along these lines, we suggest that the local cooling induced by increased sulfate aerosols over east Asia (specifically western Pacific SST), in conjunction with moist convection, gives rise to local circulation response.

Additionally, since the cooling is restricted to the western tropical Pacific (look at Figure 3.3b), there is a large-scale zonal asymmetry in SST (or nonzero zonal gradients of SST). The local circulation response which is predominantly zonal is, therefore, expected.

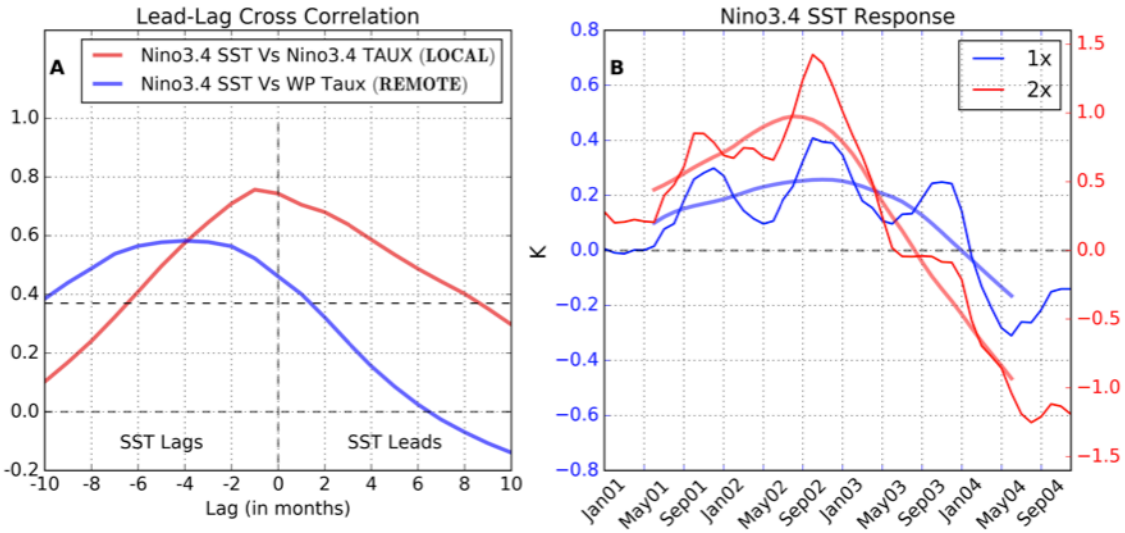

Figure 3.10 (a) **Ensemble based lead-lag cross-correlation between area averaged time series of SST and zonal wind stress responses ('2000S' – '1850S').** Red curve shows cross-correlation function between Niño3.4 SST response and Niño3.4 zonal wind stress response (Local interaction). Blue curve shows cross-correlation function between Niño3.4 SST response and tropical west Pacific zonal wind stress response (Remote forcing). These regions are highlighted in Figure 3.8. (b) **Area averaged ensemble mean monthly mean SST changes between '2000S' and '1850S' in blue, and between '2000S_2x' and '1850S' in red for fully-coupled experiments.**

3.4 CONCLUSIONS

• *Aerosols emissions from east Asia can affect the tropical Pacific climate.*

• *Significant changes in large-scale Walker circulation in response to aerosol radiative forcing.*

• *Modification of upper ocean currents over the equatorial Pacific resulting in warmer eastern tropical Pacific.*

This study addresses the transient response of the equatorial Pacific Ocean to abrupt increase in tropospheric sulfate aerosols in fully- versus partially-coupled climate model experiments. The comparison brings out the role of ocean dynamics in modulating equatorial Pacific response on seasonal to inter-annual climate timescales. We demonstrate ways in which aerosols modify the tropical atmospheric circulation that can affect ocean dynamics, and trigger a couple ocean-atmosphere response.

In addition to the southward shift of the ITCZ in response to anthropogenic sulfate forcing, the tropical circulation exhibits significant weakening of the Walker cell. The weakening is caused by aerosol-induced cooling of tropical Indian and western Pacific Ocean that results in reduced precipitation over the maritime continent and increased precipitation to the east. The resulting anomalous surface westerlies, through thermocline dynamics, warm the upper eastern equatorial Pacific Ocean. This equatorial warming in response to westerly wind stress is not simulated by the slab ocean model confirming the ocean dynamical origins of the warming. Besides the dissimilar ocean response, the thermodynamic coupling (with slab ocean) causes stronger southward shift of the tropical rain belt and weaker eastward shift (or the weakening) of the Walker cell.

Both atmospheric and oceanic responses exhibit strong seasonality. The westerly wind stress response has two maxima, one over the western Pacific during May and another over the central Pacific during October. These are related to the changes in the Walker circulation. There is a stronger atmospheric overturning response over the

maritime continent during May that weakens and shifts eastward in October. Both of the wind stress maxima are simulated, irrespective of the choice of the ocean model and play an integral part in the warming of underlying ocean in the fully-coupled case. The earlier event initiates the thermocline adjustment and warming of the upper ocean, whereas, the later event enhances the warming due to local ocean-atmosphere coupling. The warming first appears in the west during early summer, grows, and propagates eastward and peaks along with wind stress maxima over the central Pacific. This constitutes the initiation and the growth phase of the seasonal warming. It is followed by the decay caused by off-equatorial Ekman suction and poleward meridional advection along the eastern boundary.

This seasonal equatorial warming response is observed for initial three years followed by the phase reversal (cooling) in the fourth year. The phase reversal is brought about by eastward moving upwelling Kelvin wave along the equator, in accordance to ENSO's delayed oscillator paradigm. As seen in Figure 3.10b consisting of Niño3.4 SST responses, the timing of the phase reversal stays almost fixed even when the aerosol perturbation is doubled. It substantiates that barring seasonal modulation, initial growth of the warm anomaly followed by the phase reversal is driven by Bjerknes feedback and upper ocean equatorial wave dynamics. In short, the anthropogenic increase in sulfate aerosols gives rise to seasonally modulated damped oscillation of the equatorial Pacific through dynamical changes in the upper ocean.

Aerosols, natural or anthropogenic, are integral part of the climate system. Long-term changes in aerosols have caused large-scale shifts in past climates, whereas, on the

shorter timescales, the regional climate is significantly affected. In particular, increasing aerosols (or even varying aerosols) over east and southeast Asia can potentially affect the tropical Pacific climate on seasonal to inter-annual timescales, provided the perturbation is large enough. For example, the twofold increase in aerosol perturbation gives rise to around threefold increase in the tropical Pacific warming (Figure 3.10b). Unlike the previous case, the warming here reaches up to 1.5 degrees at the end of second year and rivals the background Niño state. These results are analogous to those presented by Ohba et al. 2013 in response to volcanic eruption. They showed that the rapid land cooling around the maritime continent, weakening of zonal SST gradients and associated change in Walker circulation results in El Niño, a year after tropical volcanic

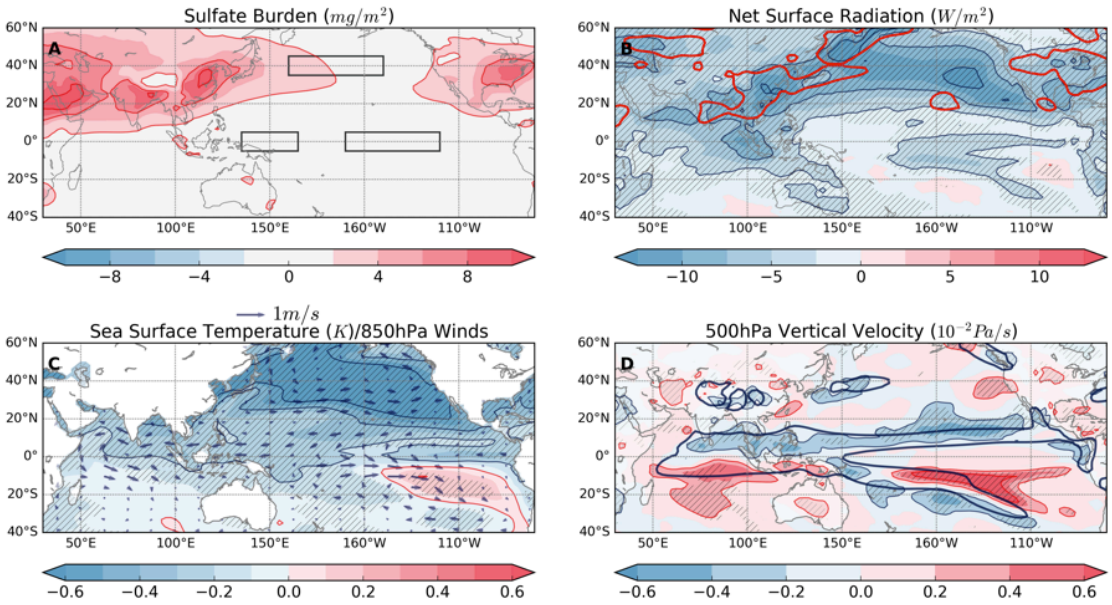

Figure 3.11 Ensemble mean fourth-year mean differences between '2000S' and '1850S' runs. Same as in Figure 3.1 but for the fourth-year mean of the fully-coupled response.

eruption. Changes in tropospheric aerosol emissions could conceivably play an important role in modulating tropical climate as well as the effect of volcanic eruption on tropical climate, and thus region's seasonal to inter-annual predictability.

CHAPTER IV

THERMODYNAMIC & DYNAMICAL COUPLED RESPONSE

4.1 INTRODUCTION

Tropical climate is strongly influenced by sea surface temperature (SST) distribution. There is greater convective activity over warmer SSTs and suppressed activity over cooler oceans (Lindzen and Nigam 1987; Sobel 2007). The rising branch of large-scale atmospheric circulation consisting of Hadley and Walker cells is anchored over the warmest tropical waters and modulates with both SST and its gradient. On seasonal timescale, the latitudinal position of ITCZ varies with maxima in solar radiation and an underlying SST (Xie 2004; Schneider et al. 2014). On decadal timescales, the precipitation maxima over the tropical Atlantic and Pacific Ocean fluctuate with the meridional mode: a coupled ocean-atmosphere mode with cross-equatorial winds and the dipolar SST pattern (Nobre and Shukla 1996; Chiang and Vimont 2004). In zonal direction, the Walker cell modulates with ENSO (Wang 2002), a quasi-periodic warming of the east equatorial Pacific Ocean, on interannual timescales. Any externally forced changes in SST distribution could therefore significantly affect the tropical climate.

But, what determines the SST distribution? Sea surface temperature over a region is jointly determined by heat flux exchange at the ocean-atmosphere interface and by the motion (dynamics) of upper ocean (Wang and McPhaden 1999; Kurian et al. 2007; Yu et al. 2010). The variations in contribution by surface fluxes versus the ocean dynamics give rise to spatiotemporal variability observed in SST distribution. One fundamental

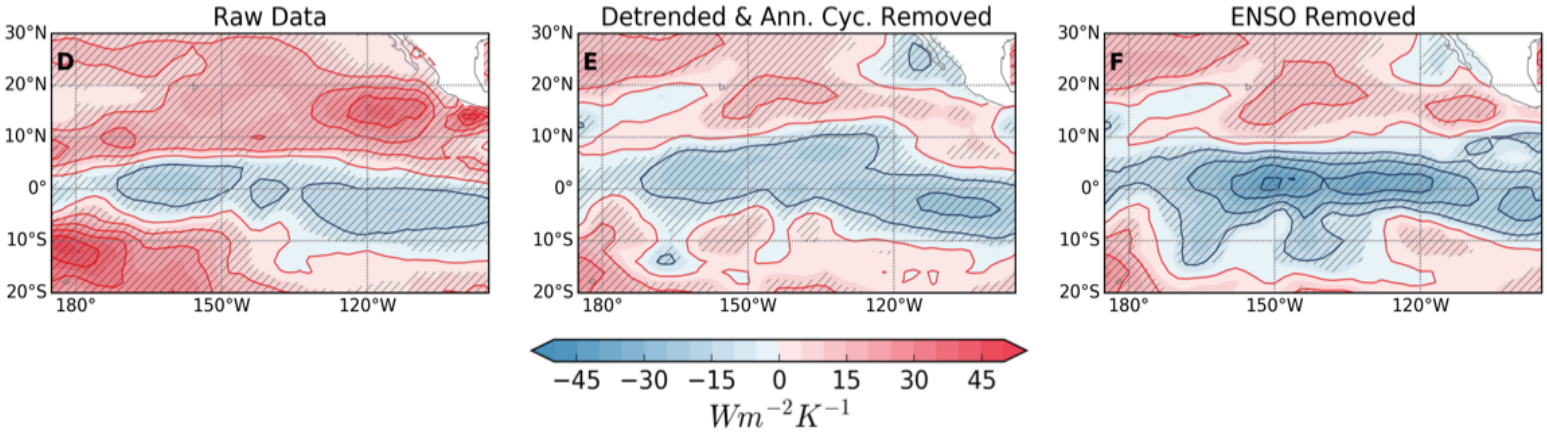

Figure 4.1 Simultaneous linear regression coefficient between monthly mean SST (ERSST v4) and net downward heat flux (NCEP/NCAR reanalysis) at the surface for 1950-2015 period. Regression coefficient over the Pacific ocean, (a) for observed monthly mean data, (b) after detrending and removing an annual cycle from the raw data, and (c) after linearly removing ENSO variability based on Nino3.4 index from the data used in (b). Stippling indicate regions exceeding 90% statistical significance according to standard t-test.

distinction between the tropics and the midlatitude can be seen in Figure 4.1 where SST is linearly regressed against the corresponding net downward surface heat flux over the Pacific basin. The negative coefficient over the tropics indicates that oceanic fluctuations force the atmosphere above. In midlatitude, however, the atmospheric fluctuations force the underlying SST (Frankignoul 1985; Saravanan and Chang 1999). As the fluctuation timescale increases (from Figure 4.1a to 4.1c), the forcing by the ocean grows stronger but forcing by the atmosphere grows weaker. It is imperative to consider both the changes in atmospheric fluxes and the ocean dynamics to predict tropical climate response to any external forcing.

Aforementioned discussion is closely related to the concept of interaction between the ocean and the atmosphere. The basic assumption is the presence of active feedbacks between the two systems and not simply one forcing another (Toba 2003; Kagan 2006). In literature, the term ocean-atmosphere coupling is often used with 'one-way' and 'two-way' coupling to distinguish between the two extremes of the interaction. Over the tropical oceans, specifically the tropical Pacific and Atlantic, the two-way interaction can be further classified into thermodynamical versus the dynamical ocean-atmosphere interaction (Saravanan and Chang 2004). The interaction is dynamical when the feedback into the atmosphere is related to changes in ocean currents and subsequent changes in upper ocean thermal structure. On the other hand, it is thermodynamical if the feedback is directly due to changes to ocean thermal structure without any dynamical changes in the ocean. Both of them are important to fully predict the tropical ocean-atmosphere state on range of timescales. ENSO or the zonal mode in the tropical Pacific

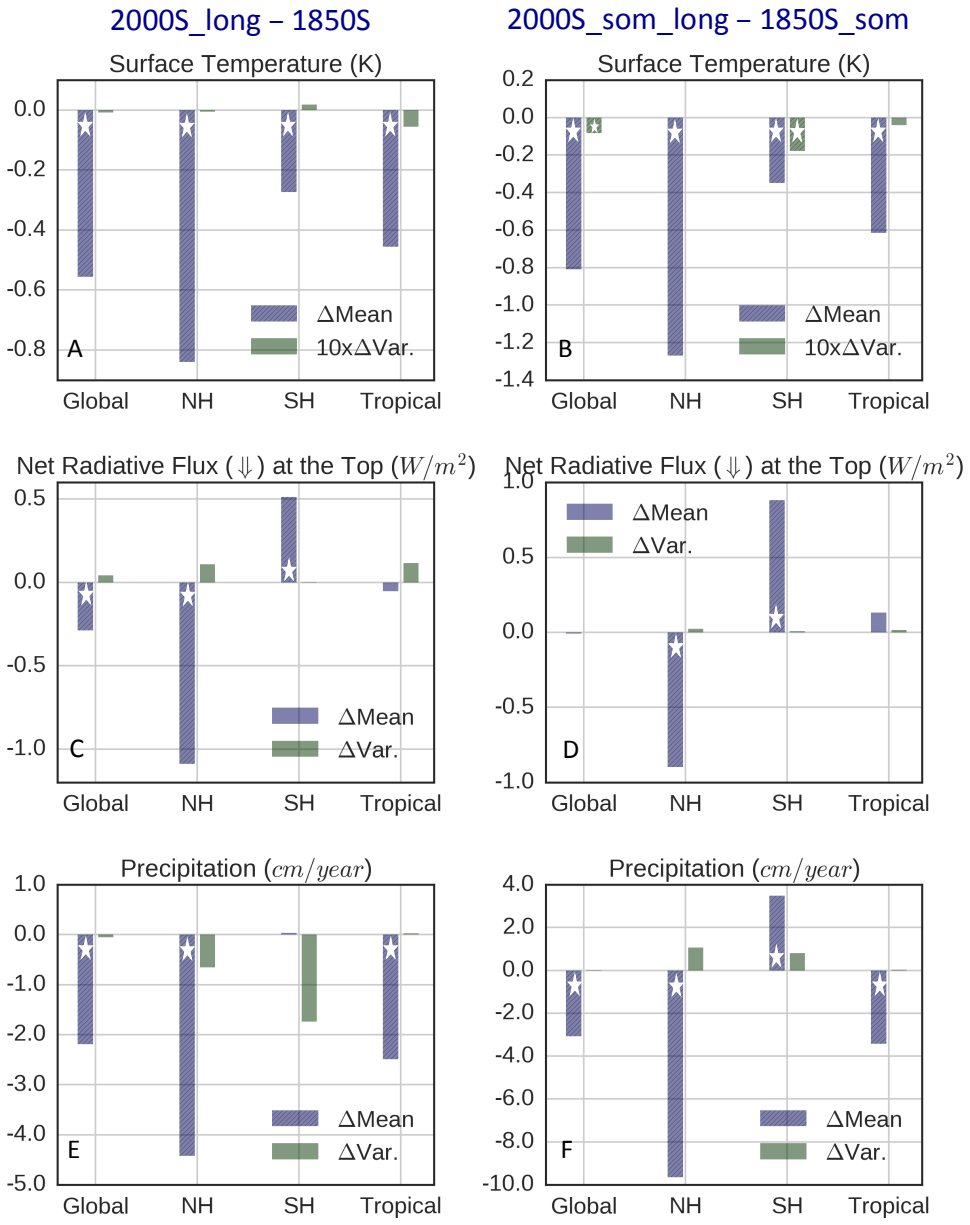

Figure 4.2 Area-averaged differences in mean and variance (of annual mean time series shown in Figure 2.2) of surface temperature, net downward radiative flux at top of the model and precipitation in (a,c,e) long-term fully-('2000S_long' – '1850S') and (b,d,f) partially-coupled ('2000S_som_long' – '1850S_som') experiments. Stars indicate statistically significant changes based on standard t and Bartlett tests.

is predominantly dynamical whereas, the Pacific Meridional Mode (PMM) is a result of thermodynamic interaction between the ocean and the atmosphere. Recent studies suggest that they are not completely independent but impact each other (Servain et al. 1999; Chang et al. 2007; Larson and Kirtman 2014). The use of full-ocean GCM versus the SOM is a natural way to separate out the two kinds of tropical ocean-atmosphere interaction and will be examined in this chapter.

The cooling of sea surface temperature is the direct consequence of increased sulfate aerosols. It cools because the radiative energy reaching the earth's surface is reduced. The greater anthropogenic aerosol concentrations over the northern hemisphere, selectively cools regions of the Pacific ocean, thereby changing local SST and its gradients that could potentially affect the climate in non intuitive ways (Ocko et al. 2014). For example, the regional warming in response to sulfate aerosols will have to be indirectly caused by changes in clouds, and atmospheric or oceanic circulation. In this chapter, we attempt to separate the role of atmosphere, ocean and their interaction in determining regional SST changes in response to sulfate aerosol forcing and its implications to regional and large-scale climate. We will be using both the fully- and the partially-coupled experiments for this purpose. Figure 4.2 compares long-term global and hemispheric mean changes in surface temperature, energy imbalance at the top, and precipitation between the fully- and the partially-coupled experiments in response to sulfate aerosol forcing. Fully- and partially-coupled responses differ not only in magnitude of the surface cooling, but also in the hemispheric energy compensation at the top of the model (Cvijanovic et al. 2013; Voigt et al. 2014). There is a perfect

compensation in partially coupled experiment between the two hemispheres leading to a zero global mean radiative imbalance. This compensation is closely related to the southward shift of the ITCZ; negative and positive precipitation response over northern and southern hemisphere in partially-coupled case indicates the southward shift, which is not apparent in the fully-coupled case.

Section 4.2 describes the methodology and brings out the fundamental differences between the two approaches of coupling ocean and atmosphere. It is followed by results in Section 4.3 in which primary mechanisms of SST response over different tropical Pacific regions is identified. Finally, section 4.4 summarizes the results and presents their implications.

4.2 METHODOLOGY

In this chapter, we examine both the short-term and the long-term SST response to sulfate aerosol forcing over the tropical Pacific ocean in fully- and partially- coupled experiments. Inter-comparison between them brings out the role of ocean dynamics, and ocean-atmosphere coupling in transient as well as equilibrium climate responses. We employ surface layer heat budget analysis to decompose SST (or surface layer temperature) response into contribution from surface fluxes versus the ocean dynamics (Wang and McPhaden 1999). The surface layer heat budget in partially- and fully-coupled cases differs substantially. The fundamental difference between the two is highlighted in Figure 4.3 using a schematic depicting the flow of heat.

The temperature of the 'slab' ocean (Figure 4.3a), with no motion and fixed depth, is primarily controlled by net heat flux input at the surface comprising of shortwave and

longwave radiative fluxes and latent and sensible turbulent heat fluxes. A net positive heat flux into the ocean would therefore warm the slab ocean, and vice versa. An additional term referred to as 'Q-flux' is essential for simulating the realistic SST distribution over the globe. This quantity simply parameterizes the heat flux divergence over every grid point. We determined climatology of the 'Q-flux' using 40 years of preindustrial control simulation (1850S) and prescribed it in various partially-coupled

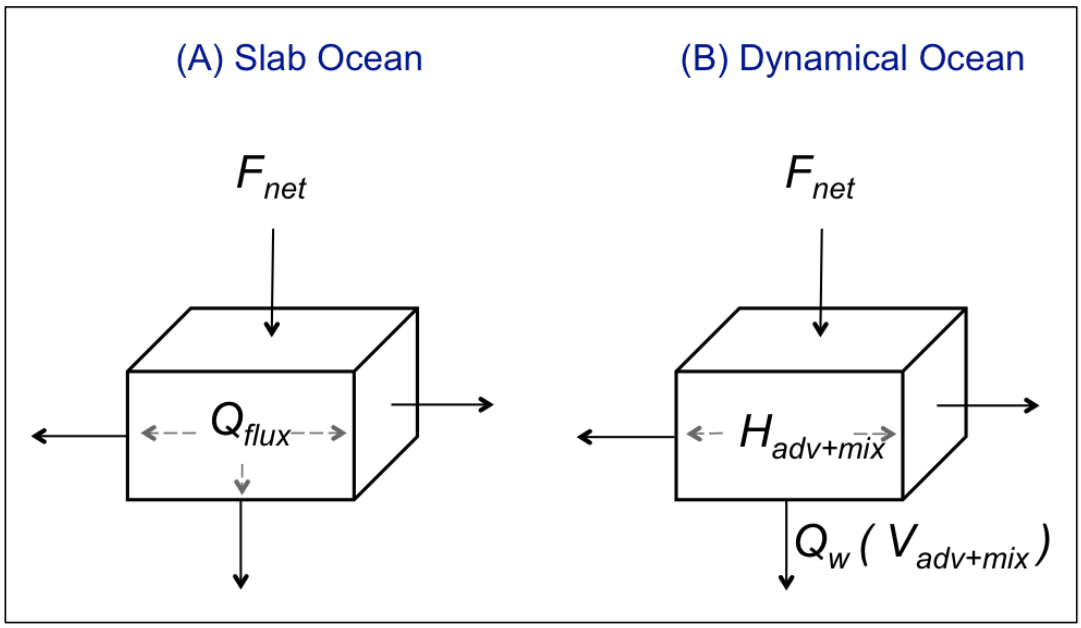

Figure 4.3 Schematic of surface layer heat budget in slab ocean versus full (or dynamical) ocean model. F_{net} in (a) and (b) represents net downward heat flux at the surface inclusive of shortwave and longwave radiative fluxes and latent and sensible turbulent heat fluxes. Q_{flux} in (a) represents a climatological net heat flux divergence out of the box in both horizontal and vertical directions; it is typically predetermined from previous fully-coupled model integration. $H_{adv+mix}$ and $V_{adv+mix}$ in (b) represent horizontal and vertical advection and mixing processes in the dynamical ocean. Q_w is the vertical heat flux due to mixing alone.

integrations. The surface layer heat budget for this case is mathematically expressed as equation 4a (Bitz et al. 2012). The rate of change of surface (or mixed) layer mean temperature, T of fixed depth, h is proportional to net surface heat flux (F_{net}) and the heat flux divergence (Q_{flux}) within the layer. Standard density and specific heat of water are used in the calculation. As there are no currents in the slab ocean, only thermodynamical ocean-atmosphere interaction is allowed in this case.

$$\frac{dT}{dt} = \frac{F_{net}}{h\rho C_p} + \frac{Q_{flux}}{h\rho C_p} \qquad 4A$$

$$\frac{\partial T}{\partial t} = \frac{F_{net}}{h\rho C_p} - u\frac{\partial T}{\partial x} - v\frac{\partial T}{\partial y} + \mathrm{R} \qquad 4B$$

$$\mathrm{R} = -\nabla \cdot \overline{\vec{u}'T'} - w\frac{\partial T}{\partial z} + \frac{Q_w}{h\rho C_p} \qquad 4C$$

On the other hand, in dynamical ocean case, with currents being predicted, both kinds of interactions are feasible. The surface layer heat budget has additional contributions from horizontal and vertical advection as well as mixing due to small-scale processes as shown in Figure 4b. The corresponding heat budget can be simply represented by equations 4b and 4c (McPhaden et al. 2002; Toba 2004; Yu et al. 2010). Temperature and currents in these equations are averaged over the depth of the layer. The residual term, R, typically consists of ocean processes that may not be determined from the monthly mean model outputs e.g., horizontal and vertical mixing due to small-scale processes. The ocean's dynamical adjustment thus makes examining surface layer heat budget in full-ocean GCM more challenging than in the slab ocean and will be validated next.

A preliminary surface layer heat budget is performed for the fully-coupled preindustrial control simulation (1850S) to test its validity. SST variations in '1850S' are partitioned into net surface heat flux, zonal and meridional advection in the surface layer over three separate regions in eastern tropical Pacific Ocean (Figure 4.4). For clarity, partitioning for only the initial 55 years is shown. These regions, namely, northeast tropical Pacific, Niño3 and southeast tropical Pacific (boxes in Figure 4.6), as we will see later, are selected to highlight the diversity in physical processes causing SST to change over the tropics.

The interannual and seasonal variability in temperature over Niño3 region (Figure 4.4a) is well reproduced on combining surface heat flux and horizontal advection (compare solid black and dashed black lines) terms. The residual (in cyan) is small except during strong El Niño and La Niña events. Seasonal variations over Niño3 are primarily contributed by surface heat flux and zonal advection terms. In contrast, the interannual variability appears to be coming from the meridional advection. Like Niño3 region, there is a good qualitative agreement in simulated and predicted surface layer temperature over southeast tropical Pacific (Figure 4.4b). But, the ratio of interannual to seasonal variations is significantly reduced over the region. The seasonal variation is primarily correlated with variation in net surface heat flux. The northeast tropical Pacific hardly undergoes any interannual variation (Figure 4.4c) and seasonal changes are again highly correlated with net surface heat flux. Amount of SST variance explained by constituents, individually or jointly is summarized in Table 4.1 for the three regions. The explained variance is always greater when all contributions are considered together

(diag. T) and is highest for the southeast tropical Pacific region. These results are consistent with those from Figure 4.1, i.e., tropical ocean forces the atmosphere above and an inverse relation holds in the midlatitude.

Figure 4.5 extends previous analysis for the annual cycle. The predicted annual cycle agrees with the simulated one over all three regions. Residuals in each are fairly weak and remain approximately constant throughout the year. The negative residual in each case imply that vertical advection and mixing would be cooling the surface layer. Both net surface heat flux and zonal advection contributes to seasonality of Niño3 SST (Figure 4.5a). The meridional advection is small, negative and leads the residual (vertical advection and mixing) by about a month. The advection by ocean currents is fairly weak over both the off-equatorial boxes with net surface heat flux solely contributing to the annual cycle variation. In the next section, we will be using heat budget analysis to understand consequences of ocean dynamics in tropical Pacific SST response to aerosol.

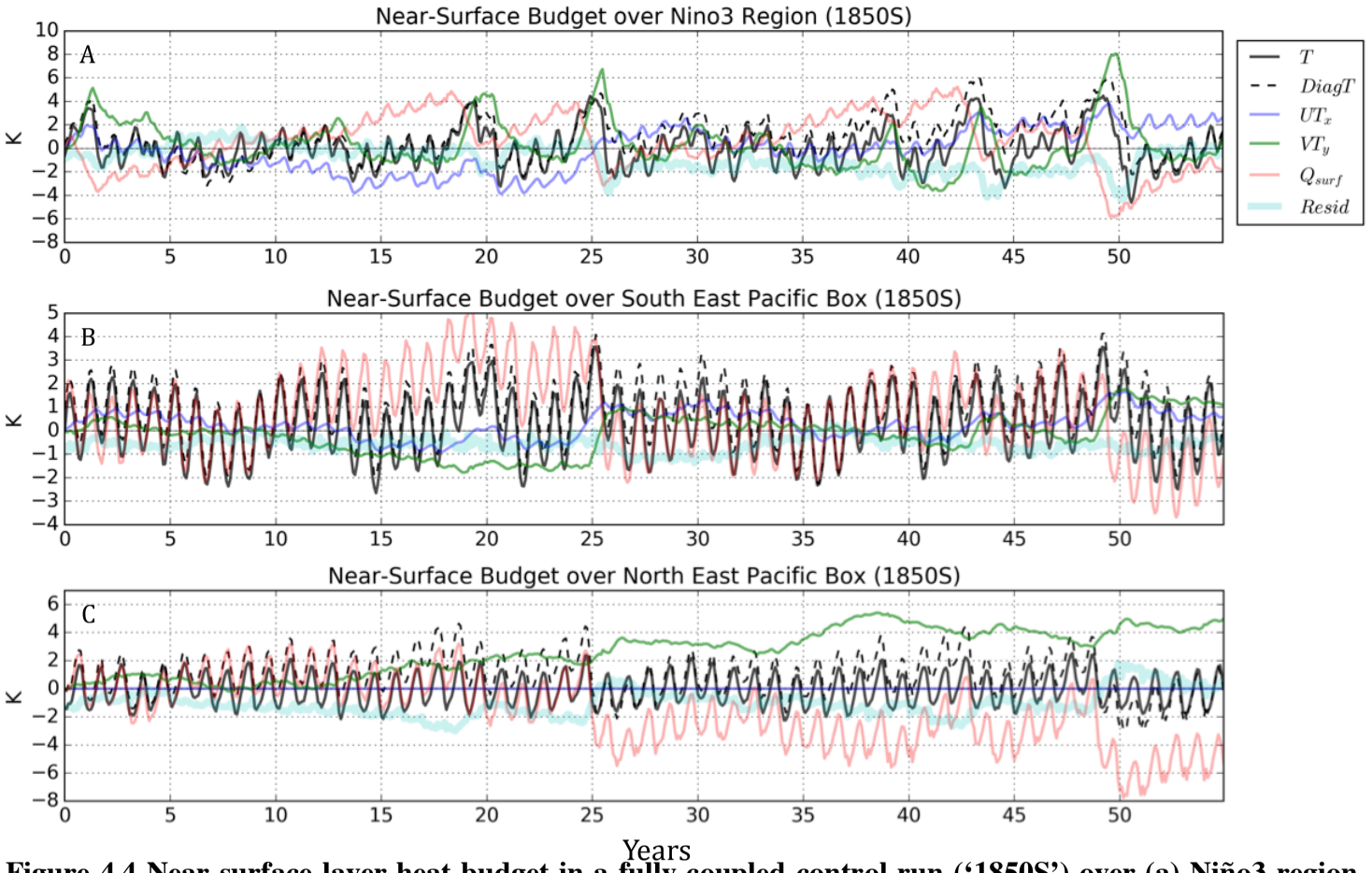

Figure 4.4 Near-surface layer heat budget in a fully-coupled control run ('1850S') over (a) Niño3 region, (b) southeast tropical Pacific, and (c) northeast tropical Pacific Ocean. Area averaged near-surface layer temperature (solid black) is diagnosed (dashed black) using net downward surface heat flux (red), zonal (blue), and meridional (green) advection. The residual in each case is plotted in thick cyan line. The budget shown is for the first 55 years of total 110 years period and is representative of the whole time series.

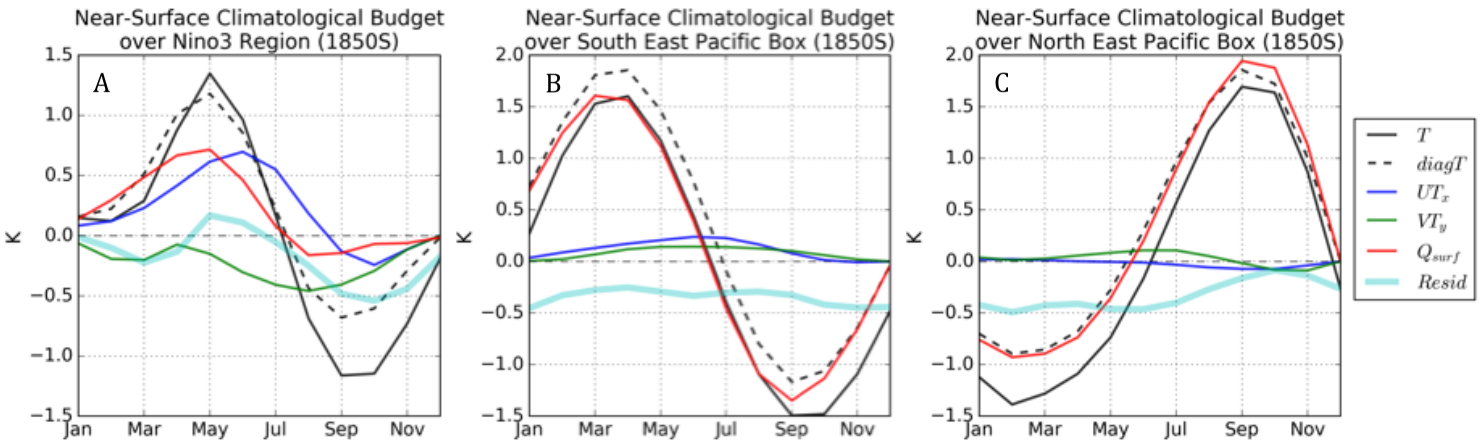

Figure 4.5 Annual cycle of near-surface layer heat budget in a fully-coupled control run ('1850S') over (a) Niño3 region, (b) southeast tropical Pacific, and (c) northeast tropical Pacific Ocean. Same as in figure 4.4 except for the annual timescale.

Table 4.1 Variance explained by terms in near-surface layer heat budget analysis

R^2 x 100 %	North EP		Nino3		South EP	
	full	minus ann_cyc	full	minus ann_cyc	full	minus ann_cyc
T vs. F_{net}	28.8	20.6	1.2	0.4	57.0	30.3
T vs. UT_x	0.4	1.4	13.6	16.5	0.6	2.6
T vs. VT_y	2.8	5.8	5.2	3.5	5.5	9.7
T vs. diag T	54.9	34.1	62.4	58.5	87.4	82.7

*Based on whole 110-year long time series.
*full and minus ann_cyc refers to data before and after removal of the annual cycle.

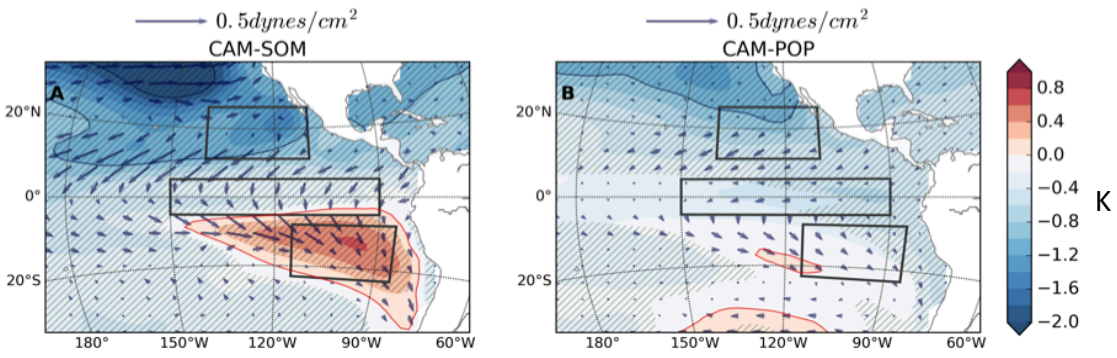

Figure 4.6 Long-term mean differences between (a) '2000S_som_long' and '1850S_som', and (b) '2000S_long' and '1850S' runs. Shading in (a) and (b) is the long-term change in SST with stippling indicating regions exceeding 90% statistical significance according to standard t-test. Vectors in (a) and (b) show corresponding surface wind stress response.

4.3 RESULTS

The long-term or equilibrium climate response to aerosols is jointly controlled by fast atmospheric adjustments and slow SST-mediated feedbacks. Figure 4.6 shows long-term mean response to sulfate aerosol forcing in both the partially- and the fully-coupled experiments. The shading in Figure 4.6 represents SST response and vectors show the

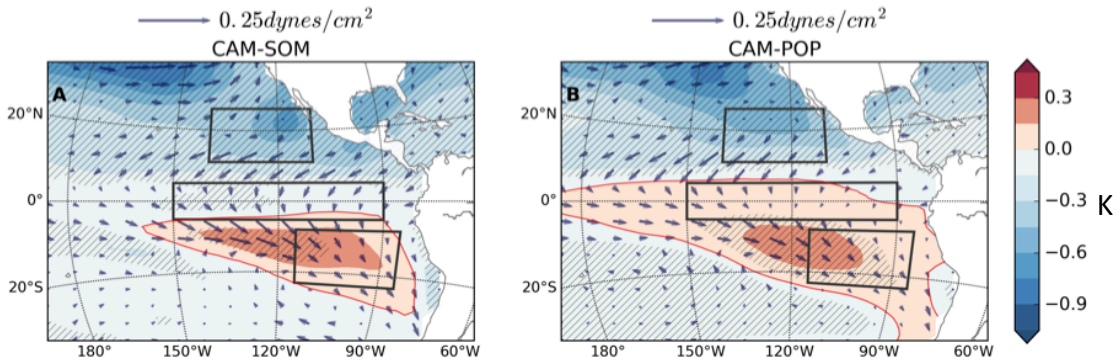

Figure 4.7 Ensemble mean short-term mean differences between (a) '2000S_som' and '1850S_som', and (b) '2000S' and '1850S' runs. Same as in Figure 4.6 except that averaging is done over both the ensemble and the integration length i.e., (a) two years for the partially-coupled, and (b) four years for the fully-coupled experiment.

corresponding wind stress response. Although fast response to aerosol perturbation would be comparable in the two experiments, the total response can be very different due to differences in slower ocean-mediated feedbacks as seen here (compare Figure 4.6a and b). The cooling over northern subtropical Pacific is stronger and southeast tropical pacific undergoes counter-intuitive warming in SOM in comparison to the fully-coupled case. Also, there are anomalous cross-equatorial surface winds across the meridional SST gradient in partially-coupled case. On the other hand, there is no southeast tropical Pacific warming in full ocean GCM and cross-equatorial winds are

very weak. The equilibrium response, certainly, depends on the choice of ocean model being used. How do ocean dynamics and dynamical coupling lead to such fundamental differences in the response?

Figure 4.7 is analogous to the mean response shown in Figure 4.6, except that it compares transient (or initial) SST and lower tropospheric circulation response to aerosols between partially- and fully-coupled experiments. This transient response corresponds to an intermediate period when fast atmospheric adjustments are completed but SST-mediated feedbacks are restricted to seasonal-interannual climatic timescales instead of longer. The response in two cases are much more comparable on shorter timescales (compare 4.7a and b) confirming the difference in long-term mean response is related to the slower feedbacks. The magnitude of northern subtropical cooling and southeast tropical warming are similar. The cross-equatorial surface winds, although weaker, can be seen in the fully-coupled response. However, only in the fully-coupled case, the equatorial warming is present along with westerly wind stress response. As explained in detail in chapter 3, the aforementioned equatorial response is related to dynamical changes in equatorial thermocline, and, therefore, is not reproduced in both long-term and short-term partially-coupled responses (Figure 4.6a and 4.7a). As time goes on, the initial tropical Pacific warming (both equatorial and off-equatorial) will disappear when both ocean dynamical adjustment and dynamical coupling are taken into account (Figure 4.6b and 4.7b). Does ocean dynamics, in long-term, play a role in transporting or diffusing the initial southeast tropical Pacific warming away?

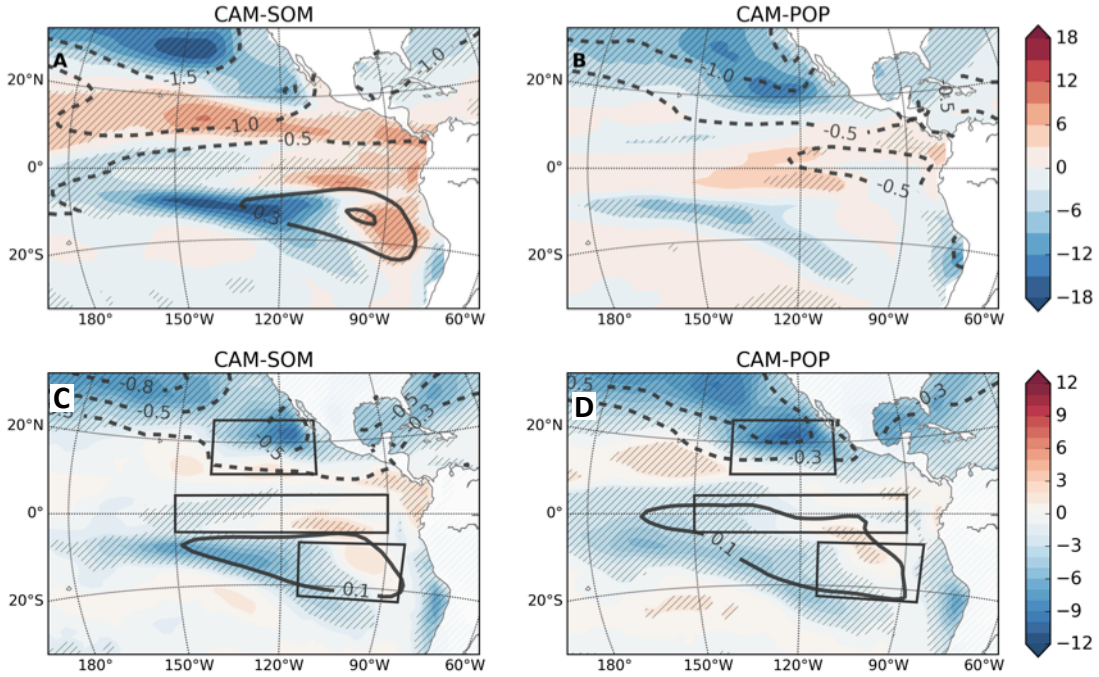

Figure 4.8 Long-term mean differences in downward surface shortwave radiative flux (in W/m^2) between (a) '2000S_som_long' and '1850S_som', and (b) '2000S_long' and '1850S' runs. Ensemble mean short-term mean differences in downward surface shortwave radiative flux between (c) '2000S_som' and '1850S_som', and (d) '2000S' and '1850S' runs. Shading in each subplot is change in shortwave radiative flux with stippling indicating regions exceeding 90% statistical significance according to standard t-test. The black contours in each subplot shows the corresponding change in SST from Figure 4.6 and 4.7.

Before decomposing the warming into contributions from surface heat flux and ocean dynamics, long-term changes in short-wave (SW) radiative flux reaching the earth surface for each of the four experiments is shown in Figure 4.8. Surface cooling over the northern subtropics in each case is directly related to reduction in incoming SW radiation. A band of positive SW flux around 10ºN in long-term partially-coupled response (Figure 4.7a) indicates southward shift of the ITCZ in response to aerosols. However, the southern tropics stays warm, in spite of reduced SW flux into the ocean (Figure 4.7a,c and d). Therefore, there must be another mechanism responsible for the

warming of the southern tropics. Long-term changes in latent heat flux, which is susceptible to changes in SST, and vice versa, are shown in Figure 4.9. The positive latent heat flux response (into the ocean) overlaps with the warmer SST, especially in partially-coupled response. Therefore, latent heat flux plays a greater role in warming of the southern tropics and the short-wave radiative flux in cooling of the extratropics. However, the surface layer heat budget analysis is required to be more conclusive and will be discussed next.

The heat budget decomposition is done for three separate regions in the eastern tropical Pacific ocean (boxes in Figure 4.6). These regions highlight the role of (a) SW

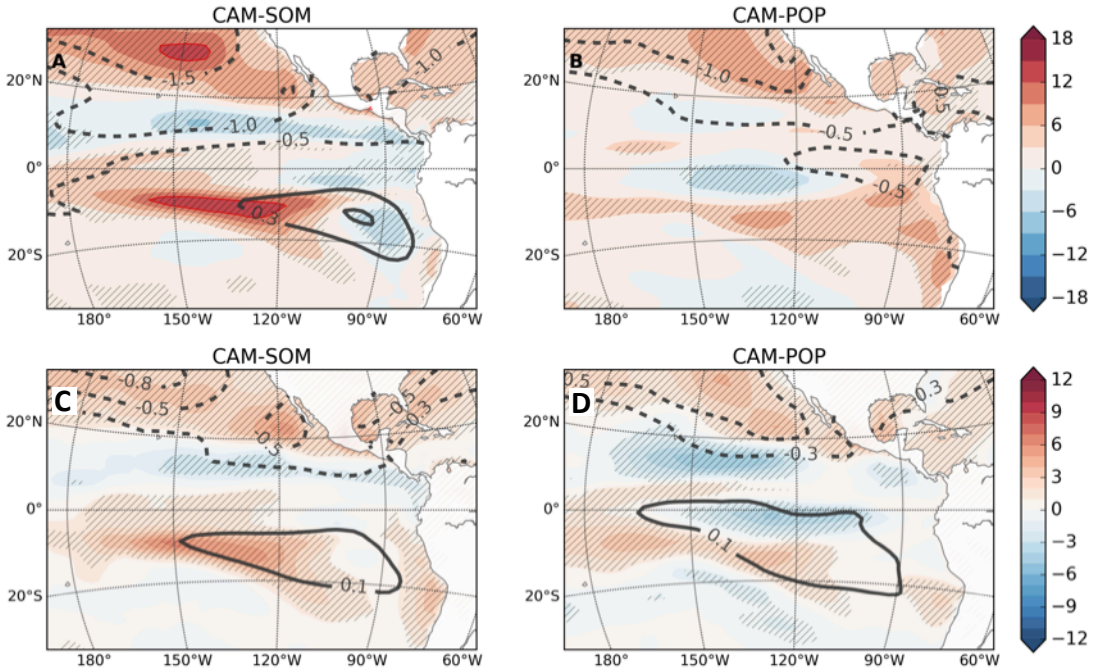

Figure 4.9 Same as in Figure 4.8 except for changes in surface latent heat flux (positive into the ocean).

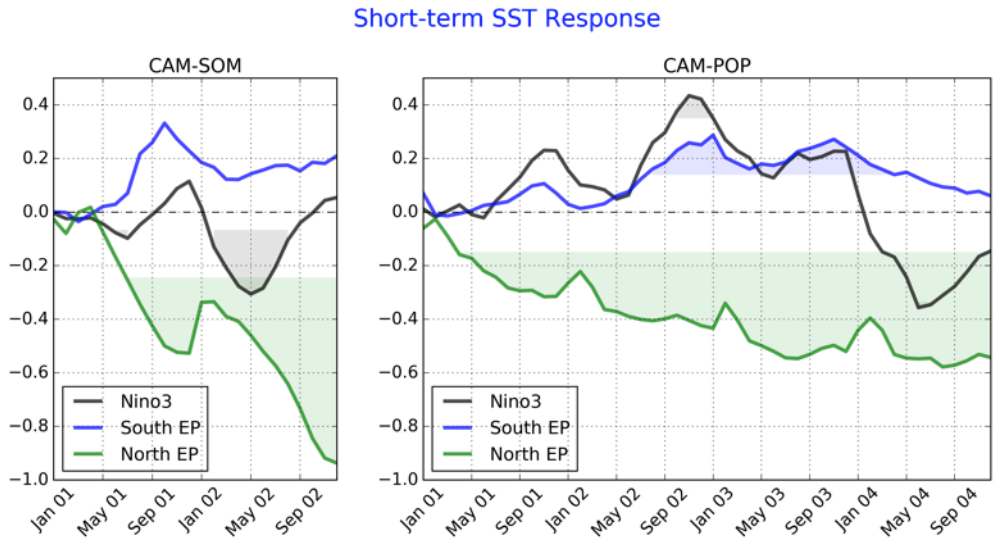

Figure 4.10 Area averaged ensemble mean monthly mean SST changes between (a) '2000S_som' and '1850S_som' for two-years in the partially-coupled experiment, and (b) '2000S' and '1850S' for four years in the fully-coupled experiment. The three regions used for averaging are shown in Figure 4.6. The shading in each highlights the period when response is statistically significant based on standard t-test.

forcing over the northeast, (b) equatorial ocean dynamics over Niño3, and (c) latent heat forcing over the southern tropics. We further restrict the analysis to transient (initial) adjustments in both partially- and fully-coupled experiments. The area-averaged transient SST response over the three regions for two types of coupling is shown in Figure 4.10. It shows initial two-years adjustments in SOM (Figure 4.10a) and four-years in full ocean GCM (Figure 4.10b). The shading in each curve highlights the statistically significant changes. The northeast tropical Pacific (in green) has a stronger cooling trend in SOM than in the full ocean GCM. The southeast tropical Pacific (in blue) in SOM has on overall increasing trend over a span two years with an isolated peak. In full ocean GCM, the southeast tropical Pacific undergoes seasonal modulation for the first three years and appears to be related to Niño3 response (in black) – a

westerly wind stress forced seasonal warming riding on top of slower ENSO like modulation (refer Chapter 3 for more details).

As seen in Figure 4.11, the decomposition of SST response in slab ocean case can be done very accurately. The dashed black line in each of the subplots is the diagnosed SST response (from surface heat fluxes) and matches the simulated SST response (solid black) quite accurately. Cooling trend over the northeast tropical Pacific (Figure 4.11a) is primarily associated with respective trend in the incoming shortwave radiation. Whereas, the seasonal jump is associated with the latent heat flux response. Contribution from longwave and sensible heat fluxes are small and partially cancels the cooling. The warming over the southeast tropical Pacific (Figure 4.11c) is jointly due to latent heat and longwave radiative flux response. The isolated peak in between is related to change in latent heat flux. The shortwave radiative flux has a cooling effect over the region. The mean Niño3 response in SOM is weak and uninteresting. Next, we examine the surface-layer heat budget for the fully-coupled response and attempt to isolate consequences of active ocean dynamics and coupling.

As opposed to the decomposition in slab ocean, the surface-layer heat budgeting in the full ocean is difficult and not very accurate. The accuracy in this case is limited by processes that remain unaccounted for in the analysis, e.g., mixing due to small-scale processes. Further, there is a loss of generality due to absence of a single criterion for choosing the layer depth. As a result, dashed lines do not exactly match with the solid black lines in Figure 4.12. In other words, the residuals are greater in budgeting in the fully-coupled case. The northeast tropical Pacific cooling (Figure 4.12a) is essentially

due to shortwave reduction and is largely compensated by positive meridional advection term. The warming over Niño3 region (Figure 4.12b) is due to all the three ocean advection terms and is compensated by every surface heat flux term. It provides a quantitative validation of conclusions drawn in chapter 3. The seasonal warming is largely contributed by the vertical advection term, whereas, the slower modulation is due to meridional advection term. The southeast tropical Pacific response (Figure 4.12c) has similar fluctuations to Niño3, but with completely different mechanism. The warming and its seasonal modulation are primarily associated with the latent heat flux response. Interestingly long wave radiation term, for the first time, is not opposing the SST response. Both vertical and meridional advection opposes this warming and could be responsible for removing or transporting the southeast tropical Pacific warming as the time goes on.

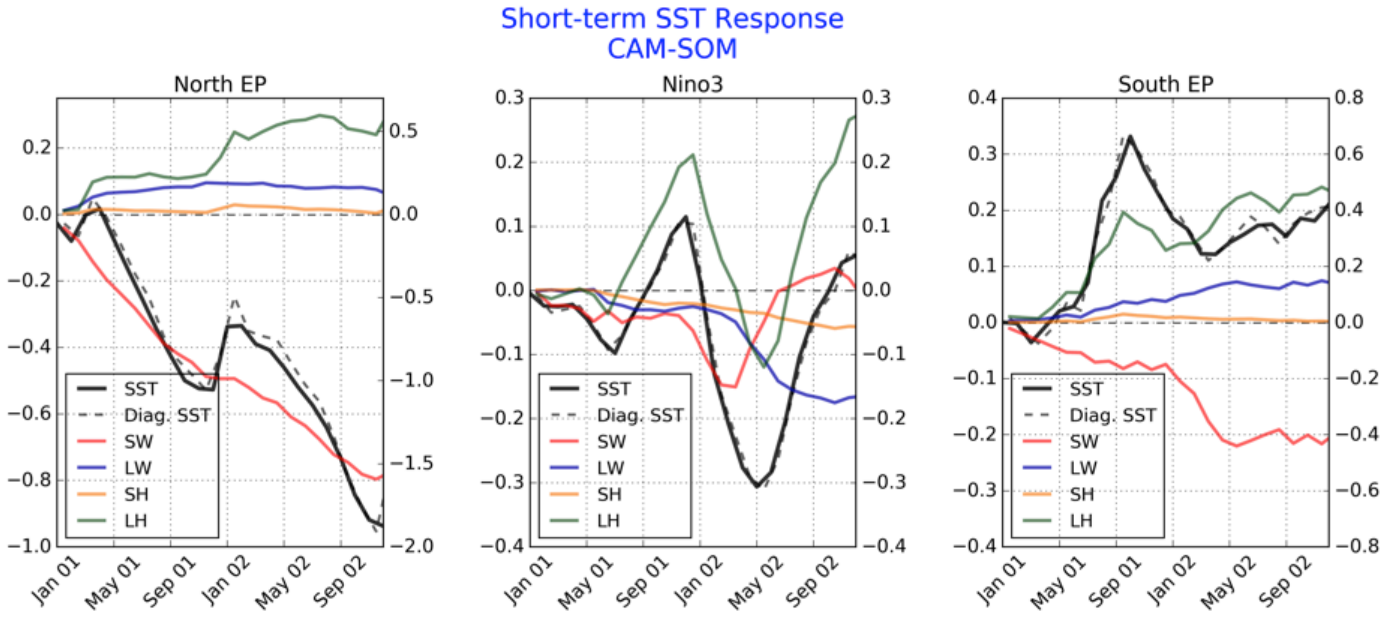

Figure 4.11 Surface-layer heat budget analysis for short-term partially-coupled experiment. Each curve represents an area average ensemble mean monthly mean difference between '2000S_som' and '1850S_som' runs. SST response (solid black; left y-axis) is partitioned into constituent surface heat fluxes (right y-axis) for (a) northeast tropical Pacific, (b) Nino3, and (c) southeast tropical Pacific boxes. The dashed black line in each subplot is the SST response diagnosed from the heat flux response.

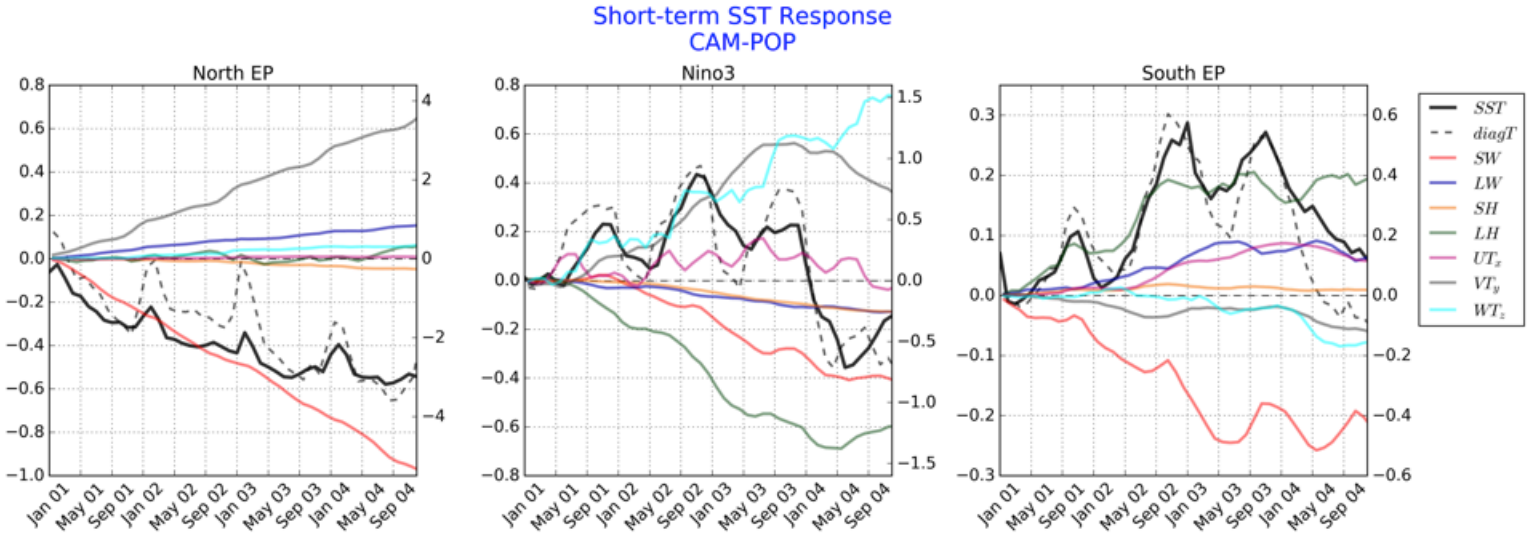

Figure 4.12 Surface-layer heat budget analysis for short-term fully-coupled experiment. Each curve represents an area average ensemble mean monthly mean difference between '2000S' and '1850S' runs. SST response (solid black; left y-axis) is partitioned into constituent surface heat fluxes and horizontal and vertical advection (right y-axis) for (a) northeast tropical Pacific, (b) Niño3, and (c) southeast tropical Pacific boxes. The dashed black line in each subplot is the SST response diagnosed by adding constituents together.

4.4 CONCLUSIONS

• *The equatorial Pacific warming in response to sulfate aerosols is due to anomalous Walker cell and dynamical ocean-atmosphere interaction.*

• *The off-equatorial warming is due to wind-induced decrease in evaporation and thermodynamic ocean-atmosphere interaction.*

• *In long-term, ocean dynamics and dynamical coupling remove the initial tropical warming response to sulfate aerosols.*

In this chapter, we compared long-term and short-term tropical Pacific SST response to sulfate aerosol forcing between partially- and fully-coupled experiments. The comparison brings out the role of ocean dynamics in determining the response on range of timescales. The surface-layer heat budget over three different regions in the eastern tropical Pacific ocean was carried out to quantitatively assess the relative contributions of surface forcing and the ocean dynamics.

We find that dynamical ocean moderates the aerosol induced cooling over the northeast tropical Pacific. The surface cooling in the fully-coupled case is weaker despite having stronger reduction in shortwave radiative flux which is associated with greater increase in cloud amount. How does ocean-atmosphere coupling impact SST-Cloud feedback and lower tropospheric stability are important to fully understand the climate response to sulfate aerosols over this region. The heat budget analysis confirms the ocean dynamical origin of initial equatorial Pacific warming. Both vertical and meridional advection responses are responsible for the seasonally modulated warming over equatorial Pacific. Surface heat flux terms partly cancel this warming and are likely

to be responding to the warming itself. Unlike the equatorial warming, off equatorial warming over southern tropics is caused by increased latent heat flux into the ocean with further enhancement by longwave radiative flux and meridional advection terms. The warming is compensated by vertical and meridional advection that could also eventually remove the warming from the long-term mean response.

Whether long-term SST changes due to aerosols, impact modes of climate variability or not is an extremely relevant question. Previous literature have shown that the two modes of tropical Pacific variability i.e., zonal and meridional modes, are susceptible to changes in SST distribution. Chiang et al. 2008 using an intermediate coupled model showed that the ENSO (or zonal mode's) variability decreases with negative inter-hemispheric thermal gradients. Consistent with their results, we observe reduction in Niño3 variability with increase in sulfate aerosols for both partially- and fully coupled cases (Figure 4.13). The representation of Pacific Meridional Mode (PMM) in long-term fully-coupled integrations were shown earlier in Figure 2.5. The PMM is better represented (closer to 20^{th} century observations) in present-day perturbed long-term integration ('2000S') than in the preindustrial control simulation ('1850S'). Is climate with present day sulfate aerosols more likely to support PMM? The extratropical forcing of PMM (corresponding to Figure 2.5) is shown in Figure 4.14. It consists of sea level pressure and surface wind stress patterns that modulate with PMM (obtained by linearly regressing SLP on PMM's principal component). The difference is related to distinct changes in pressure centers of the North Pacific Oscillation. These preliminary results suggest that inter-hemispheric SST response to anthropogenic aerosols could

potentially affect both the zonal and the meridional modes of tropical Pacific climate variability and needs to be addressed.

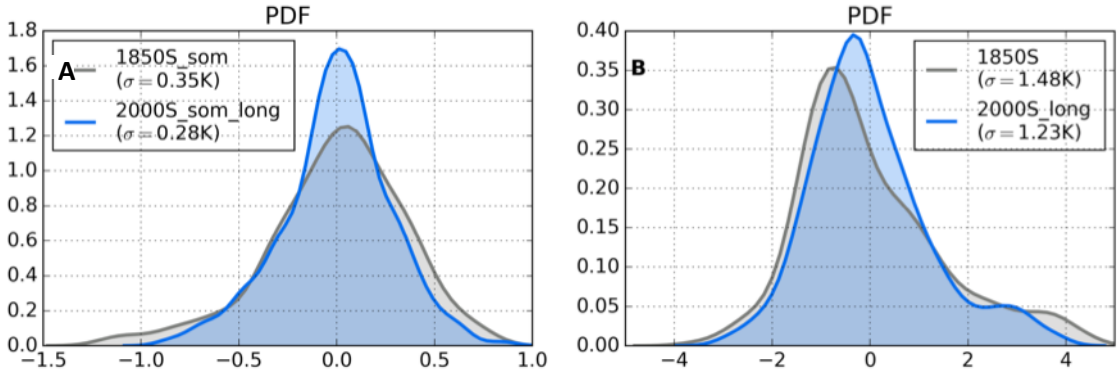

Figure 4.13 KDE based probability density function of Niño3 region monthly mean SST in (a) partially-coupled, and (b) fully-coupled long-term integrations. Grey curve is for preindustrial control runs, and blue is for present-day perturbed runs.

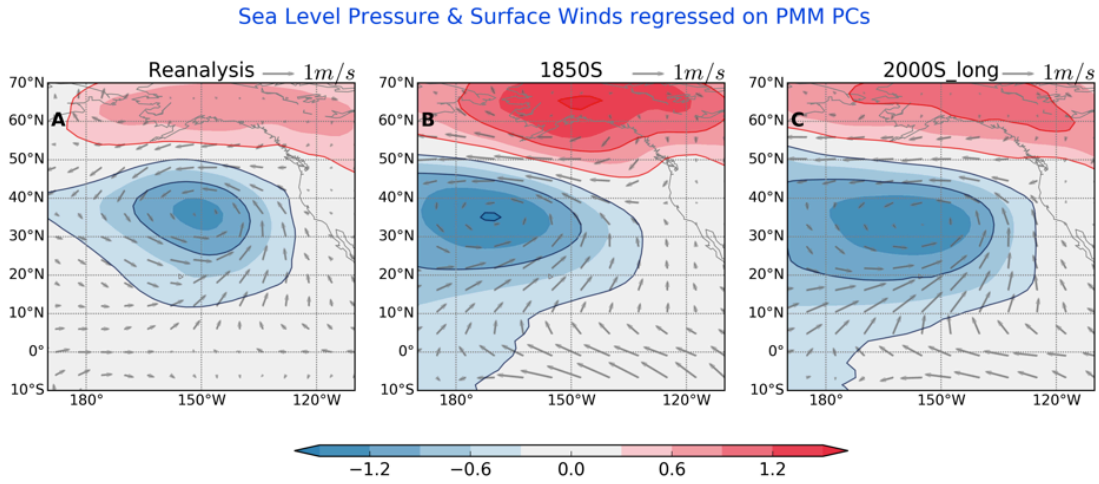

Figure 4.14 Linear regression of monthly mean sea level pressure and windstress fields with principal component time series of Pacific Meridional Mode shown in Figure 2.5. Regression coefficient over the Pacific ocean, (a) for observed (1950-2014; NCEP/NCAR Reanalysis windstress and ERSST v4) data, (b) for 60 years of fully-coupled preindustrial control simulation (1850S), and (c) for 60 years of fully-coupled present-day perturbed simulation (2000S). The shading represents sea level pressure anomaly and vectors are corresponding windstress anomalies.

CHAPTER V

TROPICAL HIGH CLOUD RESPONSE

5.1 INTRODUCTION

Aerosols and their interaction with atmospheric radiation and clouds (fast response) are imperative to accurately simulate present and future climates (Rosenfeld et al. 2014). It is important to account for extinction of shortwave and longwave radiation by aerosol particles (direct effect) to accurately determine radiative energy available at the Earth's surface, in a layer in the atmosphere, and at top of the atmosphere (Boucher 2015). It is also important to simulate aerosol-induced changes in clouds, their macrostructure- cloud fraction, liquid water content etc., and microstructure- mass and number concentrations of cloud particles, their effective sizes etc. These changes further modify the atmospheric radiation budget, and also affect precipitation formation (indirect effect; Heintzenberg and Charlson 2009). Both regional and large-scale climate is therefore susceptible to changes in aerosol amount via aerosol-radiation and aerosol-cloud interactions. At present, a relatively large uncertainty exists in quantifying aerosols' effect on clouds than radiation and is focus of this chapter.

It is more than two decades since Twomey and Albrecht (Twomey 1974; Albrecht 1989; Lohmann 2006), first proposed aerosol induced changes in clouds. Despite many advances in theoretical understanding and modeling of aerosol-cloud interaction during this period, many fundamental problems remain unsolved (Seinfeld et al. 2016). The challenges in constraining aerosol-cloud interaction in observations include inability to separate the effect of meteorology on clouds from that of aerosols, and difficulty of observing cloud micro- and macrostructure, their radiative and dynamical effects at high enough spatiotemporal resolution and extensively over the globe. Climate models encounter different challenges than those described above. The coarser resolution doesn't allow explicit representation of clouds, and aerosols' effect on them

and need to be parameterized. Accuracy of the simulated climate would then depend on that of parameterization schemes employed.

Studying aerosol-cloud interactions over a particular climate regime that supports similar large-scale environment and cloud system could reduce the meteorological noise. Studying warm (or shallow) cloud-aerosol interactions versus ice cloud-aerosol interactions would be one such example. Research carried out during last two decades or so has primarily focused on identifying and understanding links between warm clouds, rain rate and aerosols, and hence is better-understood and better represented in climate models (Stevens and Brenguier 2009). Understanding aerosols' effect on high clouds is still in early stages. In this chapter, we present preliminary analysis of simulated tropical high cloud response to increased aerosols and comment on the role of CAM5 physical parameterization schemes in it.

The chapter is organized as follows: section 5.2 presents a brief description of treatment of aerosol-cloud interaction in CAM5 along with model simulations that are analyzed. Section 5.3 consists of preliminary results followed by conclusions and implications in section 5.4.

5.2 MODEL DETAILS

In this chapter, first-year mean response to increased aerosols in both short-term fully-coupled ('2000S_short – 1850S') and uncoupled ('2000S_pres_short – 1850S_pres') experiments is examined. In CAM5, aerosols and its distribution are predicted using MAM3 scheme. Their interaction with clouds is parameterized with significant improvements with respect to warm cloud processes. However, aerosol-high cloud interaction is limited, minimally tested and needs improvements e.g., inclusion of dynamical processes that link aerosols' with invigoration of deep convection. The next subsection describes how aerosols affect clouds, specifically high clouds, in CAM5.

5.2.1 Treatment of aerosol-cloud interaction in CAM5

Like any other, state of the art atmospheric GCM, CAM5 distinguishes between atmospheric processes that are explicitly resolved versus that are not. These are loosely referred to as 'grid-scale dynamics' and 'parameterized physics', respectively. The unresolved physical processes are further subdivided into different parameterization schemes depending on what they predict. Some relevant parameterization schemes, including deep and shallow convection, cloud macro- and microphysics are shown in Figure 5.1. The graphic is a simplified representation of process ordering in CAM5; order in which different physical processes are simulated within a single time step. It is based on Park et al. 2014 and only the most relevant schemes are depicted. The dashed lines indicate that some intermediate steps have been intentionally omitted from the graphic. As can be seen, deep convection is treated separately from shallow convection, their macro-scale effects like cloud cover are differentiated from micro-scale properties like cloud droplet concentration. The interaction of radiative fluxes with atmospheric constituents and clouds is grouped under radiation parameterization and is handled separately. Finally, the cumulative effect of unresolved processes is fed back into the grid-scale dynamics and so on.

Although, it is efficient to break the 'physics' down into several different units, they are not completely independent of each other. For example, aerosol particles would be advected by large-scale dynamics, be removed by the precipitation, some of them would get activated into cloud droplets/ice affecting cloud microstructure and

macrostructure, and will eventually impact radiative budget and dynamics. In CAM5, these interactions take place over successive time steps (on order of hours).

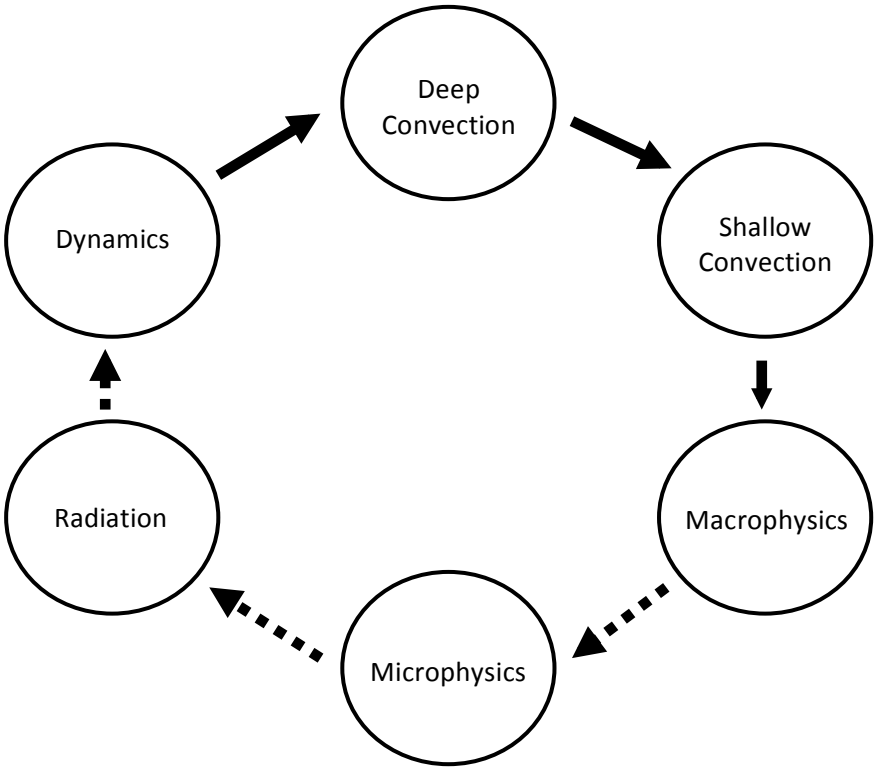

Figure 5.1 Simplified schematic representation of process-ordering in CAM5. It illustrates the sequence in which different physical processes (parameterization schemes) are simulated within a single time step (based on Park et al. 2014). The dashed lines indicate omission of certain physical processes in the graphic.

Mathematically, the effect of the small scale processes, e.g., clouds or aerosols, on grid-resolved quantities like temperature, humidity, winds etc., is introduced as source/sink terms in differential equations describing the grid-scale dynamics. For clouds containing ice particles, the rate of change of grid-mean cloud ice amount is expressed in terms of advection and various microphysical processes (right hand side) represented in the model (Equation 5.1). The parameterized microphysical processes

include deposition, sublimation, autoconversion, accretion, heterogeneous and homogeneous freezing, melting, sedimentation, convective detrainment and turbulent diffusion of cloud ice (refer to Morrison and Gettelman 2008 for more details).

$$\frac{\partial q_{ice}}{\partial t} + \frac{1}{\rho}\nabla \cdot [\rho \bar{u} q_{ice}] = \begin{bmatrix} \left(\frac{\partial q_{ice}}{\partial t}\right)_{dep} + \left(\frac{\partial q_{ice}}{\partial t}\right)_{sub} + \left(\frac{\partial q_{ice}}{\partial t}\right)_{auto} + \left(\frac{\partial q_{ice}}{\partial t}\right)_{acc} + \\ \left(\frac{\partial q_{ice}}{\partial t}\right)_{het} + \left(\frac{\partial q_{ice}}{\partial t}\right)_{hom} + \left(\frac{\partial q_{ice}}{\partial t}\right)_{mlt} + \\ \left(\frac{\partial q_{ice}}{\partial t}\right)_{sed} + \left(\frac{\partial q_{ice}}{\partial t}\right)_{det} + D(q_{ice}) \end{bmatrix} \quad \textbf{5.1}$$

In CAM5, many microphysical terms contribute to grid-mean cloud ice mixing ratio which in turn determines the amount of ice stratus (cloud fraction) present. The ice stratus fraction in CAM5 is calculated in macrophysics scheme, and is a quadratic function of relative humidity with respect to ice (Equation 5.2; A and B are constants; refer to Park et al. 2014 for more details).

$$a_{ice,stratus} = \left(\frac{RH_{ice} - A}{B}\right)^2 \quad \textbf{5.2}$$

The effect of aerosols on clouds and precipitation is fundamentally parameterized in cloud microphysics scheme, which interacts and eventually affect results of other parameterization schemes. The accuracy of model simulated aerosol-cloud interaction

depend on, (a) How physically realistic these parameterizations and their interactions are?, and (b) If all processes that are important to aerosol-cloud interaction are represented or not? In addition to the physical realism, parameterizations also need to be consistent with each other, e.g., cloud amount (or fraction; calculated in macrophysics) should be consistent with amount of hydrometeors present (calculated in microphysics). Parameterized physics in CAM5, particularly related to aerosol-cloud interaction, has considerably advanced in terms of physical realism, consistency and scope relative to its predecessor. The future generation climate models are considering the use of more generic and unified approaches to parameterize clouds and their interactions to make them internally consistent.

5.3 RESULTS

The fast climate response to sulfate aerosol forcing over the tropical Indian Ocean is shown in Figure 5.2. It consists of an ensemble mean first year mean climate response under fixed sea surface temperature conditions. Figure 5.2a shows total precipitation response that is mostly convective in nature (not shown). A significant increase in precipitation is seen over ocean on either side of the Indian peninsula and over South China Sea. The greatest reduction in precipitation, on the other hand, is confined to subtropical land over eastern Asia.

The corresponding percentage increase in high cloud fraction is shown in Figure 5.2b. In spite of having significant positive and negative precipitation anomalies over the region, the high cloud fraction is predominantly positive. Three of the four local maxima in cloud response are collocated over positive precipitation response, which suggests that

increased convection is causing high cloud response. Another maxima over the southeast tropical Indian Ocean has no corresponding increase in convection, which suggests possibility of alternate mechanisms for increase in high cloud fraction. Cloud increase is less likely to be an effect of strong nonlinearity between convection and the high cloud fraction. The vertical structure of area-averaged (box in Figure 5.2a) cloud response is shown in Figure 5.2c. The 30 member inter-ensemble spread is also highlighted along with the mean response (in black). The cloud amount increases throughout the atmospheric column but is strongest at ~150hPa; an altitude where model parameterization typically detrains hydrometeors from the deep convective cloud tops.

Figure 5.3 is an analogue of Figure 5.2 for the fully-coupled case. It consists of an ensemble mean first year mean climate response when full ocean GCM is used to predict the ocean state. In this case, the total response is a combination (not necessarily linear) of fast and slow SST mediated responses. The precipitation response (Figure 5.3a) is predominantly negative, homogeneous and weaker when compared to the fixed SST case. The three positive precipitation maxima of Figure 5.2a are not seen in this case. The sea surface temperature is reduced all around the coast (Figure 5.4a). It reiterates that SST changes and associated feedbacks have stronger impact on overall circulation response than direct (or fast) circulation response to aerosols. In spite of large-scale precipitation reduction, the high cloud response is still positive, although weaker and the imprints of local maxima from the fast response can still be seen (compare Figure 5.3b and 5.2b). The vertical profile of the response is also similar, but weaker. The 110

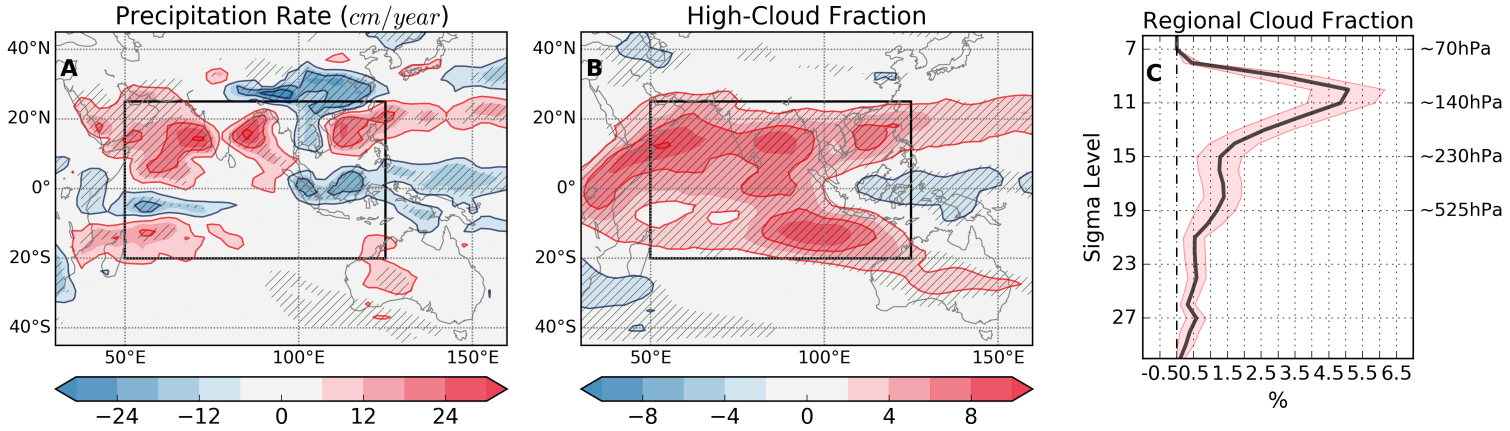

Figure 5.2 Ensemble mean first-year mean difference between uncoupled control ('1850S_pres') and perturbed ('2000S_pres_short') integrations. (a) Precipitation response, (b) increase in high cloud fraction, (c) vertical profile of area-averaged (over box in (a)) cloud fraction response and its inter-ensemble spread (standard deviation). Stippling indicate regions exceeding 90% statistical significance according to standard t-test.

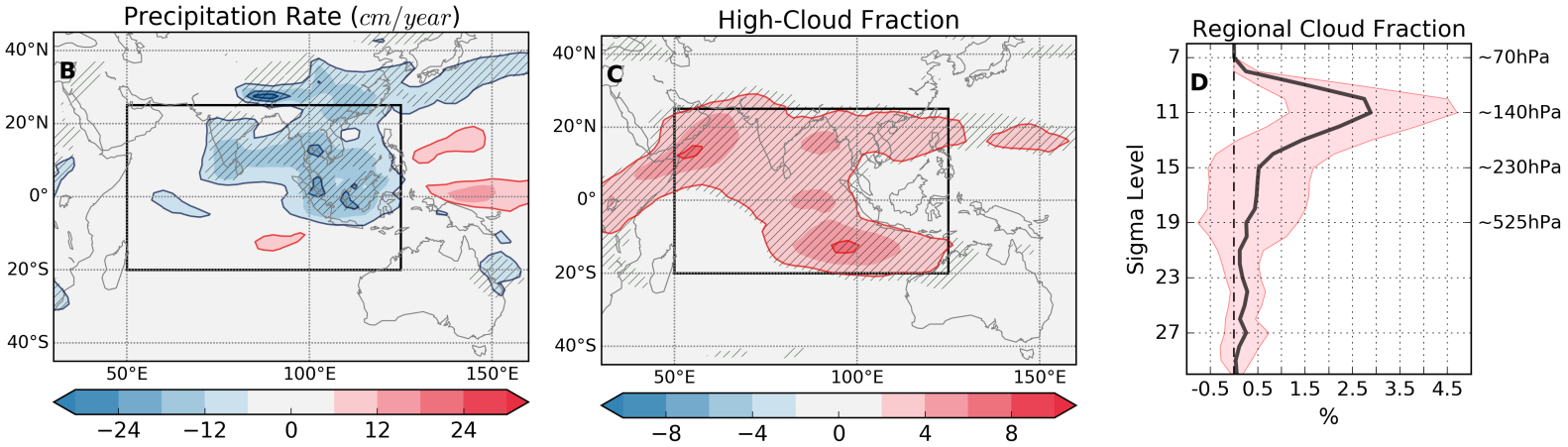

Figure 5.3 Ensemble mean first-year mean difference between full-coupled control ('1850S_pres') and perturbed ('2000S_pres_short') integrations. Same as in Figure 5.2 except for the fully-coupled case.

member inter-ensemble spread is greater indicative of higher interannual noise due to SST fluctuations.

Above results, specifically from Figure 5.2, suggest a positive relationship between precipitation and the cloud response. We examine this dependence by compositing the cloud response depending on sign of the precipitation anomaly; at a given time and a grid point, the cloud response is partitioned into two classes depending on the precipitation response. The partitioned cloud fraction response is shown in Figure 5.4b. It says that (a) cloud fraction increases with increase in (convective) precipitation, and (b) the cloud top (maxima in cloud response) also increases with increase in convection. Perhaps, there are alternate mechanisms, which are not related to the strength of convection, that lead to higher cloud amount in the upper troposphere in response to increase in aerosols (Figure 5.2b and 5.3b).

The changes in microphysical properties for the fully-coupled case are shown in Figure 5.5. Although, we are mostly interested in upper tropospheric response, the lower tropospheric response is also shown to highlight aerosols' effect on warm clouds. Figure 5.5a is a replica of Figure 5.3c. Increase in upper tropospheric cloud ice number concentration (Figure 5.5b) and mass-mixing ratio (Figure 5.5c) is consistent with increase in cloud amount. In CAM5, cloud ice effective radii are typically derived from corresponding mass and number concentrations. The response in cloud ice effective radii (Figure 5.5d) has relatively higher inter-ensemble spread when compared to the mean and is harder to interpret.

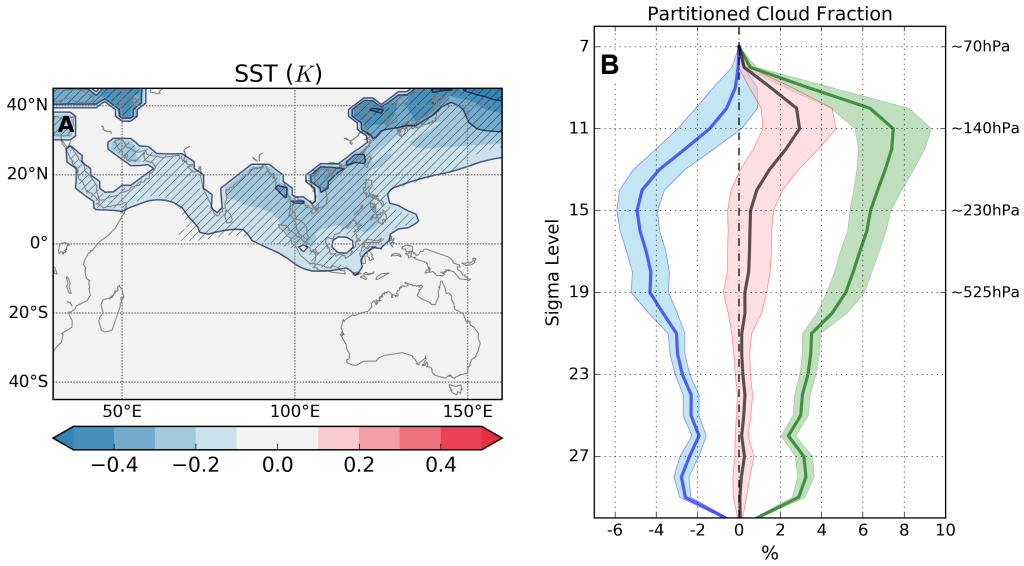

Figure 5.4 Ensemble mean first-year mean differences between fully-coupled control ('1850S') and perturbed ('2000S_short') integrations. (a) SST response. (b) Area-averaged cloud response (in black) and partitioned cloud fraction response based on positive (green) and negative (blue) local precipitation anomalies.

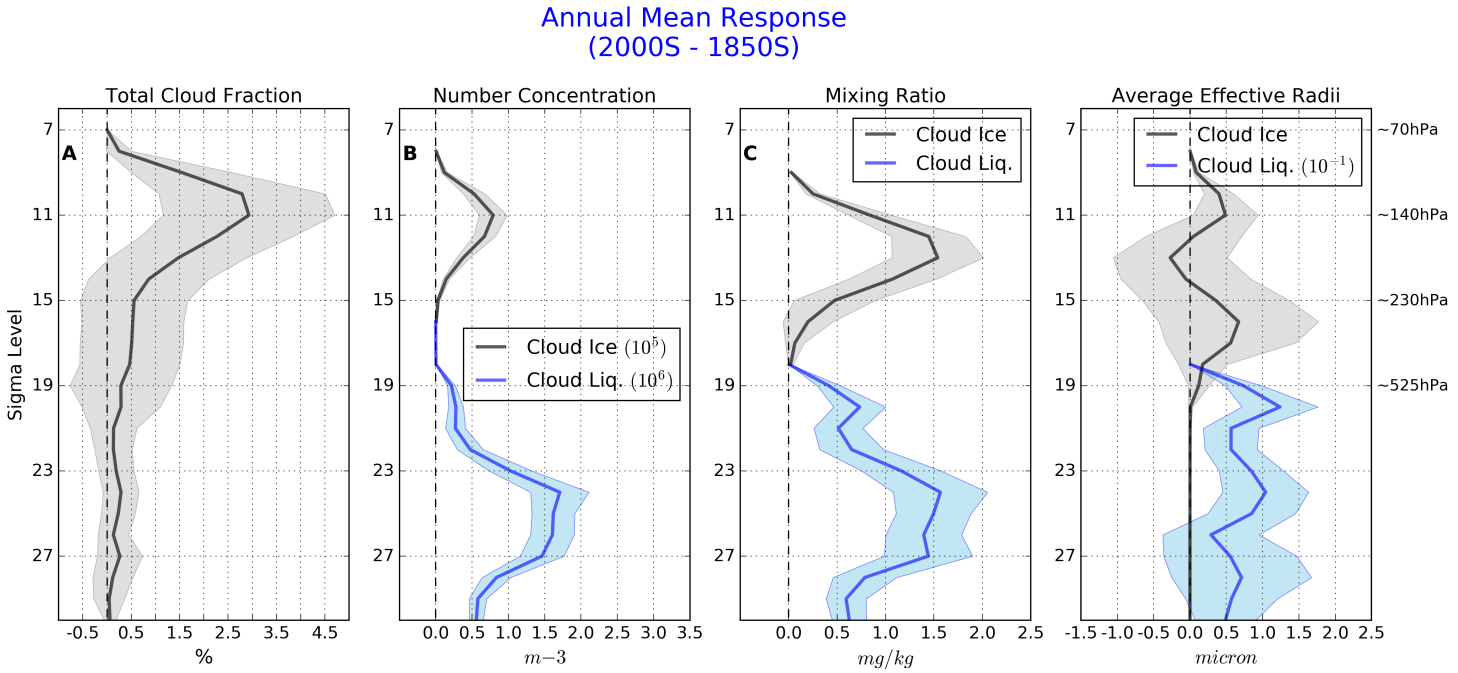

Figure 5.5 Area-averaged ensemble mean first-year mean difference between fully-coupled control ('1850S') and perturbed ('2000S_short') integrations. Vertical profile of (a) cloud fraction, (b) cloud ice, and cloud liquid number concentration, (c) their mass-mixing ratio, and (d) average effective radii response.

5.4 CONCLUSIONS

• *Increase in model simulated tropical high clouds when atmospheric aerosols are increased.*

• *A significant increase in high clouds despite large-scale, uniform decrease in deep convection.*

• *A microphysical effect: increase in cloud droplet amount due to aerosols; greater cloud ice particle formation via in-situ freezing of higher amount of cloud droplets; greater cloud fraction.*

We examined first-year mean high cloud response to sulfates over tropical Indian Ocean and discussed the role of convection and sea surface temperature in it. For this purpose, we analyzed both fully-coupled and uncoupled climate responses. Since sea surface temperature is fixed in uncoupled case, the atmospheric convection is not affected by the lower boundary but only by processes internal to the atmosphere.

There is a significant increase in high cloud fraction over the tropical Indian Ocean in response to increased sulfate aerosols. The increase is greater when SST-mediated response is prohibited in uncoupled case. Also, the precipitation response is stronger, more inhomogeneous, and is spatially correlated with the cloud response. It suggests that increase in high clouds is due to detrainment (of hydrometeors) from the deep convection. In fully-coupled case, SST-mediation uniformly suppresses convection over the region, but there is still a significant increase in the high cloud fraction. This result suggests presence of other active mechanism(s), which are independent of convection, that can increase high cloud fraction in response to increased aerosols. It is most likely a

parameterized microphysical effect as described in section 5.2.1. One or more of the microphysical processes listed earlier can increase cloud ice mixing ratio in the upper troposphere, thus, increasing super saturation, and ice stratus fraction. The proposed mechanism is consistent with the one described by Fan et al. 2013 using high frequency cloud resolved CAM5 simulations. They show that microphysical changes due to aerosols determine the cloud macrophysics response. Further, Ghan et al. 2012 showed that greater global mean high cloud fraction simulated in CAM5 with interactive aerosols is primarily due to two microphysical processes, namely, homogeneous and immersion freezing.

Whether these effects and their magnitude are realistic or not, is not yet clear, and need to be further studied. But, they certainly have an important consequence for simulated total sulfate aerosol radiative forcing (Figure 5.6 and 2.7; reprinted here for clarity). The positive radiative forcing over tropical Indian Ocean is very well correlated with the high cloud response (Figure 5.2b), and is consistent with longwave cloud radiative forcing. This regional positive radiative forcing appears to be indirectly caused by aerosols via modification of high clouds. It could have important implications for monsoonal circulation and needs to be studied and validated, extensively.

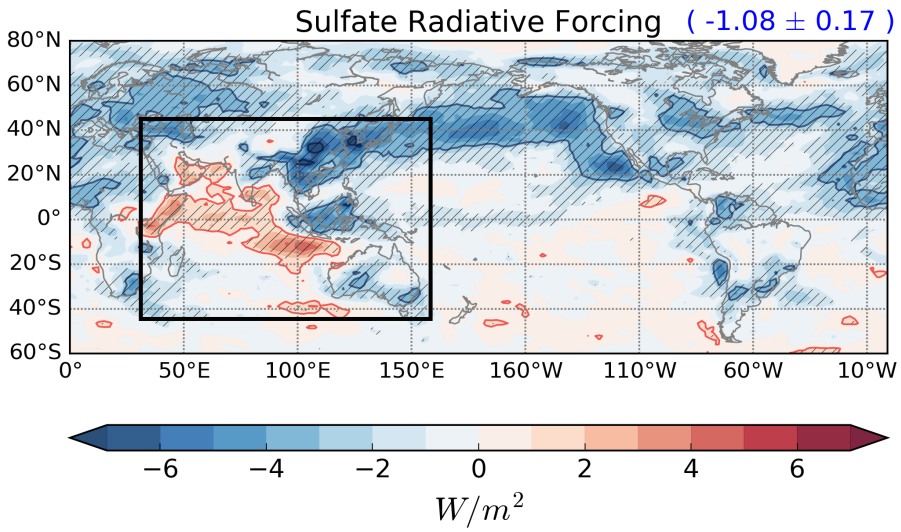

Figure 5.6 Total sulfate aerosol radiative forcing. Calculated as ensemble mean first-year mean difference in net radiative imbalance (at top of the model) between uncoupled preindustrial control ('1850S_sst') and uncoupled present day perturbed ('2000S_pres_short') integrations.

CHAPTER VI

CONCLUSIONS

This study explores impacts of anthropogenic sulfate aerosols on tropical Pacific climate using climate model experiments. Since tropical Pacific climate and its variability, e.g., ENSO, are characterized by large-scale interactions between the ocean and the atmosphere, our main objective was to identify coupled atmospheric and oceanic responses to aerosol perturbation and to understand their mechanisms. Identification of aerosol-induced changes in dynamical processes that drive ENSO in the tropical Pacific is extremely relevant for improving predictability on seasonal to long-term climate timescales.

We used suite of coupled and uncoupled climate model experiments using CESM 1.1.2 to identify and understand the regional coupled response. The role of SST, ocean dynamics and ocean-atmosphere coupling in determining the response was separated out by choosing different ocean components. The uncoupled versus coupled response distinguishes fast atmospheric response to aerosols from the slower ocean-mediated response. The choice of slab ocean versus the full Ocean GCM brings out ocean dynamical response to aerosols as well as the role of dynamical and thermodynamic ocean-atmosphere interaction in it. Further, by classifying the climate response into transient (short-term) and equilibrium (long-term) changes, we identified processes and coupled feedbacks that are active on seasonal-interannual timescales versus on multi-decadal timescales.

In CAM5, the representation of aerosol physics is much more advanced and complete than the earlier version. The parameterizations that predict aerosol distribution, clouds as well as their interactions are more physically realistic and consistent. This makes CESM 1.1.2 with CAM5 physics a leading climate model to study aerosol-climate interactions. In addition to studying the coupled climate response to aerosols, we also examined high cloud response over tropical Indian Ocean - the fast atmospheric response without any ocean feedback. The combined effect of parameterized convection and microphysical processes in high cloud response was discussed.

We find that an abrupt increase in tropospheric sulfate aerosols indirectly warms eastern tropical Pacific on seasonal-interannual timescales. The warming over equatorial region is related to dynamical changes in the upper ocean including changes in thermocline, and zonal circulation. This ocean dynamical response can be tied back to aerosol-induced tropical/subtropical surface cooling, anomalous regional atmospheric subsidence, and the Walker cell response. The seasonal-to-interannual modulation of this warming is driven by seasonal atmospheric forcing and ENSO-like ocean dynamical processes.

Off-equatorial warming response to the south is superficially similar to the one over equator, but has an entirely different formation mechanism. This off-equatorial warming is forced from the surface via reduced wind-driven evaporation (latent heat flux) over the region instead of upper ocean dynamics. It grows with time in the partially-coupled experiment because of active thermodynamic ocean-atmosphere feedback mechanism, also known as WES-feedback (Wind-Evaporation-SST). On the

other hand, the ocean dynamics, in fully-coupled case, will dissipate or transport this initial off-equatorial warming leaving a weaker and negative SST in response to increased aerosols in long-term.

We also find a consistent increase in high clouds over tropical Indian Ocean in response to increased aerosols. From a dynamical standpoint, the upper tropospheric ice cloud fraction over the tropics would be determined by detrainment from deep convective cloud tops. However, in fully-coupled case, there is large-scale uniform reduction in convection (precipitation), but a significant increase in high clouds in response to increased aerosols. This suggests an alternate mechanism via parameterized cloud microphysics: increase in cloud droplet number concentration due to increased aerosols, subsequent increase in cloud ice formation due to freezing of cloud droplets resulting in higher ice cloud fraction. This high cloud response to sulfate aerosols results in positive radiative forcing over the tropical Indian Ocean in comparison to negative forcing everywhere else on the globe and can impact the local monsoonal circulation.

These findings have important implications for the tropical Pacific climate, its variability, as well as predictability (local and remote). The contrasting long-term response between the fully- and the partially-coupled experiments highlights the effect of two different types of ocean-atmosphere coupling commonly employed to study anthropogenic climate change. The choice of ocean-atmosphere coupling significantly affects the tropical Pacific climate response and would have important implications for ITCZ and its southward shift. We also showed that sufficiently strong variations in sulfate aerosols' emissions over east Asia could affect the background Niño state on

seasonal-to-interannual timescales. It has implications for ENSO in a near-term climate change scenario, seasonal predictability, and for decadal predictions post-volcanic eruption. It could also potentially impact longer-term variability in the Pacific basin. It is essential to simulate the aerosol-induced subsidence over the East Asian region as well as to take into account the effects of ocean dynamics and dynamical coupling to accurately simulate tropical climate response to aerosols.

REFERENCES

Albrecht, Bruce A. "Aerosols, cloud microphysics, and fractional cloudiness." *Science* 245, no. 4923 (1989): 1227-1231.

Allen, Robert J., Amato T. Evan, and Ben B. B. Booth. "Interhemispheric Aerosol Radiative Forcing and Tropical Precipitation Shifts during the Late Twentieth Century." *Journal of Climate* 28, no. 20 (OCT, 2015): 8219-8246.

Ammann, Caspar M., Warren M. Washington, Gerald A. Meehl, Lawrence Buja, and Haiyan Teng. "Climate Engineering through Artificial Enhancement of Natural Forcings: Magnitudes and Implied Consequences." *Journal of Geophysical Research-Atmospheres* 115, (NOV 19, 2010): D22109.

Biasutti, M. and A. Giannini. "Robust Sahel Drying in Response to Late 20th Century Forcings." *Geophysical Research Letters* 33, no. 11 (JUN 8, 2006): L11706.

Bitz, C. M., K. M. Shell, P. R. Gent, D. A. Bailey, G. Danabasoglu, K. C. Armour, M. M. Holland, and J. T. Kiehl. "Climate Sensitivity of the Community Climate System Model, Version 4." *Journal of Climate* 25, no. 9 (MAY, 2012): 3053-3070.

Bollasina, Massimo A., Yi Ming, and V. Ramaswamy. "Anthropogenic Aerosols and the Weakening of the South Asian Summer Monsoon." *Science* 334, no. 6055 (OCT 28, 2011): 502-505.

Booth, Ben B. B., Nick J. Dunstone, Paul R. Halloran, Timothy Andrews, and Nicolas Bellouin. "Aerosols Implicated as a Prime Driver of Twentieth-Century North Atlantic Climate Variability (Vol 484, Pg 228, 2012)." *Nature* 485, no. 7399 (MAY 24, 2012): 534-534.

Boucher, Olivier. "Atmospheric Aerosols." In *Atmospheric Aerosols*, pp. 9-24. Springer Netherlands, 2015.

Bretherton, Christopher S. and Sungsu Park. "A New Moist Turbulence Parameterization in the Community Atmosphere Model." *Journal of Climate* 22, no. 12 (JUN, 2009): 3422-3448.

Cai, Wenju, Agus Santoso, Guojian Wang, Sang-Wook Yeh, Soon-Il An, Kim M. Cobb, Mat Collins, et al. "ENSO and Greenhouse Warming." *Nature Climate Change* 5, no. 9 (SEP, 2015): 849-859.

Capotondi, Antonietta, Andrew T. Wittenberg, Matthew Newman, Emanuele Di Lorenzo, Jin-Yi Yu, Pascale Braconnot, Julia Cole, et al. "Understanding ENSO

Diversity." *Bulletin of the American Meteorological Society* 96, no. 6 (JUN, 2015A): 921-938.

Capotondi, Antonietta, Yoo-Geun Ham, A. T. Wittenberg, and Jong-Seong Kug. "Climate model biases and El Niño Southern Oscillation (ENSO) simulation." *US CLIVAR Variations* 13, no. 1 (2015B): 21-25.

Carslaw, K. S., O. Boucher, D. V. Spracklen, G. W. Mann, J. G. L. Rae, S. Woodward, and M. Kulmala. "A Review of Natural Aerosol Interactions and Feedbacks within the Earth System." *Atmospheric Chemistry and Physics* 10, no. 4 (2010): 1701-1737.

Chang, C. -Y, J. C. H. Chiang, M. F. Wehner, A. R. Friedman, and R. Ruedy. "Sulfate Aerosol Control of Tropical Atlantic Climate Over the Twentieth Century." *Journal of Climate* 24, no. 10 (MAY 15, 2011): 2540-2555.

Chang, P., L. Ji, and H. Li. "A Decadal Climate Variation in the Tropical Atlantic Ocean from Thermodynamic Air-Sea Interactions." *Nature* 385, no. 6616 (FEB 6, 1997): 516-518.

Chang, P., L. Ji, B. Wang, and T. Li. "Interactions between the Seasonal Cycle and El-Niño Southern-Oscillation in an Intermediate Coupled Ocean-Atmosphere Model." *Journal of the Atmospheric Sciences* 52, no. 13 (JUL 1, 1995): 2353-2372.

Chang, Ping, Li Zhang, R. Saravanan, Daniel J. Vimont, John C. H. Chiang, Link Ji, Howard Seidel, and Michael K. Tippett. "Pacific Meridional Mode and El Niño-Southern Oscillation." *Geophysical Research Letters* 34, no. 16 (AUG 30, 2007): L16608.

Chen, Chen, Mark A. Cane, Andrew T. Wittenberg, and Dake Chen. "ENSO in the CMIP5 Simulations: Life Cycles, Diversity, and Responses to Climate Change." *Journal of Climate* 30, no. 2 (2017): 775-801.

Chiang, JCH and DJ Vimont. "Analogous Pacific and Atlantic Meridional Modes of Tropical Atmosphere-Ocean Variability." *Journal of Climate* 17, no. 21 (NOV, 2004): 4143-4158.

Chiang, John C. H., Yue Fang, and P. Chang. "Interhemispheric Thermal Gradient and Tropical Pacific Climate." *Geophysical Research Letters* 35, no. 14 (JUL 22, 2008): L14704.

Chiang, John C. H. and Andrew R. Friedman. "Extratropical Cooling, Interhemispheric Thermal Gradients, and Tropical Climate Change." *Annual Review of Earth and Planetary Sciences, Vol 40* 40, (2012): 383-412.

Christensen, Matthew W. and Graeme L. Stephens. "Microphysical and Macrophysical Responses of Marine Stratocumulus Polluted by Underlying Ships: Evidence of Cloud Deepening." *Journal of Geophysical Research-Atmospheres* 116, (FEB 1, 2011): D03201.

Collins, Matthew. "Predictions of climate following volcanic eruptions." *Volcanism and the Earth's Atmosphere* (2003): 283-300.

Cvijanovic, Ivana and John C. H. Chiang. "Global Energy Budget Changes to High Latitude North Atlantic Cooling and the Tropical ITCZ Response." *Climate Dynamics* 40, no. 5-6 (MAR, 2013): 1435-1452.

Deandreis, C., Y. Balkanski, J. L. Dufresne, and A. Cozic. "Radiative Forcing Estimates of Sulfate Aerosol in Coupled Climate-Chemistry Models with Emphasis on the Role of the Temporal Variability." *Atmospheric Chemistry and Physics* 12, no. 12 (2012): 5583-5602.

DelSole, Timothy, Michael K. Tippett, and Jagadish Shukla. "A Significant Component of Unforced Multidecadal Variability in the Recent Acceleration of Global Warming." *Journal of Climate* 24, no. 3 (FEB 1, 2011): 909-926.

Dijkstra, H. A. (2006). The ENSO phenomenon: theory and mechanisms. Advances in Geosciences, 6, 3-15.

Di Lorenzo, E., G. Liguori, N. Schneider, J. C. Furtado, B. T. Anderson, and M. A. Alexander. "ENSO and Meridional Modes: A Null Hypothesis for Pacific Climate Variability." *Geophysical Research Letters* 42, no. 21 (NOV 16, 2015): 9440-9448.

Donner, Leo, Wayne Schubert, and Richard Somerville, eds. *The Development of Atmospheric General Circulation Models: Complexity, Synthesis and Computation*. Cambridge University Press, 2011.

Donohoe, Aaron, John Marshall, David Ferreira, and David Mcgee. "The Relationship between ITCZ Location and Cross-Equatorial Atmospheric Heat Transport: From the Seasonal Cycle to the Last Glacial Maximum." *Journal of Climate* 26, no. 11 (JUN, 2013): 3597-3618.

England, Matthew H., Shayne McGregor, Paul Spence, Gerald A. Meehl, Axel Timmermann, Wenju Cai, Alex Sen Gupta, Michael J. McPhaden, Ariaan Purich, and Agus Santoso. "Recent Intensification of Wind-Driven Circulation in the Pacific and the Ongoing Warming Hiatus." *Nature Climate Change* 4, no. 3 (MAR, 2014): 222-227.

Fan, Jiwen, L. Ruby Leung, Daniel Rosenfeld, Qian Chen, Zhanqing Li, Jinqiang Zhang, and Hongru Yan. "Microphysical Effects Determine Macrophysical Response for Aerosol Impacts on Deep Convective Clouds." *Proceedings of the National Academy of Sciences of the United States of America* 110, no. 48 (NOV 26, 2013): E4581-E4590.

Frankignoul, C. "Sea-Surface Temperature Anomalies, Planetary-Waves, and Air-Sea Feedback in the Middle Latitudes." *Reviews of Geophysics* 23, no. 4 (1985): 357-390.

Friedman, Andrew R., Yen-Ting Hwang, John C. H. Chiang, and Dargan M. W. Frierson. "Interhemispheric Temperature Asymmetry Over the Twentieth Century and in Future Projections." *Journal of Climate* 26, no. 15 (AUG, 2013): 5419-5433.

Frierson, Dargan M. W., Yen-Ting Hwang, Neven S. Fuckar, Richard Seager, Sarah M. Kang, Aaron Donohoe, Elizabeth A. Maroon, Xiaojuan Liu, and David S. Battisti. "Contribution of Ocean Overturning Circulation to Tropical Rainfall Peak in the Northern Hemisphere." *Nature Geoscience* 6, no. 11 (NOV, 2013): 940-944.

Ghan, S. J. "Technical Note: Estimating Aerosol Effects on Cloud Radiative Forcing." *Atmospheric Chemistry and Physics* 13, no. 19 (2013): 9971-9974.

Ghan, S. J., X. Liu, R. C. Easter, R. Zaveri, P. J. Rasch, J. -H Yoon, and B. Eaton. "Toward a Minimal Representation of Aerosols in Climate Models: Comparative Decomposition of Aerosol Direct, Semidirect, and Indirect Radiative Forcing." *Journal of Climate* 25, no. 19 (OCT, 2012): 6461-6476.

Giannini, A., R. Saravanan, and P. Chang. "Oceanic Forcing of Sahel Rainfall on Interannual to Interdecadal Time Scales." *Science* 302, no. 5647 (NOV 7, 2003): 1027-1030.

Gill, A. E. "Some Simple Solutions for Heat-Induced Tropical Circulation." *Quarterly Journal of the Royal Meteorological Society* 106, no. 449 (1980): 447-462.

Green, Brian and John Marshall. "Coupling of Trade Winds with Ocean Circulation Damps ITCZ Shifts." *Journal of Climate* 30, no. 12 (JUN, 2017): 4395-4411.

Guilyardi, Eric, Hugo Bellenger, Mat Collins, Samantha Ferrett, Wenju Cai, and Andrew Wittenberg. "A first look at ENSO in CMIP5." *Clivar Exchanges* 17, no. 1 (2012): 29-32.

Haywood, J. and O. Boucher. "Estimates of the Direct and Indirect Radiative Forcing due to Tropospheric Aerosols: A Review." *Reviews of Geophysics* 38, no. 4 (NOV, 2000): 513-543.

He, Jie and Brian J. Soden. "Anthropogenic Weakening of the Tropical Circulation: The Relative Roles of Direct CO2 Forcing and Sea Surface Temperature Change." *Journal of Climate* 28, no. 22 (NOV, 2015): 8728-8742.

Heintzenberg, Jost and Robert J. Charlson. "Clouds in the Perturbed Climate System their Relationship to Energy Balance, Atmospheric Dynamics, and Precipitation Introduction." *Clouds in the Perturbed Climate System: Their Relationship to Energy Balance, Atmospheric Dynamics, and Precipitation* (2009): 1-15.

Held, IM and BJ Soden. "Water Vapor Feedback and Global Warming." *Annual Review of Energy and the Environment* 25, (2000): 441-475.

Hurrell, James W., M. M. Holland, P. R. Gent, S. Ghan, Jennifer E. Kay, P. J. Kushner, J. -F Lamarque, et al. "The Community Earth System Model A Framework for Collaborative Research." *Bulletin of the American Meteorological Society* 94, no. 9 (SEP, 2013): 1339-1360.

Hwang, Yen-Ting, Dargan M. W. Frierson, and Sarah M. Kang. "Anthropogenic Sulfate Aerosol and the Southward Shift of Tropical Precipitation in the Late 20th Century." *Geophysical Research Letters* 40, no. 11 (JUN 16, 2013): 2845-2850.

IPCC, 2013: Climate Change 2013: The Physical Science Basis. Contribution of Working Group I to the Fifth Assessment Report of the Intergovernmental Panel on Climate Change [Stocker, T.F., D. Qin, G.-K. Plattner, M. Tignor, S.K. Allen, J. Boschung, A. Nauels, Y. Xia, V. Bex and P.M. Midgley (eds.)]. Cambridge University Press, Cambridge, United Kingdom and New York, NY, USA, 1535 pp, doi:10.1017/CBO9781107415324.

Johnson, Nathaniel C. "How Many ENSO Flavors can we Distinguish?" *Journal of Climate* 26, no. 13 (JUL, 2013): 4816-4827.

Jones, Andy, James M. Haywood, and Olivier Boucher. "Aerosol Forcing, Climate Response and Climate Sensitivity in the Hadley Centre Climate Model." *Journal of Geophysical Research-Atmospheres* 112, no. D20 (OCT 30, 2007): D20211.

Kagan, Boris A. *Ocean Atmosphere Interaction and Climate Modeling*. Vol. 11. Cambridge University Press, 2006.

Kosaka, Yu and Shang-Ping Xie. "Recent Global-Warming Hiatus Tied to Equatorial Pacific Surface Cooling." *Nature* 501, no. 7467 (SEP 19, 2013): 403-+.

Kurian, Jaison and P. N. Vinayachandran. "Mechanisms of Formation of the Arabian Sea Mini Warm Pool in a High-Resolution Ocean General Circulation Model." *Journal of Geophysical Research-Oceans* 112, no. C5 (MAY 4, 2007): C05009.

Lamarque, J. -F, T. C. Bond, V. Eyring, C. Granier, A. Heil, Z. Klimont, D. Lee, et al. "Historical (1850-2000) Gridded Anthropogenic and Biomass Burning Emissions of Reactive Gases and Aerosols: Methodology and Application." *Atmospheric Chemistry and Physics* 10, no. 15 (2010): 7017-7039.

Larson, Sarah M. and Ben P. Kirtman. "The Pacific Meridional Mode as an ENSO Precursor and Predictor in the North American Multimodel Ensemble." *Journal of Climate* 27, no. 18 (SEP, 2014): 7018-7032.

Lehner, Flavio, Andrew P. Schurer, Gabriele C. Hegerl, Clara Deser, and Thomas L. Froelicher. "The Importance of ENSO Phase during Volcanic Eruptions for Detection and Attribution." *Geophysical Research Letters* 43, no. 6 (MAR 28, 2016): 2851-2858.

L'Heureux, Michelle L., Sukyoung Lee, and Bradfield Lyon. "Recent Multidecadal Strengthening of the Walker Circulation Across the Tropical Pacific." *Nature Climate Change* 3, no. 6 (JUN, 2013): 571-576.

Lindzen, R. S. and S. Nigam. "On the Role of Sea-Surface Temperature-Gradients in Forcing Low-Level Winds and Convergence in the Tropics." *Journal of the Atmospheric Sciences* 44, no. 17 (SEP 1, 1987): 2418-2436.

Liu, X., R. C. Easter, S. J. Ghan, R. Zaveri, P. Rasch, X. Shi, J. -F Lamarque, et al. "Toward a Minimal Representation of Aerosols in Climate Models: Description and Evaluation in the Community Atmosphere Model CAM5." *Geoscientific Model Development* 5, no. 3 (2012): 709-739.

Lohmann, U. "Aerosol Effects on Clouds and Climate." *Space Science Reviews* 125, no. 1-4 (APR, 2006): 129-137.

Maher, Nicola, Shayne McGregor, Matthew H. England, and Alexander Sen Gupta. "Effects of Volcanism on Tropical Variability." *Geophysical Research Letters* 42, no. 14 (JUL 28, 2015): 6024-6033.

Mahowald, Natalie, Daniel S. Ward, Silvia Kloster, Mark G. Flanner, Colette L. Heald, Nicholas G. Heavens, Peter G. Hess, Jean-Francois Lamarque, and Patrick Y. Chuang. "Aerosol Impacts on Climate and Biogeochemistry." *Annual Review of Environment and Resources, Vol 36* 36, (2011): 45-74.

McGregor, Shayne, Axel Timmermann, Malte F. Stuecker, Matthew H. England, Mark Merrifield, Fei-Fei Jin, and Yoshimitsu Chikamoto. "Recent Walker Circulation Strengthening and Pacific Cooling Amplified by Atlantic Warming." *Nature Climate Change* 4, no. 10 (OCT, 2014): 888-892.

McPhaden, Michael J., Stephen E. Zebiak, and Michael H. Glantz. "ENSO as an Integrating Concept in Earth Science." *Science* 314, no. 5806 (DEC 15, 2006): 1740-1745.

McPhaden, MJ. "Mixed Layer Temperature Balance on Intraseasonal Timescales in the Equatorial Pacific Ocean." *Journal of Climate* 15, no. 18 (SEP, 2002): 2632-2647.

Morrison, Hugh and Andrew Gettelman. "A New Two-Moment Bulk Stratiform Cloud Microphysics Scheme in the Community Atmosphere Model, Version 3 (CAM3). Part I: Description and Numerical Tests." *Journal of Climate* 21, no. 15 (AUG 1, 2008): 3642-3659.

Neale, Richard B., Jadwiga H. Richter, and Markus Jochum. "The Impact of Convection on ENSO: From a Delayed Oscillator to a Series of Events." *Journal of Climate* 21, no. 22 (NOV 15, 2008): 5904-5924.

Neale, R. *et al*. Description of the NCAR Community Atmosphere Model (CAM 5.0). *Tech. Rep*. Natl. Cent. for Atmos. Res., Boulder, Colo. (2010).

Neelin, JD, DS Battisti, AC Hirst, FF Jin, Y. Wakata, T. Yamagata, and SE Zebiak. "ENSO Theory." *Journal of Geophysical Research-Oceans* 103, no. C7 (JUN 29, 1998): 14261-14290.

Neelin, J. D. Climate Change and Climate Modeling. Cambridge University Press. 2010

Nobre, P. and J. Shukla. "Variations of Sea Surface Temperature, Wind Stress, and Rainfall Over the Tropical Atlantic and South America." *Journal of Climate* 9, no. 10 (OCT, 1996): 2464-2479.

Ocko, Ilissa B., V. Ramaswamy, and Yi Ming. "Contrasting Climate Responses to the Scattering and Absorbing Features of Anthropogenic Aerosol Forcings." *Journal of Climate* 27, no. 14 (JUL 15, 2014): 5329-5345.

Ohba, Masamichi, Hideo Shiogama, Tokuta Yokohata, and Masahiro Watanabe. "Impact of Strong Tropical Volcanic Eruptions on ENSO Simulated in a Coupled GCM." *Journal of Climate* 26, no. 14 (JUL, 2013): 5169-5182.

Park, Sungsu and Christopher S. Bretherton. "The University of Washington Shallow Convection and Moist Turbulence Schemes and their Impact on Climate Simulations with the Community Atmosphere Model." *Journal of Climate* 22, no. 12 (JUN, 2009): 3449-3469.

Park, Sungsu, Christopher S. Bretherton, and Philip J. Rasch. "Integrating Cloud Processes in the Community Atmosphere Model, Version 5." *Journal of Climate* 27, no. 18 (SEP, 2014): 6821-6856.

Philander, S. G. “El Niño, La Nina and the Southern Oscillation”. Vol. 46, International Geophysics Series, Academic Press. 1990

Pohlmann, H., W. A. Mueller, K. Kulkarni, M. Kameswarrao, D. Matei, F. S. E. Vamborg, C. Kadow, S. Illing, and J. Marotzke. "Improved Forecast Skill in the Tropics in the New MiKlip Decadal Climate Predictions." *Geophysical Research Letters* 40, no. 21 (NOV 16, 2013): 5798-5802.

Rosenfeld, Daniel, Meinrat O. Andreae, Ari Asmi, Mian Chin, Gerrit de Leeuw, David P. Donovan, Ralph Kahn, et al. "Global Observations of Aerosol-Cloud-Precipitation-Climate Interactions." *Reviews of Geophysics* 52, no. 4 (DEC, 2014): 750-808.

Rosenfeld, Daniel, Ulrike Lohmann, Graciela B. Raga, Colin D. O'Dowd, Markku Kulmala, Sandro Fuzzi, Anni Reissell, and Meinrat O. Andreae. "Flood Or Drought: How do Aerosols Affect Precipitation?" *Science* 321, no. 5894 (SEP 5, 2008): 1309-1313.

Rotstayn, LD and U. Lohmann. "Tropical Rainfall Trends and the Indirect Aerosol Effect." *Journal of Climate* 15, no. 15 (AUG, 2002): 2103-2116.

Russell, Lynn M., Armin Sorooshian, John H. Seinfeld, Bruce A. Albrecht, Athanasios Nenes, Lars Ahlm, Yi-Chun Chen, et al. "Eastern Pacific Emitted Aerosol Cloud Experiment." *Bulletin of the American Meteorological Society* 94, no. 5 (MAY, 2013): 709-+.

Saravanan, R. and P. Chang. "Oceanic Mixed Layer Feedback and Tropical Atlantic Variability." *Geophysical Research Letters* 26, no. 24 (DEC 15, 1999): 3629-3632.

———. "Thermodynamic Coupling and Predictability of Tropical Sea Surface Temperature." *Earth's Climate: The Ocean-Atmosphere Interaction* 147, (2004): 171-180.

Schneider, Tapio. "The General Circulation of the Atmosphere." *Annual Review of Earth and Planetary Sciences* 34, (2006): 655-688.

Schneider, Tapio, Tobias Bischoff, and Gerald H. Haug. "Migrations and Dynamics of the Intertropical Convergence Zone." *Nature* 513, no. 7516 (SEP 4, 2014): 45-53.

Schwendike, Juliane, Pallavi Govekar, Michael J. Reeder, Richard Wardle, Gareth J. Berry, and Christian Jakob. "Local Partitioning of the Overturning Circulation in the Tropics and the Connection to the Hadley andWalker Circulations." *Journal of Geophysical Research-Atmospheres* 119, no. 3 (FEB 16, 2014): 1322-1339.

Seinfeld, John H., Christopher Bretherton, Kenneth S. Carslaw, Hugh Coe, Paul J. DeMott, Edward J. Dunlea, Graham Feingold, et al. "Improving our Fundamental Understanding of the Role of Aerosol-Cloud Interactions in the Climate System." *Proceedings of the National Academy of Sciences of the United States of America* 113, no. 21 (MAY 24, 2016): 5781-5790.

Servain, J., I. Wainer, JP McCreary, and A. Dessier. "Relationship between the Equatorial and Meridional Modes of Climatic Variability in the Tropical Atlantic." *Geophysical Research Letters* 26, no. 4 (FEB 15, 1999): 485-488.

Shindell, D. T., A. Voulgarakis, G. Faluvegi, and G. Milly. "Precipitation Response to Regional Radiative Forcing." *Atmospheric Chemistry and Physics* 12, no. 15 (2012): 6969-6982.

Smith, Doug M., Ben B. B. Booth, Nick J. Dunstone, Rosie Eade, Leon Hermanson, Gareth S. Jones, Adam A. Scaife, Katy L. Sheen, and Vikki Thompson. "Role of Volcanic and Anthropogenic Aerosols in the Recent Global Surface Warming Slowdown." *Nature Climate Change* 6, no. 10 (OCT, 2016): 936-+.

Sobel, Adam H. "Simple models of ensemble-averaged precipitation and surface wind, given the sea surface temperature." *The Global Circulation of the Atmosphere, edited by T. Schneider and AH Sobel* (2007): 219-251.

Stevens, Bjorn and Jean-Louis Brenguier. "Cloud-Controlling Factors Low Clouds." *Clouds in the Perturbed Climate System: Their Relationship to Energy Balance, Atmospheric Dynamics, and Precipitation* (2009): 173-196.

Stevens, Bjorn and Graham Feingold. "Untangling Aerosol Effects on Clouds and Precipitation in a Buffered System." *Nature* 461, no. 7264 (OCT 1, 2009): 607-613.

Swanson, Kyle L., George Sugihara, and Anastasios A. Tsonis. "Long-Term Natural Variability and 20th Century Climate Change." *Proceedings of the National Academy of Sciences of the United States of America* 106, no. 38 (SEP 22, 2009): 16120-16123.

Takahashi, Chiharu and Masahiro Watanabe. "Pacific Trade Winds Accelerated by Aerosol Forcing Over the Past Two Decades." *Nature Climate Change* 6, no. 8 (AUG, 2016): 768-+.

Tao, Wei-Kuo, Jen-Ping Chen, Zhanqing Li, Chien Wang, and Chidong Zhang. "Impact of Aerosols on Convective Clouds and Precipitation." *Reviews of Geophysics* 50, (APR 17, 2012): RG2001.

Timmreck, Claudia, Holger Pohlmann, Sebastian Illing, and Christopher Kadow. "The Impact of Stratospheric Volcanic Aerosol on Decadal-Scale Climate Predictions." *Geophysical Research Letters* 43, no. 2 (JAN 28, 2016): 834-842.

Toba, Yoshiaki, ed. *Ocean-atmosphere interactions*. The Rosen Publishing Group, 2003.

Tokinaga, Hiroki, Shang-Ping Xie, Clara Deser, Yu Kosaka, and Yuko M. Okumura. "Slowdown of the Walker Circulation Driven by Tropical Indo-Pacific Warming." *Nature* 491, no. 7424 (NOV 15, 2012): 439-443.

Twomey, S. "Pollution and the planetary albedo." *Atmospheric Environment (1967)* 8, no. 12 (1974): 1251-1256.

Vecchi, Gabriel A. and Brian J. Soden. "Global Warming and the Weakening of the Tropical Circulation." *Journal of Climate* 20, no. 17 (SEP 1, 2007): 4316-4340.

Voigt, Aiko, Sandrine Bony, Jean-Louis Dufresne, and Bjorn Stevens. "The Radiative Impact of Clouds on the Shift of the Intertropical Convergence Zone." *Geophysical Research Letters* 41, no. 12 (JUN 28, 2014): 4308-4315.

Voigt, Aiko, Robert Pincus, Bjorn Stevens, Sandrine Bony, Olivier Boucher, Nicolas Bellouin, Anna Lewinschal, Brian Medeiros, Zhili Wang, and Hua Zhang. "Fast and Slow Shifts of the Zonal-Mean Intertropical Convergence Zone in Response to an Idealized Anthropogenic Aerosol." *Journal of Advances in Modeling Earth Systems* 9, no. 2 (JUN, 2017): 870-892.

Wang, CZ. "Atmospheric Circulation Cells Associated with the El Niño-Southern Oscillation." *Journal of Climate* 15, no. 4 (2002): 399-419.

Wang, CZ and J. Picaut. "Understanding ENSO Physics - A Review." *Earth's Climate: The Ocean-Atmosphere Interaction* 147, (2004): 21-48.

Wang, WM and MJ McPhaden. "The Surface-Layer Heat Balance in the Equatorial Pacific Ocean. Part I: Mean Seasonal Cycle." *Journal of Physical Oceanography* 29, no. 8 (AUG, 1999): 1812-1831.

Williams, KD, A. Jones, DL Roberts, CA SeNiño r, and MJ Woodage. "The Response of the Climate System to the Indirect Effects of Anthropogenic Sulfate Aerosol." *Climate Dynamics* 17, no. 11 (AUG, 2001): 845-856.

Williamson, D. L., J. T. Kiehl, V. Ramanathan, R. E. Dickinson, and J. J. Hack, 1987: *Description of the NCAR Community Climate Model (CCM1)*. NCAR Technical Note

Wu, Zhaohua, Norden E. Huang, John M. Wallace, Brian V. Smoliak, and Xianyao Chen. "On the Time-Varying Trend in Global-Mean Surface Temperature." *Climate Dynamics* 37, no. 3-4 (AUG, 2011): 759-773.

Xie, SP. "The Shape of Continents, Air-Sea Interaction, and the Rising Branch of the Hadley Circulation." *Hadley Circulation: Present, Past and Future* 21, (2004): 121-152.

Yu, Jin-Yi, Hsun-Ying Kao, and Tong Lee. "Subtropics-Related Interannual Sea Surface Temperature Variability in the Central Equatorial Pacific." *Journal of Climate* 23, no. 11 (JUN, 2010): 2869-2884.

Zhang, Rong, Thomas L. Delworth, Rowan Sutton, Daniel L. R. Hodson, Keith W. Dixon, Isaac M. Held, Yochanan Kushnir, et al. "Have Aerosols Caused the Observed Atlantic Multidecadal Variability?" *Journal of the Atmospheric Sciences* 70, no. 4 (APR, 2013): 1135-1144.